Mechanisms of nuclear movement during muscle development in Drosophila:

Author: Mary Ann Collins

Mechanisms of nuclear movement during muscle development in *Drosophila*

Mary Ann Collins

A dissertation submitted to the Faculty of the Department of Biology

in partial fulfillment of the requirements for the degree of

Doctor of Philosophy

Boston College
Morrissey College of Arts and Sciences
Graduate School

January 2020

ABSTRACT

Mechanisms of nuclear movement during muscle development in *Drosophila*

Mary Ann Collins

Advisor: Eric S. Folker, Ph.D.

Skeletal muscle is a syncytial cell type in which the multiple nuclei are evenly spaced along the cell periphery. During muscle development, the myonuclei undergo an elaborate set of movements to achieve this precise positioning throughout the muscle. The importance of proper nuclear positioning is highlighted by the correlation between mispositioned nuclei and muscle disease. However, the mechanisms that govern this energetically expensive process as well as the influence nuclear positioning has on muscle cell function remains to be elucidated.

The goal of this thesis is to determine the molecular factors and subsequent mechanisms that regulate nuclear movement and how such pathways are disrupted in various muscle diseases. Since many of the key cellular features are conserved between *Drosophila* and mammalian muscles, we utilize *Drosophila* musculature as a model system to study myonuclear positioning during muscle development. In this thesis, we provide the first evidence that nuclei experience attractive and repulsive interactions with one another as they actively migrate. Furthermore, we demonstrate that these nucleus-nucleus interactions are critical for proper nuclear positioning, and that they are distinctly regulated by genes that are associated with two different muscle diseases, Emery-Dreifuss muscular

dystrophy and Centronuclear myopathy (Chapter 2). We then elaborate upon the genetic mechanisms through which CNM-linked genes regulate nuclear positioning (Chapter 3). Finally, we show that proper nuclear movement requires both the separation of nuclei from their neighbors as well as the transmission of force, that is generated from the cytoskeleton, to move nuclei within the cell (Chapter 4).

Together, the work presented in this thesis provides new perspective and mechanistic insights into the genetic factors and physical forces that regulate nuclear movement during muscle development and how such pathways are disrupted in disease, while emphasizing the importance of studying such dynamic processes within an *in vivo* system.

DEDICATION

This dissertation is wholeheartedly dedicated to the four most fearless and courageous women who continue to inspire me every single day.

In loving memory of Pearl E. Schweitzer

ACKNOWLEDGEMENTS

I am deeply indebted to the many people who have helped me along this incredible journey.

First and foremost, I would like to express my utmost gratitude to my advisor, Dr. Eric Folker: Thank you for your incredible mentorship over these past five years. I have learned a tremendous amount from your guidance – scientifically, professionally, and personally. You have taught me the value of patience and the importance of having confidence, not only in my data but in myself as well. I will always appreciate your honest feedback, continuous support, and incredible persistence. Your passion for research is inspiring and has constantly motivated me throughout this dissertation. Thank you for making me into the scientist that I am today.

I would like to extend my deepest appreciation to my dissertation committee, Dr. David Burgess, Dr. Vicki Losick, Dr. Daniel Kirschner, and Dr. Sarah McMenamin: Thank you for your additional guidance and advice. I have enjoyed sharing my scientific progress with you as well as our stimulating discussions about my work. Your insightful questions, thoughtful ideas, and diverse perspectives have been invaluable to both my research and my scientific training alike.

To my lab mates, Dr. Alexander Auld, Torrey Mandigo, and Alexandra Burgess: Thank you for your friendship and encouragement over the years. I will forever cherish the many hours we spent laughing, complaining, troubleshooting, daydreaming, and joking around together. You are amazing scientists, colleagues, and friends; I cannot wait to see what amazing things you will accomplish in the future.

I would also like to extend my sincere thanks to the undergraduate students of the Folker Lab, especially Gabriella Vazquez, Jaclyn Camuglia, Tiffany Shu, Allie Coon, Riya Thomas, and Arshdeep Singh: Thank you for your hard work, dedication, scientific contributions, and above all else, your friendship as well as the copious amounts of coffee you've brought me to help keep me sane. It has been an absolute pleasure mentoring you and watching you grow over the years.

To my best friend and fellow Jersey girl, Dr. Alyssa Antropow: I am truly grateful for our many years of friendship – since our first day of college all the way through graduate school and beyond. Whether it is to commiserate or celebrate, thank you for always being there for me and for your shared love of Moscato and pizza.

To my parents, Mary Lou and Thomas Collins, and my sister Nancy: Thank you for always supporting my dreams and aspirations, no matter how ambitious. Your unconditional love, encouragement, and understanding have meant the absolute world to me. None of this would have been possible without you. I love you all so much.

Finally, to Dave: Despite the long-distance, thank you for making your love and support felt all the way from San Francisco to Boston. Out of all our adventures together, graduate school has been by far the most challenging yet rewarding, and I am incredibly proud of what we have accomplished. Thank you for always believing in me, especially during times of self-doubt. I am forever grateful for you and cannot wait to start the next chapter of our lives, meu amor.

TABLE OF CONTENTS

LIST OF FIGURES & TABLES

CHAPTER 1

INTRODUCTION

1.1 NUCLEAR MOVEMENT: A CONSERVED PROCESS

As the largest organelle in the cell, the nucleus is the principal organizational center of eukaryotic cells. Textbook diagrams and illustrations often depict the nucleus as a giant stationary sphere that sits idly in the center of the cell. Despite this classical representation, the position of the nucleus is extremely dynamic. This active process of nuclear movement is conserved in all eukaryotes, from unicellular and mononucleated cell types to more complex multicellular systems. Furthermore, the precise position of the nucleus is crucial for a variety of cellular and developmental processes.

Nuclear positioning is of particular importance during cell division: primarily to establish the division plane and ensure equal distribution of genetic material. In the budding yeast, *Saccharomyces cerevisiae*, the nucleus is positioned into the bud neck in order to properly distribute DNA between the mother cell and daughter cell (Yeh et al., 1995; Shaw et al., 1998; ten Hoopen et al., 2012). Similarly, in the fission yeast, *Schizosaccharomyces pombe*, the nucleus is actively positioned in the middle of the cell, where it serves as a spatial cue for the location of the division plane (Tran et al., 2001; Almonacid & Paoletti, 2010). For multicellular organisms, the migration of the male and female pronuclei are essential during the early stages of egg fertilization. After fertilization, the male and female pronuclei move toward each other and fuse in the middle of the egg (Reinsch & Karsenti, 1997). Thus, proper positioning of the two pronuclei is necessary for the even division of

the zygote and further development of the blastomere. Positioning of pronuclei can also result in asymmetric divisions, as seen during the first cell division of *Caenorhabditis elegans*. In this scenario, the female pronucleus moves towards the anterior of the zygote to meet with the male pronucleus. This movement is part of the process that divides the zygote asymmetrically to form two daughter cells that differ in size and developmental fate (Colombo et al., 2003). In addition to cell division, movement of the nucleus has also been observed during other phases of the cell cycle. In vertebrate neuroepithelium, nuclei of neuronal precursor cells undergo interkinetic nuclear migration: a set of characteristic cell-cycle dependent nuclear movements along the apico-basal axis (Baye & Link, 2008; Del Bene, 2011). Nuclei positioned on the apical side of the neuroepithelium begin to migrate at the start of G1 and continue to move basally through S-phase. As the cell cycle progresses, these nuclei must migrate back towards the apical side before the neuronal precursor cells can divide. This reversible movement is thought to create the necessary space for neighboring cells to divide, thereby maximizing the number of epithelial cells within the apical surface (Spear & Erickson, 2012), and may also regulate cell-cycle exit as well as cell fate determination (Del Bene et al., 2008).

Nuclei in non-dividing cells also move to regulate other developmental processes beyond the context of cell division, such as cellular organization, morphology, polarization, and migration. Analogous to interkinetic nuclear movement, nuclei of photoreceptor cells in the developing optic epithelium of *Drosophila* move basally and then apically to establish the characteristic arrangement of cells in the ommatidium (Patterson et al., 2004). In the hypodermis of *C. elegans*, nuclei in neighboring hyp7 precursor cells exchange positions to allow for their subsequent fusion and formation of the hyp7 syncytium (Starr

et al., 2001). In migrating cells, the nucleus is positioned toward the rear of the cell, far from the protruding front. During fibroblast migration, reward movement of the nucleus allows for forward positioning of the centrosome towards the leading edge (Gomes et al., 2005). The resulting polarization is established and maintained through the harnessing of retrograde-moving actin cables over the nuclear surface to push the nucleus towards the rear (Luxton et al., 2010). In addition to migrating fibroblasts, this characteristic rearward nuclear movement has been observed in many other cell types, such as such as fish keratocytes (Small et al., 1995), astrocytes (Etienne-Manneville & Hall, 2001), and epithelial cells (Desai et al., 2009). For migrating neurons, nuclear movement is especially challenging, as these cells navigate through a dense environment of neural tissue. Through the coordination of contractile forces generated by the actin and microtubule cytoskeletal networks, the nucleus is pushed into the leading process of the neuron (Vallee et al., 2009; Trivedi & Solecki, 2011).

Coordinating the movement and position of the nucleus becomes increasingly challenging in cells that contain multiple nuclei within a shared cytoplasm, known as syncytia. To achieve their multinucleated state, some syncytia arise from multiple nuclear divisions without cytokinesis. One such example is the formation of the *Drosophila* syncytial blastoderm, in which nuclei divide in a parasynchronous wave. During embryonic development, cellularization of the syncytium requires the movement of the nuclei towards the cortex of the embryo prior to the invagination of the plasma membrane (Mazumdar & Mazumdar, 2002). Similarly, nuclei in the syncytial hyphae of filamentous fungi, like *Aspergillus nidulans* and *Ashbya gossypii*, divide asynchronously. During hyphal growth, these nuclei actively migrate and are evenly distributed throughout the cell to adequately

nourish the rapidly growing hypha (Xiang & Fischer, 2004; Dundon et al., 2016; Gibeaux et al., 2017). Other syncytial cell types, like skeletal muscle, form from multiple cell fusion events. Unlike the syncytial embryo or fungal hyphae, skeletal muscle cells are post-mitotic and therefore do not divide. Rather, new nuclei are incorporated from mononucleated myoblasts that fuse into the growing myotube (Capers, 1960). As the myotube matures into a myofiber, these nuclei undergo a specific pattern of movements to achieve even spacing and maximal distance from one another at the periphery of the muscle.

The examples above represent a small yet diverse subset of cellular processes that require proper positioning of the nucleus. While the position and movement of the nucleus has been well described in each of these systems, what remains unclear are the mechanistic details in how this active process is regulated. Furthermore, little to no work has been done to investigate how movement of the nucleus impacts cellular development and function, and thus, the purpose of this movement remains poorly understood.

1.2 NUCLEAR MOVEMENT IN SKELETAL MUSCLE

Perhaps the most striking example of nuclear movement is within myofibers, the cellular unit of skeletal muscle. Muscle fibers are a unique cell type, due to their specialized cellular organization and architecture. Skeletal muscle tissue is arranged as a bundle of multiple muscle fascicles that are composed of bundles of individual muscle cells. Each muscle cell, also known as a myofiber, can span several centimeters in length, up to 50 μm in diameter, and contain five times as much volume than most smaller mononucleated cells (Bruusgaard et al., 2003). Within each myofiber is a highly organized contractile network of myofibrils which are comprised of repeating sections of sarcomeres. Each sarcomere is

composed of an alternating parallel arrangement of thin actin filaments overlapping with thick myosin filaments (Huxley, 1953; Huxley, 1957). Contraction of the sarcomere relies on the generation of force produced by the cyclic formation of cross-bridges between actin and myosin (Huxley & Hanson, 1954; Huxley & Niedergerke, 1954). Prior to contraction, actin is coated in tropomyosin and troponin, which regulate cross-bridge formation by blocking the myosin-binding sites on the thin filaments. As the muscle rapidly depolarizes, calcium ions are released into the cell and bind to troponin, which subsequently removes tropomyosin from the thin filaments (Lehman et al., 1994; Brown & Cohen, 2005). With the myosin binding sites now exposed, myosin will cross-bridge with actin and pull on the thin filaments. The pulling forces generated cause the thin filaments to slide past the thick filaments, and as a result, the sarcomere shortens and the muscle contracts (Huxley, 1969). Thus, this highly ordered architecture is essential for skeletal muscle to robustly generate force while maintaining its strength and plasticity.

Due to the syncytial nature and massive size of skeletal muscle, each fully mature myofiber can contain hundreds of nuclei. As previously mentioned, these myonuclei are precisely positioned at the periphery of the cell, located between the sarcomeres and the plasma membrane, and are equally spaced out along the length of the myofiber (Bruusgaard et al., 2003; Lei et al., 2009). Although the function of this patterning remains unknown, the peripheral positioning of myonuclei is a hallmark characteristic of skeletal muscle. However, prior to reaching their final position, each nucleus goes through an elaborate set of long-range movements as the muscle develops and matures (Roman & Gomes, 2018). This section will discuss the different types of nuclear movements, and the mechanisms that regulate each step, within the context of muscle development, repair, and disease.

1.2.1 Myonuclear movement during muscle development

Myonuclei begin their journey during fusion, a critical step in myogenesis that establishes the muscle syncytium (Fig. 1.1). Prior to fusion, muscle precursor cells will differentiate to form mononucleated myoblasts that proliferate before exiting the cell cycle and acquire the ability to fuse (Hutcheson et al., 2009; Biressi et al., 2007). These post-mitotic myoblasts will then begin to merge with an immature muscle fiber, called a myotube. Fusion is a multistep process that involves the initial recognition and adhesion of the myoblast to the myotube, subsequent breakdown of the myoblast plasma membrane, exchange of cytoplasmic material, and ultimate fusion of the two cells (Abmayr & Pavlath, 2012; Kim et al., 2015). After a myoblast fuses, it will deposit its nucleus into the growing myotube. This newly incorporated nucleus will then rapidly migrate toward the center of the premature fiber (Kelly & Zacks, 1969; Englander & Rubin, 1987). As more myoblasts fuse into the growing myotube, each newly incorporated nucleus will actively move to the center to join the other nuclei already present.

In cultured mouse muscle (C2C12) cells, nuclear centration has been shown to be microtubule (MT) dependent, driven by the dynein/dynactin complex, and regulated by Cdc42 and the polarity proteins Par3 and Par6 (Cadot et al., 2012). When a new myoblast nucleus is deposited into the myotube, Par6 is recruited to its nuclear envelope and activated by Cdc42 to regulate dynein-dependent MT polarization at the nuclear surface. Microtubules emanating from the migrating nucleus interact with the cluster of nuclei already positioned in the center of the myotube. Forces generated by dynein anchored at the nuclear envelope will pull on MTs emanating from the myotube nuclei to move the newly incorporated nucleus towards the center. Alternatively, dynein at the nuclear

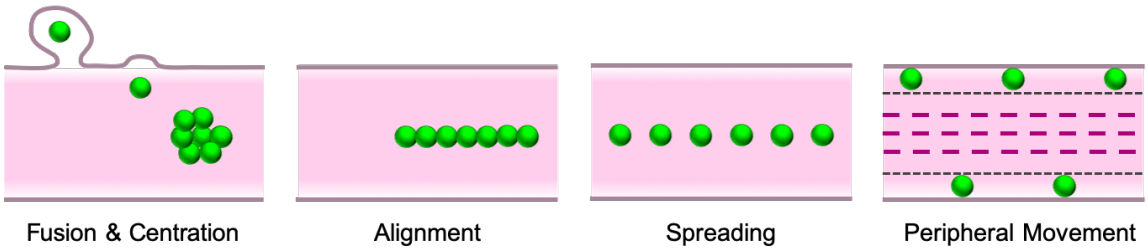

Figure 1.1: Nuclear movement in mammalian skeletal muscle during development. During fusion, newly incorporated myonuclei (green) are moved to the center of the muscle (pink) where they cluster with previously incorporated nuclei. Myonuclei then align within the center of the cell before moving apart and becoming evenly spread to maximize their internuclear distance. Finally, the myonuclei move to the periphery of the muscle which coincides with the formation of a fully-developed sarcomere (purple).

envelope of the myotube nuclei can pull on the MTs of the migrating myoblast nucleus, resulting in its movement from the periphery towards the center of the cell.

Once fusion is complete, the nuclei that are all clustered together begin to move apart from one another. In mammalian myotubes, nuclei first align in a single row along the length of the growing fiber at the onset of differentiation. Nuclear alignment requires the relocalization and anchoring of centrosomal proteins, including PCM-1, pericentrin, and Akap450, to the nuclear envelope by the KASH-domain (Klarsicht, ANC-1, Syne homology) protein, nesprin-1 (Espigat-Georger et al., 2016; Gimpel et al., 2017). At the nuclear surface, these centrosomal proteins recruit kinesin and dynein motors, which are required for MT nucleation and subsequent lateral movement of nuclei along these microtubules.

Following alignment, nuclei spread out from one another to achieve even spacing throughout the length of the myotube. Nuclear spreading coincides with the later stages of muscle differentiation, during which the myotube matures into a myofiber. In addition to anchoring centrosomal proteins to the nuclear envelope, nesprin-1 can also directly recruit kinesin around the nucleus, through an interaction with kinesin light chain (Wilson & Holzbaur, 2015). Although these two functions of nesprin-1 are independent of one

another, the recruitment of centrosomal proteins and kinesin are both required for proper nuclear alignment and spreading. With kinesin, nuclei can be moved through two proposed mechanisms. The first describes kinesin moving nuclei indirectly through the sliding of anti-parallel microtubules that push adjacent nuclei apart (Metzger et al., 2012). Alternatively, kinesin can pull the nucleus as a giant cargo as it processes along the anti-parallel MT network, resulting in their lateral movement (Wilson & Holzbaur, 2012; Wilson & Holzbaur, 2015).

Another type of nuclear movement occurs during nuclear spreading which involves the rotation of nuclei. Similar to spreading, nuclear rotation depends on nesprins recruiting kinesin, as well as dynein, to the nuclear envelope. In this model, the coordinated action of kinesin towards the MT plus (+) end and dynein toward the MT minus (-) end results in the rotation of the nucleus and its net movement (Wilson & Holzbaur, 2012). The direction and speed of rotation depends on the number and distribution of these opposing motors around the nucleus as well as the polarity of the local MT network. Interestingly, it was noted that although nuclei rotate independently from one another, at least one nucleus rotates every time two nuclei cross paths. This type of movement has also been observed in the *C. elegans* hypodermis, in which nuclei display bidirectional movements during migration and rotated to roll past cytoplasmic granules (Fridolfsson & Starr, 2010). Therefore, myonuclei may rotate as a way to avoid obstacles present in the cytoplasm that can block their lateral movement as they spread throughout the myotube.

After spreading, nuclei migrate to the periphery of the myofiber where they will remain anchored to maintain their final position and even distribution. In cultured mammalian muscles, peripheral nuclear movement coincides with the last stages of

myofibril formation. As the full contractile network is established, the nuclei must squeeze through the surrounding sarcomeres to reach the muscle periphery. In contrast to earlier movements, peripheral nuclear migration does not rely on the MT network. Instead, this type of movement is dependent on the actin cytoskeleton and the intermediate filament desmin. Specifically, the actin nucleation protein N-WASP and its target, the Arp2/3 complex, polymerize γ-actin, which then drives the rearrangement of desmin filaments into organized networks at the Z-line of sarcomeres (Falcone et al., 2014; Roman et al., 2017). Once organized, the desmin networks can now crosslink neighboring sarcomeres to one another. When these crosslinked myofibrils contract, the force generated pushes the nuclei out to the periphery of the muscle, where the distance between adjacent nuclei is maximized.

Myonuclear movement during skeletal muscle development is diverse. Although this complex set of movements has been extensively characterized, we are only beginning to uncover the molecular factors and genetic mechanisms driving these different types of movements. However, these genetic mechanisms fail to explain why nuclei associate and dissociate at specific stages of myogenesis. Therefore, it is equally important to understand how nuclei physically interact with each other to coordinate their movement and position within muscle and the impact such nuclear interactions have on the development and function of skeletal muscle.

1.2.2 Myonuclear movement during muscle repair

While myonuclear movement is predominately studied during myogenesis, nuclei are thought to undergo a similar pattern of movement during muscle repair, as centrally

positioned nuclei are a classic morphological feature of damaged muscles (Carlson, 2003; Dubowitz et al., 2007; Yin et al., 2013). Post-development, adult skeletal muscle is stable, with infrequent turnover of myonuclei and sporadic fusion of satellite cells to compensate for muscle turnover caused by daily wear and tear (Schmalbruch & Lewis, 2000). However, in response to injury, skeletal muscle undergoes a highly orchestrated repair process that relies on the dynamic interaction between the injured myofiber and mononucleated satellite cells (Chargé & Rudnicki, 2004; Yin et al., 2013). First, an active satellite cell will fuse with the damaged fiber and deposit its single nucleus at the periphery of the muscle. Rather than maintaining this peripheral position, it is thought that the newly incorporated nucleus moves in towards the center of the myofiber before moving back out to the muscle periphery. (Dubowitz et al., 2007). In cross-sections of regenerating muscle, central nuclei are often observed in discrete portions of the myofiber, suggesting that fusion of satellite cells, and their nuclei, happens focal to the site of injury, rather than diffusely around the muscle (Blaveri et al., 1999). Thus, nuclear movement may contribute to the ability of skeletal muscle fibers to repair themselves after injury. While the significance of myonuclear positioning is still a matter of debate, this specific pattern of movement during both myogenesis and muscle repair illustrates that nuclear positioning, and its maintenance, must be essential.

1.2.3 Mispositioned nuclei in muscle disease

The importance of myonuclear positioning to muscle cell function is further emphasized by diseased muscle (Fig. 1.2). Muscle biopsies taken from patients with various muscle disorders reveal myofibers with an increase in the number of centrally positioned nuclei (>25% compared to <3% in healthy individuals) as well as clusters of

nuclei at the cell periphery (Folker & Baylies, 2013). This pathological feature has been recognized for over 50 years and is used as a key histological marker for diagnosing and differentiating muscle diseases from neurological disorders (Spiro et al., 1966; Dubowitz et al., 2007). Yet despite the prevalence of mispositioned nuclei, the correlation between nuclear positioning and disease pathogenesis remains largely unknown and widely debated. Those arguing that nuclear position is not critical believe that mispositioned nuclei are simply a consequence of muscle dysfunction, as central nuclei are often seen during ongoing muscle repair. Conversely, recent work has indicated that that mispositioned nuclei contribute to progressive muscle weakness (Folker et al., 2012; Metzger et al., 2012; Schulman et al., 2014), and that proper nuclear positioning is essential for the assembly and stability of the sarcomeres (Auld & Folker, 2016). Therefore, it is possible that newly incorporated nuclei move to the center of the muscle fiber during repair to regulate the assembly of damaged myofibrils. This function for myonuclei may also suggests that the correct positioning of nuclei throughout the muscle is critical for maintaining proper muscle function.

1.3 MUSCLE DISEASE & DISORDERS

Muscle disease encompasses a heterogenous group of inherited disorders, generally characterized by irreversible degeneration or incomplete development of the muscle tissue. Although specific muscle diseases are individually rare, the combined prevalence of all inherited muscular dystrophies and myopathies is about 20-25 in 100,000 individuals (Theadom et al., 2014). Each disorder varies in severity, age of onset, pattern of inheritance, and affected muscle groups (Mercuri & Muntoni, 2013). Symptoms can include muscle

weakness and wasting, joint stiffness, contractures, facial weakness, difficulty swallowing, respiratory issues, and in severe cases, cardiac failure. At the cellular level, the main histological features of diseased muscles include hypotonia with rounded myofibers, altered nerve innervation, large cytoplasmic vacuoles, fibrosis, and most notably, mispositioned nuclei within the center of myofibers (Dubowitz et al., 2007). While therapy and medication can help manage some of these symptoms, there is currently no treatment that can stop or reverse the progressive muscle wasting caused by any muscle disease.

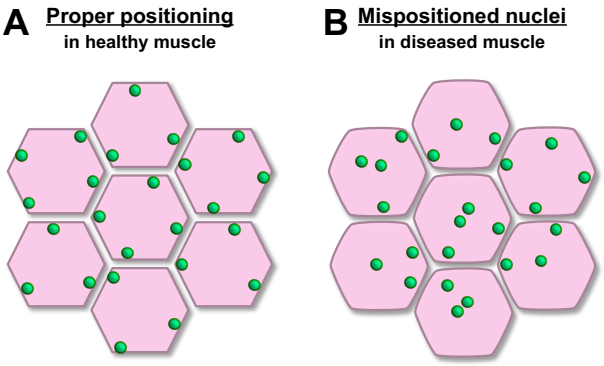

Figure 1.2: Nuclear position in healthy muscle versus diseased muscle. Schematic of a cross section of muscle (pink) from a healthy individual (**A**) versus a cross section of diseased muscle (**B**). In healthy muscle, nuclei (green) are positioned at the periphery of the muscle cell with even spacing to maximize their distance from one another. In patients afflicted with muscle diseases, nuclear positioning is severely aberrant. Nuclei are found within the center of the myofiber along with clustering of nuclei out at the muscle periphery.

In an attempt to understand the underlying pathology, research efforts have mainly focused on identifying the genes associated with muscle diseases. While many of the genes associated with each individual disorder have been identified, the cellular role of each protein is not clear. More directly, it is unknown whether common phenotypes, such as mispositioned nuclei, arise from the disruption of a single pathway or multiple parallel pathways. This lack of understanding regarding the basic genetic mechanisms and cellular processes that govern muscle cell development and organization represents a significant obstacle to potential therapeutic development. Work in this thesis aims to address these questions using two different disease models, Emery-Dreifuss Muscular Dystrophy (EDMD) and Centronuclear myopathy (CNM), to uncover the genetic mechanisms

regulating nuclear movement to understand how nuclear position is impacted in different muscle diseases.

1.3.1 Emery-Dreifuss Muscular Dystrophy & the LINC Complex

Emery-Dreifuss muscular dystrophy (EDMD) is a rare, often slowly progressive muscle disorder primarily affecting voluntary muscle groups. Named after the two physicians to first describe the disorder, EDMD is characterized by three main clinical features: 1) contractures of the joints, tendons, and muscles, 2) muscle degeneration and atrophy, and 3) cardiac abnormalities and congestive heart failure (Emery & Dreifuss, 1966; Emery, 2000; Madej-Pilarczyk, 2018). Though symptoms typically present during adolescence, the age of onset, severity, and progression of EDMD can vary, from early onset with severe presentation in childhood to late onset with slow progression in adulthood (Bonne et al., 2004). Muscle biopsies show mild to moderate myopathic features, with variation in fiber size and mild fibrosis (Mittelbronn et al., 2006; Fidzianska et al., 2010), as well as mispositioned nuclei with altered nuclear morphology and disrupted chromatin organization (Sewry et al., 2001; Favreau et al., 2003). Genetically, EDMD is a heterogenous disorder with X-linked recessive, autosomal dominant, and autosomal recessive forms (Meinke et al., 2011). Although the frequency of EDMD is estimated at 1/100,000 for the X-linked form, only a few rare autosomal cases have been described (Di Barletta et al., 2000). EDMD results from mutations in the genes *EMD* (Bione et al., 1994), *LMNA* (Bonne et al., 1999; Di Barletta et al., 2000), and *SYNE1/2* (Zhang et al., 2007). These genes code for proteins that localize to the nucleus, specifically within the nucleoskeleton or another specialized structure called the Linker of Nucleoskeleton and Cytoskeleton (LINC) complex (Crisp et al., 2006; Tapley & Starr, 2013; Sosa et al., 2013).

The LINC complex is a multi-protein complex that spans both layers of the nuclear envelope and physically links the nucleus and the cytoskeleton (Fig. 1.3). This connection is critical for the mechanical properties of the nucleus in sensing, generating, and transmitting forces across the nuclear membrane (Lombardi & Lammerding, 2011; Navarro et al., 2016). The LINC complex itself is composed of KASH-domain proteins, called Nuclear envelope spectrin-repeat proteins (or Nesprins) in mammals, and the SUN proteins, SUN1 and SUN2. KASH-proteins share a conserved Klarsicht, ANC-1 and Syne Homology (KASH) transmembrane domain that specifically recruits them to the outer nuclear membrane (Zhang et al., 2001). In mammals, four separate *SYNE* genes have been identified which encode different nesprin proteins that interact with specific cytoskeletal elements. The EDMD-associated genes, *SYNE1/2* code for the multi-isomeric and ubiquitously expressed nesprin-1 and -2, respectively. In addition to a KASH-domain, the

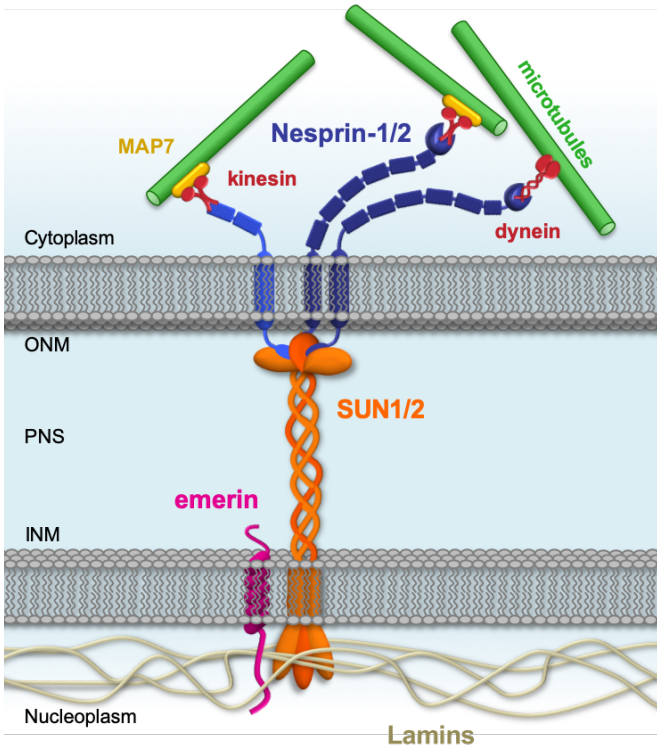

Figure 1.3: The Linker of the Nucleoskeleton and Cytoskeleton (LINC) Complex. The LINC complex physically couples the nucleus to the cytoskeleton. At its core, the LINC complex is comprised of KASH-domain proteins (blue) and SUN-domain proteins (orange). In the inner nuclear membrane (INM), the SUN proteins associate with the nuclear lamina (tan), chromatin, and emerin (magenta). Within the perinuclear space (PNS), the SUN proteins also interact with the KASH-domain proteins, called nesprins-1 and nesprin-2 in mammals. These KASH-domain proteins can extend out from the outer nuclear membrane (ONM) into the cytoplasm where they can interact with various cytoskeletal elements, like microtubules (green) through the motor proteins, kinesin and dynein (red), and other MT-associated proteins, like MAP7 (yellow). Through the LINC complex, the nuclear membrane can sense and respond to changes in the environmental mechanical state. Disruptions to this connection are associated with the muscle disease, Emery-Dreifuss muscular dystrophy.

giant isoforms of nesprin-1 and -2 contain a calponin homology (CH) domain, which binds to actin filaments, as well as a long central rod domain composed of multiple spectrin repeats that supports interactions with other proteins such as emerin and lamins (Zhang et al., 2001; Starr & Fischer, 2005; Rajgor & Shanahan, 2013). Nesprin-1 and -2 can also bind to the microtubule cytoskeleton via kinesin-1 and dynein (Wilson & Holzbaur, 2015; Gimpel et al., 2017). In the perinuclear space, nesprins interact with the SUN proteins, which span the inner nuclear membrane and are defined by their C-terminal Sad1p, UNC-84 (SUN) domain (Malone et al., 1999; Luxton & Starr, 2014). In turn, SUN proteins interact with the nucleoskeleton, specifically with the nuclear lamina (Haque et al., 2006), nuclear pore complex components (Chen et al., 2014), and chromatin (King et al., 2008).

The nuclear lamina is a network of intermediate filaments composed of A-type and B-type lamins, which provides mechanical stability to the nucleus and contributes to many processes within the nucleus including chromatin organization, DNA replication, transcription, and epigenetics (Dechat et al., 2008). Encoded by the *LMNA* gene, A-type lamins (lamin A/C) are composed of a N-terminal head, an α-helical rod domain made of heptad repeats, and a globular C-terminal tail that adopts an immunoglobulin-like fold (Helbling-Leclerc et al., 2002). A-type lamins form dimers through their rod domain and can interact with chromatin (Bruston et al., 2010) as well as other nuclear proteins, such as nesprin-1 (Mislow et al., 2002), nesprin-2 (Yang et al., 2013), and emerin (Sakaki et al., 2001), through binding sites located in the rod domain and C-terminal tail. *LMNA* has also been associated with a wide variety of diseases collectively called laminopathies, including autosomal dominant and recessive forms of EDMD (Worman & Bonne, 2007). Many of the *LMNA* mutations that cause muscle disease affect buried residues at the core of the

immunoglobulin-like fold. Such mutations may destabilize the C-terminus tail, resulting in a loss of structurally functional lamin A/C.

Similar to lamins, emerin has a variety of proposed functions in the nucleus, including the regulation of gene expression, intra- and intercellular signaling, chromatin dynamics, and nuclear structure (Holaska & Wilson, 2007). Embedded in the inner nuclear membrane, emerin is a founding member of the LEM-domain (Lap2β, emerin and MAN1) proteins, through which it binds to a host of transcription factors and regulates the expression of their target genes (Koch & Holaska, 2014). Additionally, emerin was shown to regulate the expression of many muscle- and cardiac-specific genes (Bakay et al., 2006; Melcon et al., 2006; Koch & Holaska, 2012). Approximately 95% of mutations in the emerin gene *EMD* result in complete loss of emerin protein and leads to X-linked EDMD, which makes up nearly 40% of all EDMD cases (Bonne et al., 2003).

Although ubiquitously expressed, disruptions in nesprin-emerin-lamin interactions might play a muscle-specific role in the pathogenesis of EDMD. To support this notion, two separate hypotheses have been proposed to explain the underlying disease mechanism. The first, dubbed the "gene regulation" hypothesis, proposes that because the lamina plays a role in chromatin organization, mutations in LINC complex components could disrupt the interactions between the nuclear lamina and chromatin. Such disruptions could alter the expression of transcription factors in a tissue-specific manner or change the expression pattern of tissue-specific genes (Frock et al., 2006; Dialynas et al., 2010).

Recent evidence strongly supports a second hypothesis based on the structural function of the LINC complex and its ability to couple the nucleoskeleton with the cytoskeleton. According to the "structural" hypothesis, EDMD and other muscle-

associated laminopathies arise when the integrity of the nuclear envelope and lamina are compromised and can no longer protect the nucleus from mechanical stress. (Isermann & Lammerding, 2013; Meinke et al., 2014). Since skeletal muscle is under constant physical stress from contractile forces, weakening of these structural networks can alter the balance of forces transduced onto the nucleus and render the muscle cell susceptible to mechanical damage (Zhang et al., 2007; Banerjee et al., 2014; Bertrand et al., 2014). Furthermore, the LINC complex and associated proteins all play a critical role in proper nuclear positioning and movement within muscle (Lei et al., 2009; Mattioli et al., 2011; Elhanany-Tamir et al., 2012), as defects in this process are implicated in impaired muscle function.

1.3.2 Centronuclear Myopathy & the "MAD" pathway

Centronuclear myopathy describes a rare early-onset muscle disease characterized by the abundance of nuclei localized in the center of myofibers (Jungbluth et al., 2008; Jungbluth et al., 2018). Like other congenital myopathies, clinical features of CNM are usually detected at birth or may develop during early childhood and can vary in severity, from mild to life-threatening. Symptoms include contractures at birth, skeletal and facial abnormalities, reduced fetal movements, developmental delays in motor skills, as well as hypotonia and progressive muscle weakness (Jungbluth & Gautel, 2014; Gonorazky et al., 2018). Several forms of CNM have been described, with the majority of cases attributed to mutations in the genes *MTM1* (Laporte et al., 1996), *BIN1* (Nicot et al., 2007), and *DNM2* (Bitoun et al., 2005). All these genes code for proteins that participate in various aspects of membrane trafficking and remodeling, which are essential for the morphological development and physiological maintenance of skeletal muscle (Fig. 1.4). Mutations in a few additional genes have also been reported to lead to CNM phenotypes, to a lesser

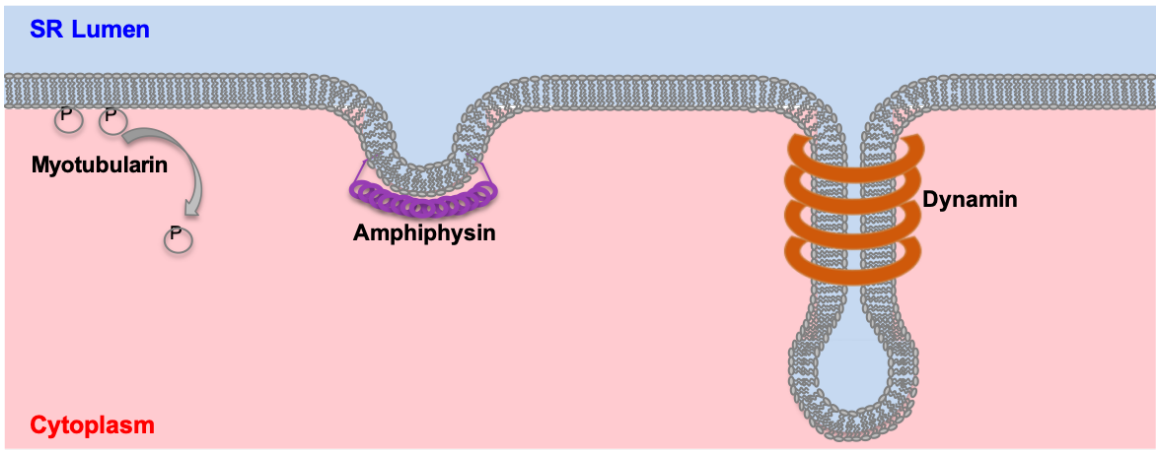

Figure 1.4: The myotubularin, amphiphysin, and dynamin "MAD" pathway. Myotubularin, amphiphysin-2, and dynamin-2 are all intricately involved in various aspects of membrane formation, shaping, and remodeling. Such processes are critical for the trafficking of organelles, like endosomes, lysosomes, and mitochondria, as well as the formation of muscle-specific membrane structures like the sarcoplasmic reticulum and transverse-tubules (T-tubules) invaginations. Centronuclear myopathy is linked to mutations affecting lipid phosphatase activity of myotubularin (*MTM1*) and alters membrane remodeling activity of amphiphysin (*BIN1*) and dynamin (*DNM2*). Thus, CNM has been traditionally classified as a disease of the T-tubule network.

degree: the skeletal muscle ryanodine receptor *RYR1* (Jungbluth et al., 2007), the muscle-specific protein kinase *SRPK3* (Nakagawa et al., 2005), a phosphoinositide phosphatase *JUMPY* (Tosch et al., 2006), and *TTN* which codes for the massive sarcomeric protein, titin (Ceyhan-Birsoy et al., 2013).

Mutations in *MTM1* are associated with the most severe subtype of CNM called myotubular myopathy, also referred to as X-linked CNM or X-linked MTM (Laporte et al., 1996; McEntagart et al., 2002; Hnia et al., 2012). *MTM1* encodes myotubularin, a lipid phosphatase that binds to specific phosphoinositides, through its lipid binding PH-GRAM domain (Tsujita et al., 2004; Choudhury et al., 2006). Myotubularin also regulates lipid activity via its catalytic PTP domain, which dephosphorylates phosphoinositides and promotes their turnover (Blondeau et al., 2000; Taylor et al., 2000). Thus, myotubularin is involved in the formation and trafficking of certain organelles, like endosomes, lysosomes, and mitochondria (Hnia et al., 2011), as well as muscle-specific membrane structures like

the sarcoplasmic reticulum and transverse-tubules (T-tubules) invaginations (Laporte et al., 2001; Amoasii et al., 2013).

Autosomal forms of CNM may arise due to mutations in *BIN1*, which encodes bridging integrator-1, also known as amphiphysin-2, (Nicot et al., 2007; Böhm et al., 2014). Similar to myotubularin, amphiphysin-2 is involved in membrane remodeling pathways, such as endocytosis, trafficking, apoptosis, and formation of the T-tubule network (Prokic et al., 2014). The most distinctive feature of *BIN1* is its specialized BAR domain that contains an additional amphipathic helix at the N-terminus (Peter et al., 2004; Frost et al., 2009). Through this N-BAR domain, amphiphysin-2 senses and preferentially binds to curved membrane structures, where it induces further curvature and subsequent tubulation of the membrane (McMahon & Gallop, 2005). At its C-terminus, *BIN1* contains a Src homology (SH3) domain that is thought to bind to the proline-rich regions of dynamin 2 and N-WASP (Yu et al., 1994; Owen et al., 1998). Although *BIN1* is ubiquitously expressed, the muscle-specific isoform contains an additional phosphoinositide-binding motif that preferentially binds to specific lipids and may potentially target amphiphysin-2 to the T-tubule network (Butler et al., 1997; Nicot et al., 2007). Additionally, this PI motif can inhibit the SH3 domain from binding to its targets, like dynamin (Kojima et al., 2004), providing a possible mechanism *BIN1* regulation specifically in muscle.

DNM2 codes for dynamin-2, a large GTPase that assembles into helical arrays and acts as a mechanochemical scaffold to constrict and deform biological membranes (Shpetner & Vallee, 1989). Dynamin-2 possesses a catalytic GTPase domain that hydrolyzes GTP, as well as a GTPase effector domain (GED), believed to self-regulate its activity (McNiven, 2005). Dynamin-2 is also capable of self-assembly, mediated by a

middle domain (MD) that coordinates intermolecular interactions (Hinshaw & Schmid, 1995; Ramachandran et al., 2007). Through its lipid-binding pleckstrin homology (PH) domain, dynamin-2 is targeted to membrane surfaces. Once bound, dynamin-2 participates in a multitude of membrane-based processes including the formation, trafficking, and recycling of secretory vesicles for endocytosis (Jones et al., 1998; Gold et al., 1999; van Dam & Stoorvogel, 2002; González-Jamett et al., 2013), tubulation of the T-tubule network (Praefcke & McMahon, 2004), and apoptosis (Soulet et al., 2006). Additionally, the proline-rich domain (PRD) facilitates interactions with a variety of SH3-domain proteins and suggests additional roles for dynamin-2 in regulating other cellular processes, such as centrosome cohesion (Thompson et al., 2004) and fusion events like those observed during myogenesis (Leikina et al., 2013). Mutations in *DNM2* are associated with the autosomal dominant form of CNM (Bitoun et al., 2005; Durieux et al., 2010; Böhm et al., 2012), with the majority of mutations found within the MD, PH, and GED domains, thus affecting dynamin-2 self-assembly, membrane localization, and GTPase activity, respectively.

Together, myotubularin, amphiphysin-2, and dynamin-2 are commonly referred to as the "MAD" pathway (Jungbluth et al., 2009). Furthermore, since these proteins are intricately involved in various aspects of membrane formation, shaping, and remodeling, CNM has traditionally classified as a disease of the T-tubule network (Dowling et al., 2009; Al-Qusairi et al., 2009; Toussaint et al., 2011; Fugier et al., 2011; Durieux et al., 2010; Chin et al., 2015). Studies using various animal models deficient of the CNM-linked genes reproduce the phenotypic abnormalities in muscle morphology, as observed in human patients, including disrupted T-tubule structure, triad assembly, sarcomere architecture, and calcium signaling. However, the most common and prominent pathological phenotype

of CNM is aberrantly positioned nuclei. Furthermore, recent work has directly demonstrated that nuclear positioning in muscle is an early event in myogenesis that precedes myofibril assembly (Auld & Folker, 2016), and therefore occurs prior to the formation of a fully developed T-tubule network (Flucher et al., 1993). Yet the genetic mechanisms of how these proteins regulate the dynamic process of nuclear positioning remain largely unknown.

1.4 MODEL ORGANISM TO STUDY MYONUCLEAR MOVEMENT: *DROSOPHILA MELANOGASTER*

Our lack of understanding regarding the mechanisms that drive myonuclear movements largely stems from the fact that it is difficult to investigate the function of the nucleus, and the position of the nucleus, during muscle development. There are several systems available for studying myonuclear positioning and muscle cell development. Mouse models are routinely used as the model organism of choice for studying mammalian muscle function and disease (Zhang et al., 2007; Iyer et al., 2017). While modern technology has made it possible to investigate the subcellular structure of mammalian muscle (Oddoux et al., 2013), the temporal resolution of this *in vivo* system is severely limited. Since mouse embryonic development occurs *in utero*, it is not possible to examine long-range nuclear movements that occur over the course of myogenesis, in real developmental time.

Instead, mammalian cell culture systems have been primarily used to investigate myonuclear movement, as they are optically clear and amenable to high-resolution time-lapse microscopy. *In vitro* studies using C2C12 myoblasts have shed light on some of the

mechanisms that govern myonuclear positioning (Wilson & Holzbaur, 2012; Cadot et al., 2012; Falcone et al., 2014; Wilson & Holzbaur, 2015; Gache et al., 2017). While nuclei in these cultured cells are dynamic, there is one key difference their behavior and movement. Culture myotubes are inherently artificial as they lack the necessary spatial cues and surrounding cellular attachments that play an integral role in muscle organization. Hence a major drawback to such *in vitro* systems is that they do not recapitulate the constraints of development in an organism, nor can they be used to evaluate muscle function.

In recent years the fruit fly, *Drosophila melanogaster*, has emerged as a powerful model system to study the process of myonuclear movement. Compared to other model organisms, there are many technical advantages of using *Drosophila*. Unlike mammals, *Drosophila* have a short reproductive cycle and can produce a large number of externally laid eggs daily. Additionally, *Drosophila* develop quickly, with embryonic development completed within 24 hours and fully mature larvae within a few days. *Drosophila* embryos are also transparent and can be easily prepared for time-lapse imaging (Richardson et al., 2007; Kim et al., 2015; Auld et al., 2018). Thus, the dynamics of nuclear movement during myogenesis can be observed *in vivo* as the embryos develops.

1.4.1 Conserved features of skeletal muscle between *Drosophila* and mammals

Most importantly, many of the basic developmental principles and cellular hallmarks that define skeletal muscle are highly conserved between the mammals and *Drosophila* (Taylor, 2006; Piccirillo et al., 2014). Similar to mammalian skeletal muscle, the somatic musculature of the *Drosophila* embryo is derived from the mesoderm germ layer. *Drosophila* muscles are also formed from the iterative fusion of mononucleated myoblasts into a growing myotube (Chen et al., 2003). Post-fusion, the general

mechanisms of muscle development, patterning, and differentiation are also conserved between the two systems (Schulman et al., 2015). As a result, many of the key structural features of skeletal muscle are remarkably similar. *Drosophila* muscles contain the same contractile unit, the sarcomere, composed of tandem arrays of thin actin filaments and thick myosin filaments. *Drosophila* muscles also contain multiple myonuclei within a shared cytoplasm that move throughout myogenesis.

Yet a major difference between the two systems is how the muscle architecture is organized. In *Drosophila*, the myofibers are fully functional muscles without the complex bundling arrangement as seen in mammals. This simplified features makes *Drosophila* muscles much more amenable to high spatial and temporal imaging than their mammalian counterparts. An additional strength of the *Drosophila* system is that embryonic and larval muscles do not undergo muscle repair (Piccirillo et al., 2014). Therefore, mispositioned nuclei represent a bona fide phenotype and not a sign of ongoing muscle repair. Taken together, these features make *Drosophila* an ideal system to dynamically image the precise position of myonuclei as the muscle develops.

1.4.2 Myonuclear movement in *Drosophila* embryos

During embryonic development, myonuclei undergo a complex set of well-characterized movements in the lateral transverse (LT) muscles (Fig. 1.5), which are analogous to nuclear movements observed in mammalian muscle (Folker et al., 2012; Metzger et al., 2012). During fusion, myonuclei in the LT muscles begin clustered together within the center of the muscle. Once fusion is completed at stage 15 (10:20 – 11:20 h after egg laying, AEL), the single cluster of myonuclei begin to separate into two distinct groups. Each group of nuclei will migrate directionally to opposite muscle poles, with one moving

toward the ventral end of the LT muscle and the other toward the dorsal end. At stage 16 (11:20 – 16 h AEL), each group of nuclei reaches their respective position within the end of the muscle. However, nuclear positioning is not completed until these nuclei move back towards the center and evenly distribute themselves along the length the myofiber (16 – 20 h AEL) (Folker et al., 2012; Metzger et al., 2012; Folker et al., 2014).

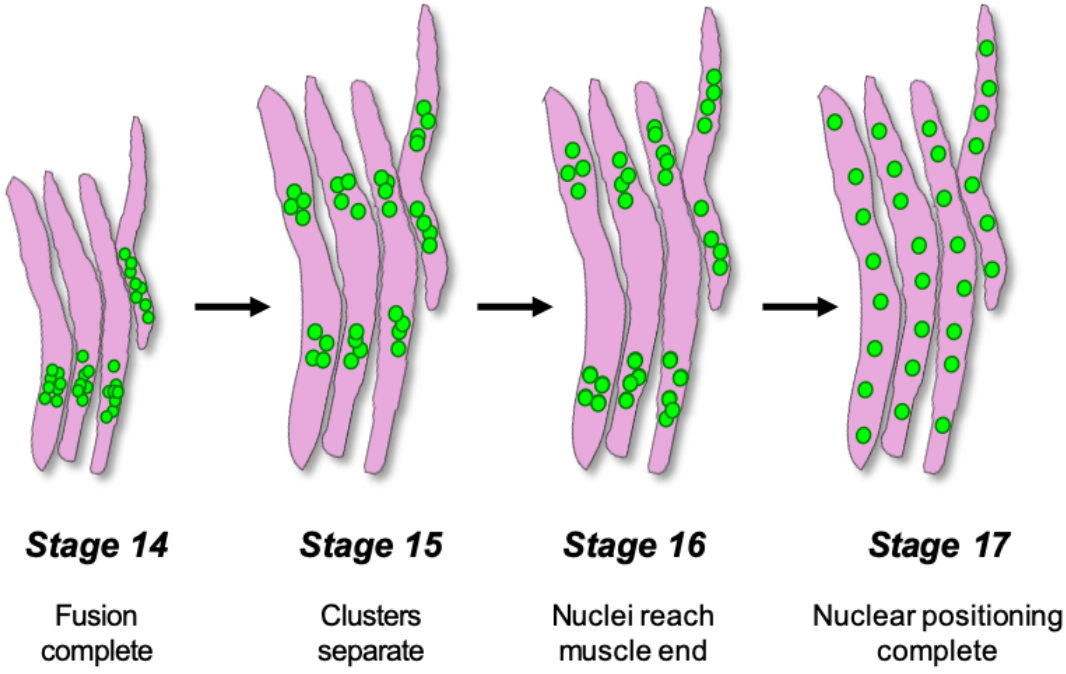

Figure 1.5: Myonuclear movement in *Drosophila* skeletal muscle during embryonic development. Schematic showing the dynamic process of myonuclear movement in the lateral transverse muscles (purple) of a *Drosophila* embryo. At stage 14, nuclei (green) in the LT muscles begin clustered together. Once fusion is completed, nuclei begin to separate into two distinct groups that migrate directionally as tightly associated clusters towards opposite muscle poles. At stage 16, each group of nuclei reaches their respective position within the end of the muscle. Nuclear positioning is completed when these nuclei dissociate from their cluster and move back towards the center, spacing themselves out along the length of the myofiber.

Drosophila combines genetic manipulability, *in vivo* muscle function assays, and optical tractability making it an ideal model organism to investigate the mechanisms driving myonuclear movement. Although some of the specific movements differ slightly between *Drosophila* and mammalian muscle, many of the same nuclear and cytoskeletal elements are responsible for moving and positioning myonuclei in both systems. Recent

work using *Drosophila* has identified conserved roles for the LINC complex in myonuclear movement during the embryonic and larval stages of muscle development (Elhanany-Tamir et al., 2012; Folker et al., 2012; Metzger et al., 2012; Folker et al., 2014). Furthermore, the LINC complex is critical for the interaction between the nucleus and the sarcomere and contributes to the assembly and stability of the myofibril network (Auld & Folker, 2016). All of these conclusions relied on high-resolution and time-lapse imaging of muscles at distinct stages of myogenesis. Thus, by using *Drosophila* muscle as a model system, it is possible to identify novel genetic pathways and molecular mechanisms of myonuclear positioning as well as test for physiological impact within a single system.

1.5 REMAINING QUESTIONS

Work over the last several decades has started to uncover the mechanisms that regulate nuclear movement. However, most of what we know about nuclear positioning has been derived from studies using mononucleated cells. The limited mechanistic understanding is in part driven by the complexity that many nuclei in a single cytoplasm creates. Hence, little is known about the mechanisms used by syncytial cells, like skeletal muscle, to coordinate the movement and position of their multiple nuclei. Do muscles use the same regulatory mechanisms and molecular factors to move their multiple nuclei as mononucleated cells? Another intriguing aspect related to myonuclear movement is the correlation between mispositioned nuclei and muscle disease. Despite being the most prominent phenotype, we still do not know whether mispositioned nuclei arise from the disruption of a single pathway or multiple parallel pathways. Furthermore, do the genes that are associated with different muscle diseases play an active role in regulating nuclear

movement, and if so, how? This question is of particular interest with respect to genes that code for proteins that do not directly localize to the nucleus. Lastly, although the complex pattern of movements has been extensively characterized, there are many aspects of myonuclear movement that remain unexplored. What drives nuclei to associate together and then separate from one another during specific points in muscle development? How are such physical interactions between nuclei regulated? Given the mechanical environment of muscle cells, how do physical forces, generated by the nuclei and the cell alike, influence these physical interactions?

This work aims to elaborate upon our current understanding of how nuclei move and interact with one another to coordinate their position during muscle development. To address these questions, we applied a combination of genetic and biophysical approaches with a variety of microscopy techniques, ranging from standard confocal imaging to super-resolution and nonlinear optical methods. In the first two chapters, we explore such pathways within a disease context through the correlation between mispositioned nuclear and muscle disease. First, we investigate how genes linked to EDMD and CNM regulate nuclear movement through distinct disease-specific mechanisms (Chapter 2). Secondly, we expanded upon the hypothesis that CNM-linked genes disrupt the association interactions between nuclei through interactions with the cytoskeleton (Chapter 3). Finally, this thesis concludes with new insights into the physical interactions that exist between nuclei as they migrate (Chapter 4).

CHAPTER 2

NUCLEAR POSITIONING IS DISRUPTED BY DISTINCT MECHANISMS IN EMERY-DREIFUSS MUSCULAR DYSTROPHY AND CENTRONUCLEAR MYOPATHY

The content in this chapter was adapted from the following publication:

Collins, M.A., Mandigo, T.R., Camuglia, J.M., Vazquez, G.A., Anderson, A.J., Hudson, C.H., Hanron, J.L., and Folker, E.S. (2017) Emery–Dreifuss muscular dystrophy–linked genes and Centronuclear myopathy–linked genes regulate myonuclear movement by distinct mechanisms. *Molecular Biology of the Cell*. **28**:2303–2317.

2.1 ABSTRACT

Muscle cells are a syncytium in which the many nuclei are positioned to maximize the distance between adjacent nuclei. Although mispositioned nuclei are correlated with many muscle disorders, it is not known whether this common phenotype is the result of a common genetic mechanism. To answer this question, we disrupted the expression of genes linked to Emery–Dreifuss muscular dystrophy (EDMD) and Centronuclear myopathy (CNM) in *Drosophila* and evaluated the position of the nuclei. We found that the genes linked to EDMD and CNM were each necessary to properly position nuclei. However, the specific phenotypes were different. EDMD-linked genes were necessary for the initial separation of nuclei into distinct clusters, suggesting that these factors relieve interactions between nuclei. CNM-linked genes were necessary to maintain the nuclei within clusters as they moved toward the muscle ends, suggesting that these factors were necessary to maintain interactions between nuclei. Together these data suggest that nuclear position is disrupted by distinct genetic mechanisms in EDMD and CNM.

2.2 INTRODUCTION

Based on their abundance and their repetitive structure, myofibers – the cellular units of skeletal muscle – have long been a model system to identify cell-biological mechanisms that underlie development. Many features of myofiber structure, however, such as their syncytial nature, are specialized for muscle cells. During the development of an individual muscle cell, many mononucleated myoblasts fuse to form a syncytial myofiber that can contain up to thousands of nuclei (Kim et al., 2015), each of which is

precisely positioned. Most nuclei are distributed evenly throughout the muscle, with a small cluster of nuclei associated with the neuromuscular junction (Bruusgaard et al., 2003; Bruusgaard et al., 2006). Disruptions in the distribution of nuclei have been correlated with muscle disease for several decades (Dubowitz et al., 2007). As previously mentioned, two muscle diseases in which mispositioned nuclei are abundant are EDMD (Sewry et al., 2001) and CNM (Spiro et al., 1966). It is not clear, however, whether the position of the nuclei is a consequence of ongoing muscle repair or mispositioned nuclei contribute to muscle weakness and muscle deterioration. More fundamentally, it is not known whether mispositioned nuclei in disparate muscle diseases arise from common or distinct mechanisms.

To determine whether mispositioned nuclei are the result of a common cellular disruption or are due to disease-specific cellular defects, we evaluated the position of nuclei in *Drosophila* that had disruptions in genes linked to EDMD or CNM. Each of the genes mutated in patients with EDMD encodes for a protein that is localized to the nucleoskeleton or the nuclear envelope (Meinke et al., 2011). Based on this localization, the function of some EDMD-linked genes with respect to nuclear position has been tested in muscle (Zhang et al., 2009a; Dialynas et al., 2010; Elhanany-Tamir et al., 2012), cultures of myoblast-derived cells (Cadot et al., 2012; Wilson & Holzbaur, 2015), and other cell types (Gundersen & Worman, 2013).

In mammals, *SYNE1* and *SYNE2* are necessary for the clustering of nuclei at the postsynaptic side of the neuromuscular junction (Zhang et al., 2007; Zhang et al., 2009a). Furthermore, nesprin proteins and SUN proteins regulate the distribution of nuclei throughout the muscle in *Drosophila* embryos and larvae (Elhanany-Tamir et al., 2012)

and in mammalian cell culture systems (Wilson & Holzbaur, 2015). In addition, emerin is essential for nuclear movement during cell migration (Chang et al., 2013). However, these experiments were all completed in different systems, making it difficult to compare the functions of each factor with respect to nuclear movement during muscle development *in vivo*.

Despite the name Centronuclear myopathy, there has been little investigation of the causes or consequences of mispositioned nuclei with respect to CNM. The genes mutated in patients with CNM encode for proteins that regulate the development and structure of the T-tubule in skeletal muscle or the release of calcium in skeletal muscle (Jungbluth et al., 2007). Therefore, it is believed that defects in Ca^{2+} signaling and T-tubule structure underlie CNM. However, we recently demonstrated that the movement of nuclei in muscle is an early event in muscle development that precedes myofibril assembly (Auld & Folker, 2016) and therefore precedes a fully developed T-tubule network (Flucher et al., 1993).

Furthermore, it was recently demonstrated that the proteins linked to CNM have additional cellular functions. Specifically, amphiphysin-dependent activation of N-WASP was demonstrated to be a prerequisite for triad formation (the junction between the T-tubules and the sarcoplasmic reticulum) and was necessary for proper movement of nuclei to the periphery of a cultured myofiber system (Falcone et al., 2014). In addition, amphiphysin contributed to the attachment between the nucleus and the cytoskeleton and nuclear movement in culture (D'Alessandro et al., 2015). The latter function suggests that nuclear position may be regulated by the concerted actions of amphiphysin (and perhaps other CNM-linked genes) and the proteins linked to EDMD that localize to the nucleus.

We compared the effects of genes linked to CNM and EDMD during muscle development in *Drosophila* embryos. This system combines a short developmental timeline with optical clarity and rich genetic resources, which made it possible to measure the precise distribution of nuclei during muscle development. Consistent with previous reports (Elhanany-Tamir et al., 2012), the LINC complex, which has been linked to EDMD, contributed to embryonic myonuclear positioning. In addition, the CNM-linked genes *Amphiphysin* (*Amph*) and *myotubularin* (*mtm*) are also necessary for positioning myonuclei in the embryo. However, the effects of the CNM-linked genes were milder and are mechanistically distinct. CNM-linked genes and EDMD- linked genes exhibit different genetic interactions with the microtubule motors dynein and kinesin. Furthermore, live-embryo time-lapse microscopy of myonuclear movement was used to demonstrate that the loss of *Amphiphysin* caused reduced interactions between nuclei, whereas the loss of *bocksbeutel* (*Drosophila* emerin) caused enhanced interactions between nuclei. Thus, nuclear position is likely disrupted by distinct genetic mechanisms in different muscle disorders.

2.3 RESULTS

2.3.1 Muscle-specific depletion of EDMD- and CNM-linked genes disrupt myonuclear position in the *Drosophila* embryo

During embryonic muscle development in *Drosophila*, the nuclei undergo a complex set of movements, which involve 1) the separation of nuclei into two distinct clusters, 2) the directed movement of these clusters toward their respective ends of the

muscle, and 3) the dispersion of nuclei throughout the myofiber. To determine whether genes that have been linked to EDMD and CNM contribute to active nuclear positioning in *Drosophila*, we investigated the function of *Otefin* (*Drosophila* emerin), *bocksbeutel* (*Drosophila* emerin), *klaroid* (*Drosophila* SUN), *klarsicht* (*Drosophila* nesprin), Amphiphysin, and myotubularin during embryonic development. Each gene was specifically depleted from the muscle using the GAL4/UAS system. UAS-RNA interference (RNAi) expression, using RNAi lines that were validated by reverse transcriptase PCR (RT-PCR) (Table 2.1), was driven from embryonic stage 12 through larval development under the control of *DMef2-GAL4*.

Genes	Control	RNAi
Ote	1.00	0.25
bocks	1.00	0.35
koi	1.00	0.20
klar	1.00	0.40
mtm	1.00	0.62
Amph	1.00	0.30

Table 2.1: Relative expression of EDMD- and CNM-linked genes when knockdown by UAS-RNAi.

We measured the position of nuclei in the lateral transverse (LT) muscles of stage 16 (16 h after egg lay [AEL]) embryos, as previously described (Folker et al., 2012). In control embryos, the nuclei in each LT muscle were positioned in two separate clusters, with one near the dorsal end of the muscle and the other near the ventral end of the muscle (Fig. 2.1 A). *DMef2-GAL4*-mediated depletion of *Ote*, *bocks*, or *koi* caused an increase in the distance between the dorsal end of the muscle and the nearest nucleus in each genotype (Fig. 2.1 A-C). Across the entire population, depletion of *klar* did not affect the average position of nuclei. However, 20% of LT muscles in *klar*- and *bocks*-depleted embryos had all of their nuclei positioned near the ventral end of the muscle. In addition, expression of RNAi against *klar* driven by the mesodermal enhancer *twist-GAL4*, which acutely expresses from stage 8 through stage 13, did cause a statistical difference in the position of nuclei in the embryo (Fig. 2.2 A-C). These data indicate that the effects of *klar*, *bocks*, *Ote*,

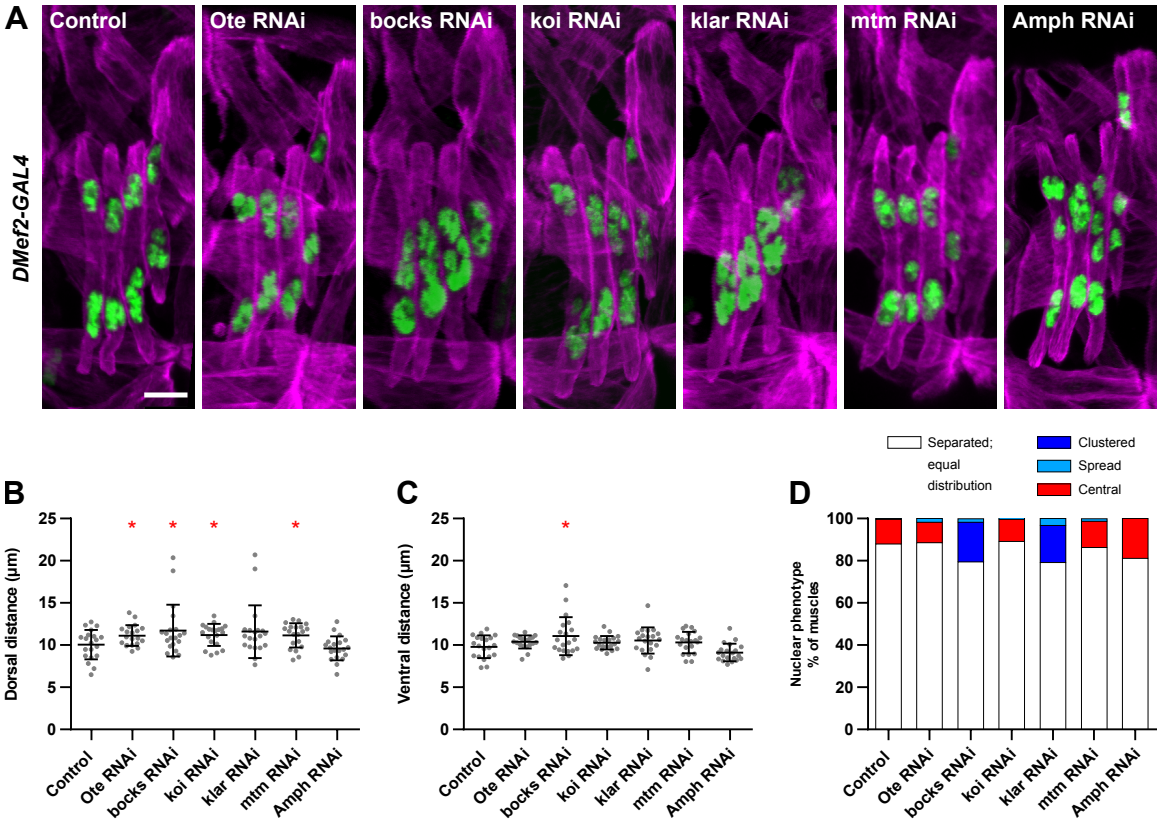

Figure 2.1: Muscle-specific knockdown of EDMD- and CNM-linked genes effects nuclear positioning muscle autonomously in *Drosophila* embryos. (**A**) Immunofluorescence images of the lateral transverse (LT) muscles in one hemisegment from stage 16 (16 hours AEL, after egg lay) embryos that expressed the indicated UAS-RNAi constructs under the control of *DMef2-GAL4*. Muscles in magenta, myonuclei in green. Scale bar, 10 µm. (**B,C**) Graphs indicating the distance between the dorsal end of the muscle and the nearest nucleus (**B**) and between the ventral end of LT muscles and the nearest nucleus (**C**) in embryos that expressed the indicated UAS-RNAi constructs driven with *DMef2-GAL4*. (**D**) The frequency at which each nuclear positioning phenotype was observed in each of the indicated UAS-RNAi constructs was driven with *DMef2-GAL4*. For (B) and (C), each data point indicates the average distance within a single embryo. Error bars indicate SD from 20 embryos. Student's t-test was used for comparison to controls. *P < 0.05.

and *koi* on nuclear position are muscle autonomous and occur during embryonic development. In contrast, *DMef2-GAL4*-driven expression of *mtm* RNAi caused only a mild mispositioning of the nuclei relative to the dorsal end of the muscle (Fig. 2.1 B), and RNAi against *Amph* had no effect on the position of myonuclei (Fig. 2.1 A-C). Together these data suggest that the activities of CNM- and EDMD-linked genes are temporally distinct.

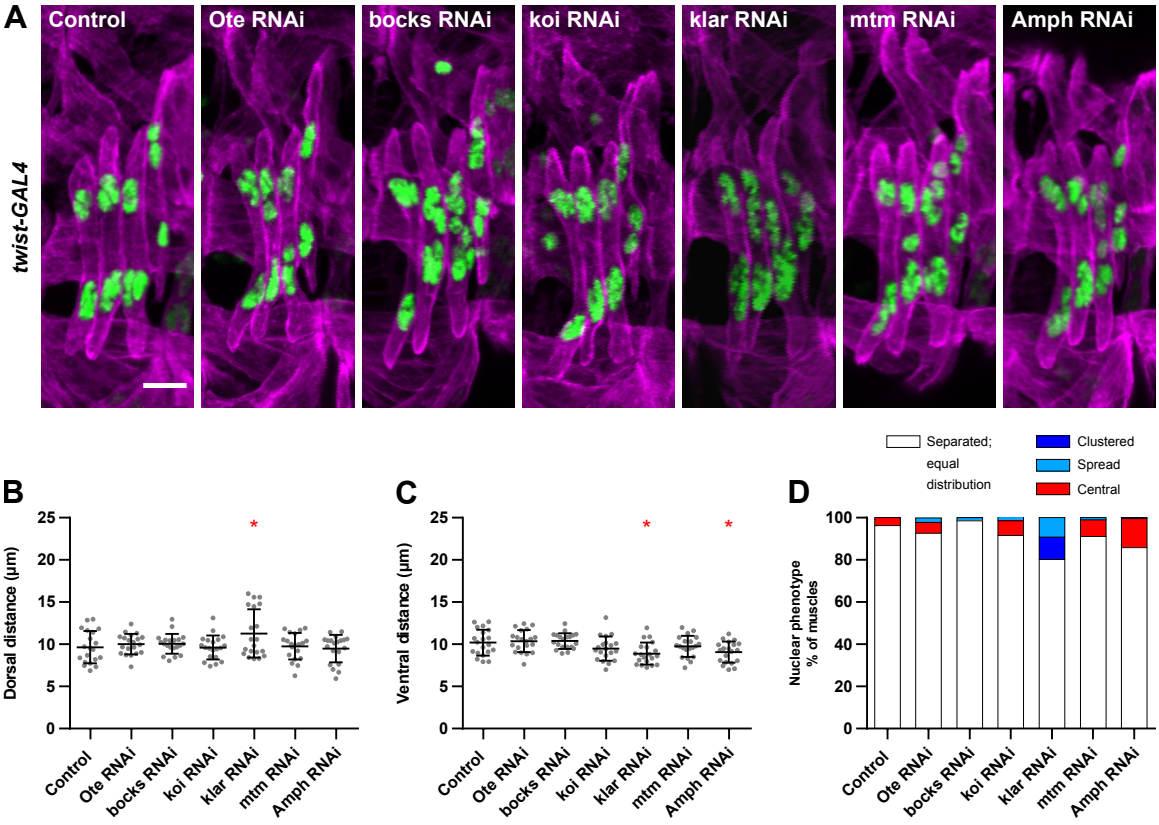

Figure 2.2: Mesoderm-specific knockdown of EDMD- and CNM-linked genes effects nuclear positioning muscle autonomously in *Drosophila* embryos. (**A**) Immunofluorescence images of the LT muscles in one hemisegment from stage 16 (16 hours AEL) embryos that expressed the indicated UAS-RNAi constructs under the control of *twist-GAL4*. Muscles in magenta, myonuclei in green. Scale bar, 10 µm. (**B,C**) Graphs indicating the distance between the dorsal end of the muscle and the nearest nucleus (**B**) and between the ventral end of LT muscles and the nearest nucleus (**C**) in embryos that expressed the indicated UAS-RNAi constructs driven with *twist-GAL4*. (**D**) The frequency at which each nuclear positioning phenotype was observed in each of the indicated UAS-RNAi constructs was driven with *twist-GAL4*. For (B) and (C), each data point indicates the average distance within a single embryo. Error bars indicate SD from 20 embryos. Student's t-test was used for comparison to controls. *P < 0.05.

2.3.2 The EDMD-linked genes, *bocksbeutel* and *klarsicht*, distinctly affect embryonic myonuclear position from the CNM-linked gene *Amphiphysin*

To test whether the variation of phenotypes seen in the RNAi experiments was due to variation in RNAi efficiency, we tested embryos that were homozygous for either the $bocks^{DP01391}$ or the $klar^{1}$ null allele (Welte et al., 1998). In $bocks^{DP01391}$ and $klar^{1}$ embryos, nuclei were clustered near the ventral end of the muscle (Fig. 2.3 A), with nuclei positioned 53 and 43% farther from the dorsal ends of muscles in $bocks^{DP01391}$ and $klar^{1}$ embryos,

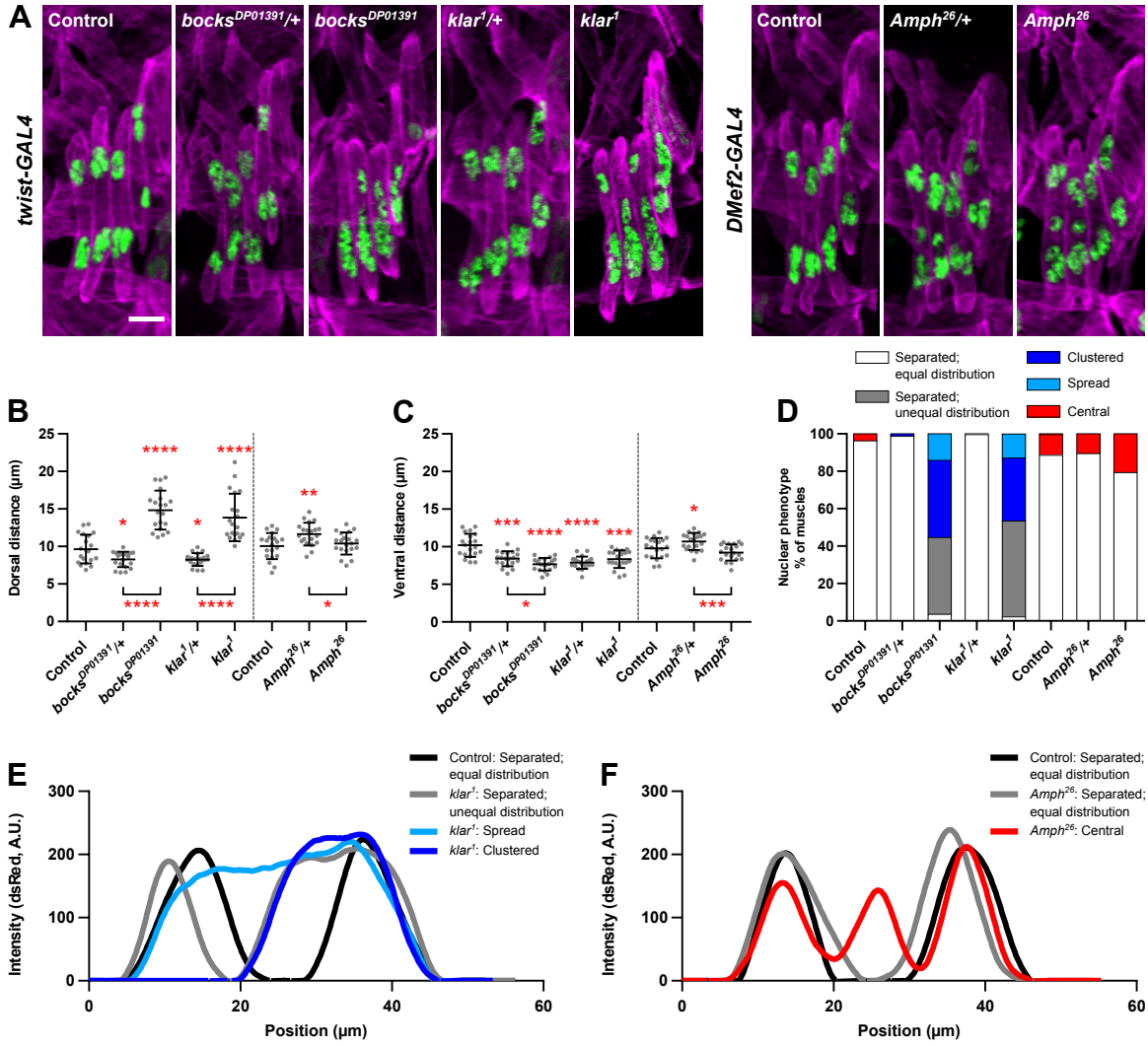

Figure 2.3: *Bocksbeutel*, *klarsicht*, and *Amphiphysin* are necessary for proper myonuclear position in *Drosophila* embryos. (**A**) Immunofluorescence images of the LT muscles in one hemisegment from stage 16 (16 hours AEL) embryos for the indicated genotypes. Muscles in magenta, myonuclei in green. Scale bar, 10 µm. (**B,C**) Graphs indicating the distance between the dorsal end of the muscle and the nearest nucleus (**B**) and between the ventral end of LT muscles and the nearest nucleus (**C**) in embryos for the indicated genotypes. (**D**) The frequency at which each nuclear positioning phenotype was observed in each of the indicated genotypes. (**E,F**) Averaged linescans of DsRed intensity for each nuclear phenotype observed in *klar*^{1} mutants (**E**) and *Amph*^{26} mutants (**F**) compared to controls. Position correlates to the length of the muscle. Dorsal end position corresponds to 0 µm. For (B) and (C), each data point indicates the average distance within a single embryo. Error bars indicate SD from 20 embryos. Student's t-test was used for comparison to controls. *P < 0.05, **P < 0.005, ***P < 0.0005, ****P < 0.00005.

respectively (Fig. 2.3 B). In addition, compared with controls, nuclei were 25 and 18% closer to the ventral muscle ends in *bocks*^{DP01391} and *klar*^{1} embryos, respectively (Fig. 2.3 C). The null allele for Amph, *Amph*^{26} (Zelhof et al., 2001), did not affect the position of nuclei relative to the muscle ends (Fig. 2.3 A-C).

There was an increase, however, in the appearance of individual nuclei near the center of the muscle in *Amph*^{26} embryos. Furthermore, in a small number of *bocks*^{DP01391} and *klar*^{1} embryos, a single nucleus appeared to be positioned near the dorsal end of the muscle. Therefore, we further measured the distribution of nuclei within the muscle. First, we determined the distribution of nuclei by linescan analysis of the apRed (nuclei) signal in the LT muscles in each genotype (Fig. 2.3 E and F). In both *twist-GAL4*, *apRed* and *DMef-GAL4, apRed* control embryos, there were two peaks: one near the dorsal end and one near the ventral end of the muscle (Fig. 2.3 D, E, and F). Analysis of *klar*^{1} embryos revealed three distinct phenotypes (Fig. 2.3 D and E). In *klar*^{1} embryos with a nucleus near the dorsal end of the muscle, there were distinct peaks, but the breadth of the peak near the ventral end was greater than the breadth of peak near the dorsal end, indicating that the ventral cluster is larger. In *klar*^{1} embryos with a single cluster of nuclei, the intensity profile showed a single broad peak near the ventral end of the muscle. Finally, in embryos with a spread phenotype, the nuclei extend from the dorsal portion of the muscle to the ventral portion of the muscle without any discernible gaps, which would appear as troughs in the intensity profiles. Similar data were obtained by analysis of *bocks*^{DP01391} embryos. These data suggest that the distribution of nuclei between the dorsal and ventral clusters is disrupted by the loss of *klarsicht* or *bocksbeutel*.

To support these data, we measured the areas of the clusters of nuclei. The size of the dorsal cluster of nuclei was reduced in *bocks*^{DP01391} and *klar*^{1} embryos compared with controls (Fig. 2.4 A). Conversely, the area of the ventral cluster of nuclei was increased in *bocks*^{DP01391} and *klar*^{1} embryos compared with controls (Fig. 2.4 B). The total area of the muscle filled by the nuclei was equal in *bocks*^{DP01391}, *klar*^{1}, and control embryos (Fig.

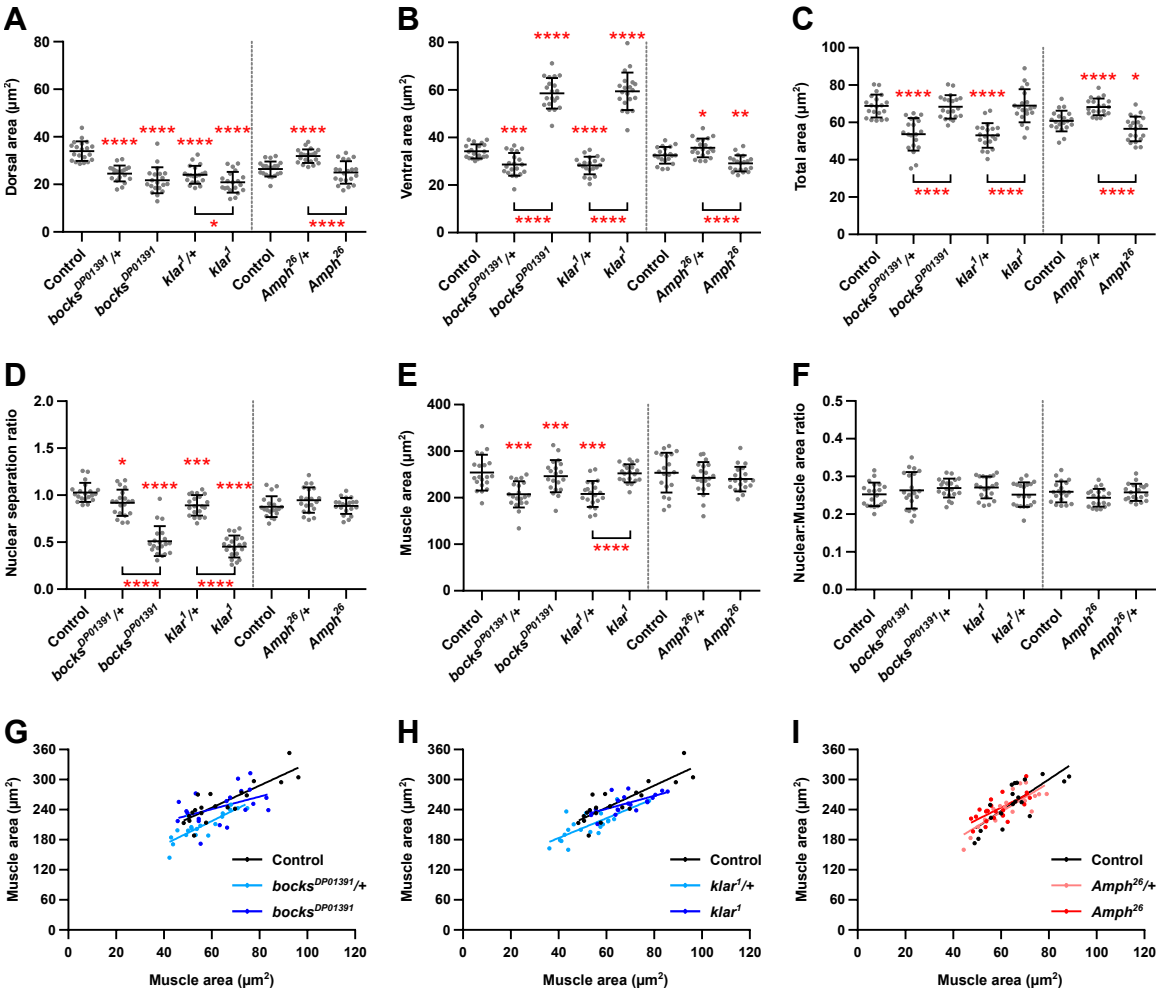

Figure 2.4: *Bocksbeutel* and *klarsicht* are necessary for proper distribution of nuclei into clusters in *Drosophila* embryos. (**A–C**) Graphs indicating the area of nuclei located near the dorsal end of the muscle (**A**), area of nuclei located near the ventral end of the muscle (**B**), and total area of the muscle occupied by nuclei (**C**) for the indicated genotypes. (**D**) The relative distribution of nuclei between the dorsal half of the muscle and the ventral half of the muscle in each of the indicated genotypes. (**E,F**) Graphs indicating the area of muscle (**E**) and the total nuclear area to muscle area ratio for the indicated genotypes (**F**). (**G–I**) Total nuclear area plotted as a function of muscle area for *bocks*^{DP01391} (**G**), *klar*^{1} (**H**), and *Amph*^{26} (**I**) compared to controls and respective heterozygotes. For (A-F) each data point represents the average area within a single embryo. Error bars indicate SD from 20 embryos. Student's t-test was used for comparison to controls. *P < 0.05, **P < 0.005, ***P < 0.0005, ****P < 0.00005.

2.4 C). The total area filled by nuclei, however, was reduced in both *bocks*^{DP01391} and *klar*^{1} heterozygotes compared with controls. The decrease in nuclear areas can be explained as a function of decreased muscle size. To maintain animals with the null mutations of *bocks*^{DP01391} and *klar*^{1}, each allele is carried over the *TM6b* balancer, which also carries the *Tb*^{1} dominant mutation (Lattao et al., 2011), resulting in short, wide muscles (Fig. 2.4 E).

To control for these differences in muscle size across all genotypes, we determined the percentage of total muscle area that was occupied by all nuclei. In all genotypes tested, nuclei comprised ~25% of the total muscle area (Fig. 2.4 F), and the sum of nuclear areas correlated with muscle size in all genotypes (Fig. 2.4 G-I).

Finally, the ratio of the size of the dorsal cluster of nuclei compared with the ventral cluster of nuclei was significantly reduced in $bocks^{DP01391}$ and $klar^{1}$ embryos compared with controls and heterozygotes (Fig. 2.4 D). In controls, the average ratio was ~1, whereas in $bocks^{DP01391}$ and $klar^{1}$ embryos, the cluster of nuclei near the ventral end of the muscle was on average twice as large as the cluster near the dorsal end. In total, these data suggest that *bocksbeutel* and *klarsicht* are required for the separation of nuclei and their distribution into two distinct clusters of equal size that then move to opposed ends of the muscle.

Similar analysis was completed on $Amph^{26}$ embryos. In $Amph^{26}$ embryos, nuclei were properly distributed between the dorsal and ventral ends, with only slight differences compared with controls (Fig. 2.3 D and F). However, in 20% of muscles, there was an additional peak near the center of the cell, indicating that there was a mispositioned nucleus. This central nucleus was on average equidistant from both the dorsal cluster and the ventral cluster of nuclei (Fig. 2.3 F). These data are supported by the measurements of cluster size. The dorsal cluster in $Amph^{26}$ embryos is smaller, but insignificantly so, than with control embryos (Fig. 2.4 A). The ventral cluster in $Amph^{26}$ embryos is smaller than with control embryos (Fig. 2.4 B). The total area occupied by nuclei is also slightly smaller in $Amph^{26}$ embryos than with controls (Fig. 2.4 C). However, the ratio of the size of the dorsal cluster compared with the ventral cluster of nuclei is equal in $Amph^{26}$ embryos and control embryos (Fig. 2.4 D). These data suggest that separation of nuclei into distinct

clusters of equal size is not affected by the loss of *Amphiphysin*. However, the presence of central nuclei suggests that clusters of nuclei are not properly maintained during migration toward the muscle end. Furthermore, that the ratio of the size of the dorsal cluster compared with the ventral cluster is not affected suggests that the nuclei that occupy the center of the muscle originate from dorsal and ventral clusters with equal frequency.

On the basis of these measurements, we counted the frequency of distinct phenotypes (Fig. 2.3 D). In controls, nuclei were properly separated into two distinct, dorsal and ventral groups of equal size in most embryos (96%, *twist-GAL4*, *apRed*; 90%, *DMef-GAL4, apRed*). In $Amph^{26}$ embryos, nuclei were separated into distinct clusters, but centrally mispositioned nuclei were identified in 20% of muscles, compared with <10% of muscles in controls (Fig. 2.3 D). In contrast, central nuclei were not found in either $bocks^{DP01391}$ or $klar^{1}$ embryos. However, nuclei were clustered near the ventral end of 41 and 33% of the muscles in $bocks^{DP01391}$ or $klar^{1}$ embryos, respectively. In addition, in 14% $bocks^{DP01391}$ embryos and in 13% of $klar^{1}$ embryos, nuclei were spread through the center of the myofiber, with no distinct dorsal or ventral clusters (Fig. 2.3 D).

Similar analysis of embryos that had undergone muscle-specific RNAi-mediated depletion produced similar data. Central nuclei were found at an increased frequency in embryos that expressed RNAi under the control of *DMef2-GAL4* or *twist-GAL4* (Fig. 2.1 D and Fig. 2.2 D). In addition, muscle-specific depletion of *bocks* and *klar* caused phenotypes that resembled the nulls. Specifically, in ~20% of embryos, the nuclei were in a single cluster near the ventral end of the muscle rather than in two clusters near either end of the muscle (Fig. 2.1 A-D and Fig. 2.2 A-D).

Together these data suggest that the EDMD-linked genes, *bocksbeutel* and *klarsicht*, and the CNM-linked gene *Amphiphysin* are all necessary for nuclear movement during embryonic muscle development. In addition, the function of each factor with respect to nuclear position is muscle autonomous. However, the specific contributions of the EDMD-liked genes are distinct from the contributions of the CMN-linked gene. Nuclei are in a single cluster when *bocks* or *klar* is disrupted suggests that these factors are necessary to separate nuclei from one another. Conversely, nuclei found in the center of the muscle when *Amph* is disrupted suggests that *Amph* is necessary to maintain the interactions between nuclei.

2.3.3 Dynamic attractive and repulsive interactions between myonuclei are regulated independently by EDMD- and CNM-linked genes

To test these hypotheses directly, we analyzed the movement of myonuclei during embryonic development. In control embryos, dorsal clusters of nuclei and ventral clusters of nuclei moved away from one another at a rate of ~5 μm/h (Fig. 2.5 A-B and Supp. Movie 1) as previously described (Folker et al., 2014). During this movement, nuclei remained within their respective clusters and did not change direction (Fig. 2.5 A and Supp. Movie 1). In $bocks^{DP01391}$ embryos, nuclei remained in a single cluster without splitting into separate clusters (Fig. 2.5 A and Supp. Movie 2). However, on the occasion that a single nucleus did escape from a cluster, it moved directly toward the dorsal end of the muscle at a rate of >6 μm/h (Fig. 2.5 B and Supp. Movie 2). This demonstrated that nuclei are in a single cluster because the cluster cannot be resolved and not because nuclei move back to their starting point. In addition, the fact that the rare nuclei that escape the cluster do move

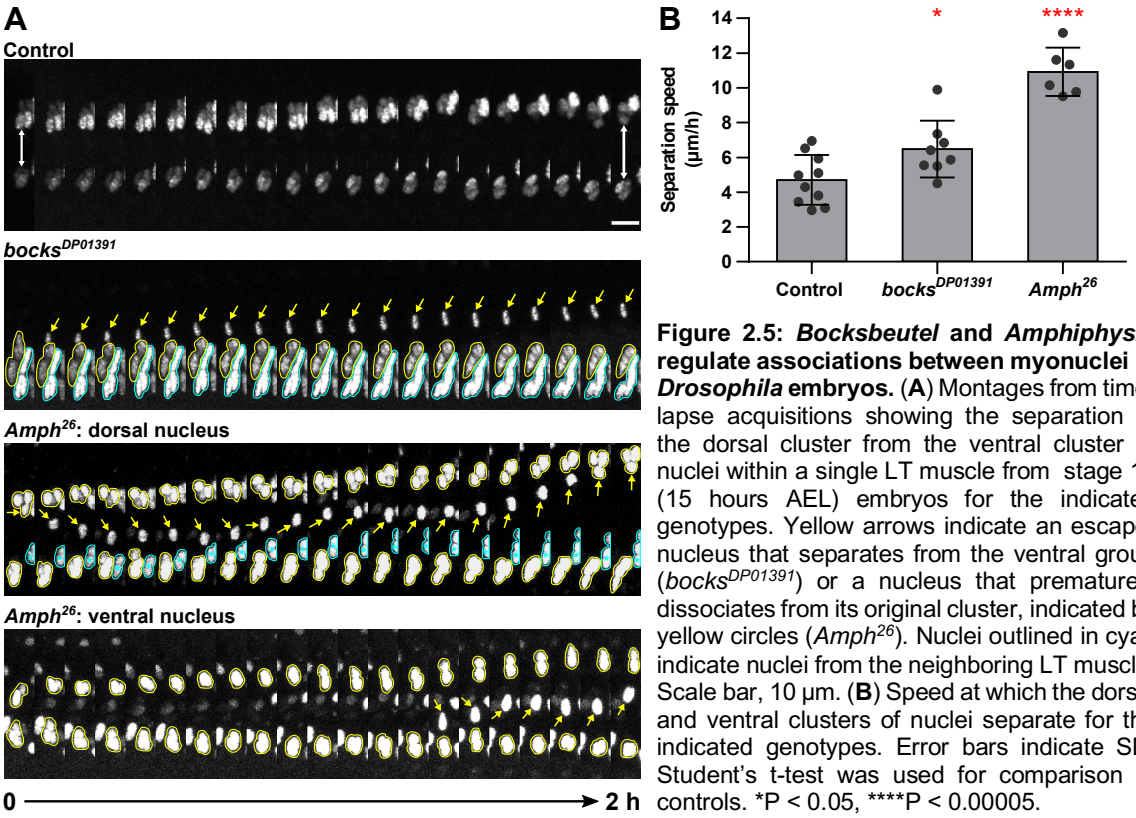

Figure 2.5: *Bocksbeutel* and *Amphiphysin* regulate associations between myonuclei in *Drosophila* embryos. (**A**) Montages from time-lapse acquisitions showing the separation of the dorsal cluster from the ventral cluster of nuclei within a single LT muscle from stage 15 (15 hours AEL) embryos for the indicated genotypes. Yellow arrows indicate an escaper nucleus that separates from the ventral group (*bocks*^{DP01391}) or a nucleus that prematurely dissociates from its original cluster, indicated by yellow circles (*Amph*^{26}). Nuclei outlined in cyan indicate nuclei from the neighboring LT muscle. Scale bar, 10 µm. (**B**) Speed at which the dorsal and ventral clusters of nuclei separate for the indicated genotypes. Error bars indicate SD. Student's t-test was used for comparison to controls. *P < 0.05, ****P < 0.00005.

directionally to a proper position suggests that the machinery and directional cues for myonuclear movement are present.

Nuclear movement in *Amph*^{26} embryos was significantly different. The clusters of nuclei were only loosely associated as they moved toward the muscle end. Nuclei regularly dissociated from a cluster and moved into the middle of the muscle (Fig. 2.5 A and Supp. Movie 3 and 4). Furthermore, nuclei dissociated from both the dorsal and ventral cluster of nuclei and moved either back to their original cluster (Supp. Movie 3) or to the other cluster (Supp. Movie 4) without preference. Finally, the clusters of nuclei moved significantly faster in *Amph*^{26} embryos than with either control or *bocks*^{DP01391} embryos. These data explain the relatively low abundance of centrally positioned nuclei in embryos (Fig. 2.1 D and Fig. 2.3 D). Because the nuclei occupy the center of the muscle transiently before moving to either the dorsal or ventral cluster, central nuclei were found only in a subset of

muscles by fixed-embryo analysis. Together these data suggest that *bocksbeutel* is necessary for the separation of nuclei from one another, and *Amphiphysin* is necessary to maintain the association of nuclei with one another.

2.3.4 *Bocksbeutel* genetically interacts with the microtubule motors, dynein and kinesin, to regulate embryonic myonuclear positioning

To determine whether there are distinct genetic interactions between the EDMD-linked and CNM-linked genes and established pathways known to affect nuclear positioning, we tested genetic interactions between microtubule motors and *bocksbeutel* and *Amphiphysin* with respect to nuclear positioning in embryos. We completed double-heterozygote experiments to evaluate the genetic interactions between $bocks^{DP01391}$ and both $Dhc64C^{4-19}$ and Khc^{8}. The position of myonuclei in embryos that were $Dhc64C^{4-19}$/+, $bocks^{DP01391}$/+ double heterozygotes was different from that with each individual heterozygote (Fig. 2.6 A-D). However, the phenotype was an intermediate of the individual heterozygotes. The distance between the muscle end and the nearest nucleus in $Dhc64C^{4-19}$/+, $bocks^{DP01391}$/+ double heterozygotes was increased compared with the same distance in $bocks^{DP01391}$/+ embryos. However, compared with $Dhc64C^{4-19}$/+ embryos, the distance between the muscle end and the nearest nucleus was decreased in $Dhc64C^{4-19}$/+, $bocks^{DP01391}$/+ double heterozygotes (Fig. 2.6 C and D). These data suggest that *Dynein* and *bocksbeutel* do not interact to regulate myonuclear movement in embryos. However, there was a clear interaction between $bocks^{DP01391}$ and Khc^{8} with respect to the distribution of nuclei. With respect to the nuclear separation ratio, more nuclei were positioned within the ventral end of the muscles in the Khc^{8}/+; $bocks^{DP01391}$/+ embryos than in $bocks^{DP01391}$/+

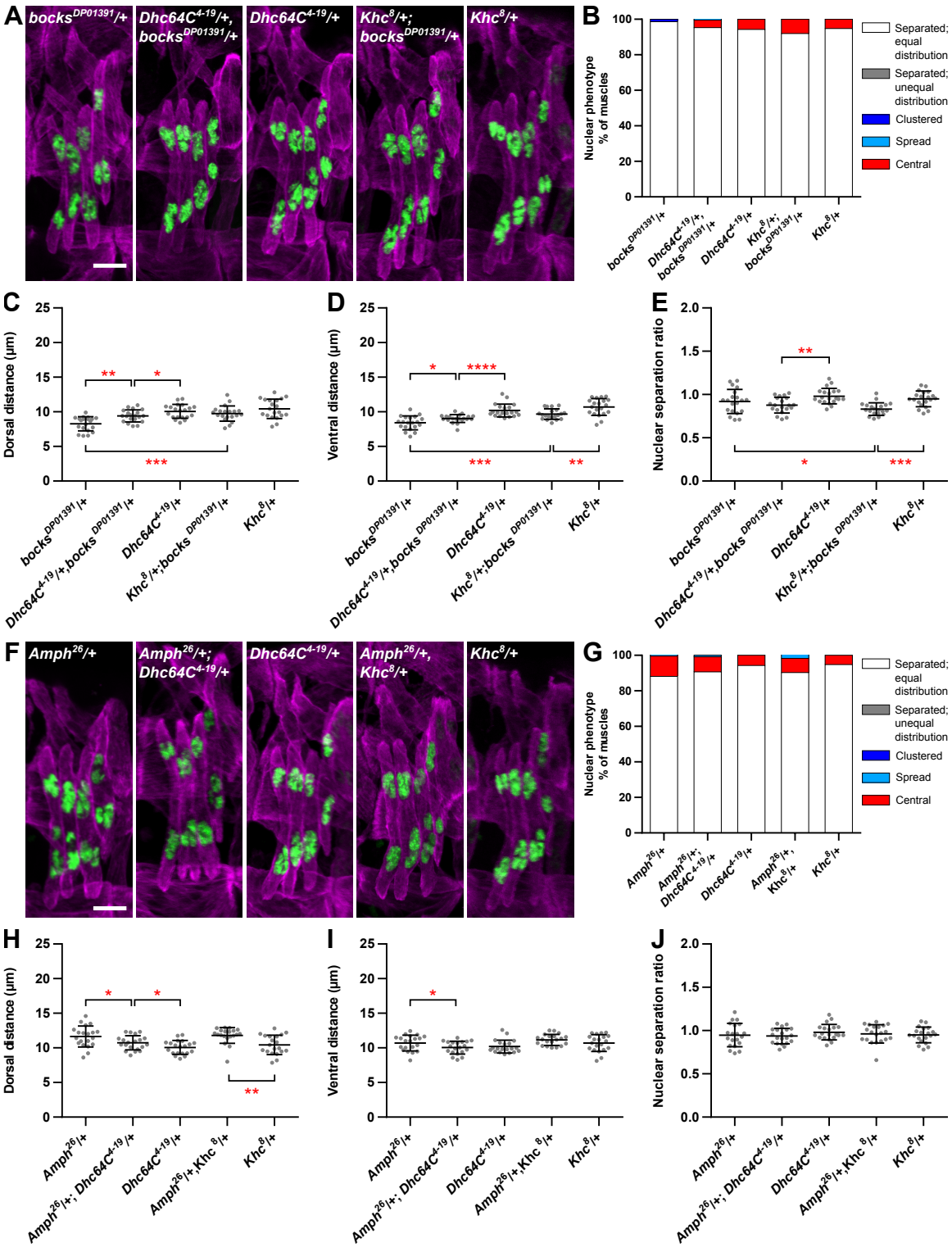

Figure 2.6: *Bocksbeutel* genetically interacts with dynein and kinesin to affect nuclear positioning in *Drosophila* embryonic muscles. (**A,F**) Immunofluorescence images of the LT muscles in one hemisegment from stage 16 (16 hours AEL) embryos for the indicated genotypes. Muscles in magenta, myonuclei in green. Scale bar, 10 µm. (**B,G**) The frequency at which each nuclear positioning phenotype was observed in each of the indicated genotypes. (**C,D,H,I**) Graphs indicating the distance between the dorsal end of the muscle and the nearest nucleus (**C,H**) and between the ventral end of the muscle and the nearest nucleus (**D,I**) in the

indicated genotypes. (**E,J**) The relative distribution of nuclei between the dorsal half of the muscle and the ventral half of the muscle in each of the indicated genotypes. For (C–E) and (H–J), each data point indicates the average distance within a single embryo. Error bars indicate SD from 20 embryos. Student's t-test was used for comparison to controls. *P < 0.05, **P < 0.005, ***P < 0.0005, ****P < 0.00005.

and Khc^{8}/+ embryos (Fig. 2.6 E). In addition, qualitative analysis of the phenotypes also indicated an interaction between $bocks^{DP01391}$ and Khc^{8} (Fig. 2.6 B). The frequency of central nuclei in the Khc^{8}/+; $bocks^{DP01391}$/+ double heterozygote is increased compared with either single heterozygote. Similarly, we completed double-heterozygote experiments to evaluate the genetic interactions between $Amph^{26}$ and both $Dhc64C^{4-19}$ and Khc^{8} (Fig. 2.6 F). No genetic interaction was observed with either motor protein with respect to myonuclear position, nuclear distribution, or phenotypes (Fig. 2.6 G-J). Together these data indicate that *bocksbeutel* regulates nuclear positioning in embryos through a microtubule motor-dependent mechanism, whereas *Amphiphysin* regulates nuclear positioning through a microtubule motor-independent mechanism.

2.4 DISCUSSION

We used *Drosophila* musculature to investigate whether aberrant nuclear position that is related to EDMD and CNM results from a common mechanism. We find that disruption of EDMD- and CNM-linked genes in *Drosophila* recapitulates the phenotypes of mispositioned nuclei evident in the human diseases (Table 2.2). Furthermore, the mechanism by which embryonic nuclear position is disrupted is muscle autonomous. However, these data also strongly indicate that the specific phenotype is different, depending on whether EDMD- or CNM-linked genes are disrupted.

	Genotypes	Nuclear Phenotypes			
		Dorsal Distance	Ventral Distance	Central	Clustered
EDMD	*Ote RNAi*	+	–	–	–
	koi RNAi	+	–	–	–
	bocks RNAi	+	+	–	+
	klar RNAi	+	+	–	+
	bocks^{DP01391}/+	–	–	–	–
	bocks^{DP01391}	+	+	–	+
	klar^{1}/+	–	–	–	–
	klar^{1}	+	+	–	+
CNM	*mtm RNAi*	+	–	–	–
	Amph RNAi	–	+	+	–
	Amph^{26}/+	–	–	–	–
	Amph^{26}	–	–	+	–

Table 2.2: Summary of all nuclear positioning defects in each of the tested genotypes.

In interpreting these data, it is important to note that each of the alleles used is a null. However, only the *emerin* mutation leading to EDMD is believed to be a complete loss of function. The *Amph/BIN1* mutations that have been linked to CNM, and the *SYNE1* and *SYNE2* mutations that have been linked to EDMD are missense mutations. The effect of these specific mutations that cause disease is a critical next step. Nevertheless, that the functions of these genes with respect to nuclear position are disrupted by null mutations indicates that these are functions to explore in disease models.

In embryos with disrupted expression of *Amphiphysin* (CNM-linked gene), there is an increase in the frequency of nuclei that populate the center of the muscle. The increased number of central nuclei suggests that the clusters of nuclei are not tightly maintained as they move toward the ends of the muscles. More directly, nucleus-nucleus interactions may be inhibited. Conversely, *bocksbeutel* and *klarsicht*, two of the EDMD-linked genes that encode for nuclear envelope proteins, are necessary for the dissociation of nuclei from one another. This suggests that nucleus-nucleus interactions are too tightly maintained. Together these data suggest that the two sets of genes have opposing functions with respect to nucleus-nucleus interactions and nuclear movement. These conclusions are supported

by live-embryo time-lapse microscopy, which clearly demonstrated that most nuclei are stuck within a single cluster in *bocks*^{DP01391} embryos, whereas nuclei dissociate from clusters at a high frequency in *Amph*^{26} embryos. In addition, the speeds at which the clusters of nuclei separate from each other is increased in *bocks*^{DP01391} embryos and increased to a greater degree in *Amph*^{26} embryos. This suggests that the interactions between nuclei restrict nuclear movement. Therefore, when such interactions are inhibited in *Amph*^{26} embryos, nuclei can move more freely in terms of both direction and speed. This is complicated by the observation that nuclei move faster in *bocks*^{DP01391} embryos than in controls. One explanation for this is that the nucleus that escapes and moves dorsally has limited interactions with other nuclei and therefore is free to move more quickly.

It is important to note that the interactions between nuclei are likely indirect. The proteins encoded for by *klarsicht* and *bocksbeutel* are nesprin and emerin proteins, respectively. Each of these proteins can localize to the outer nuclear envelope and regulate interactions between the nucleus and the cytoskeleton (Starr & Han, 2002; Salpingidou et al., 2007; Chang et al., 2013). Additionally, in muscle, the nuclear envelope is crucial for the organization of the microtubule cytoskeleton (Tassin et al., 1985; Espigat-Georger et al., 2016). Therefore, it is likely that nucleus-nucleus interactions are mediated by the cytoskeleton. Consistent with this, loss of either *bocks* or *Amph* disrupts microtubule organization (Collins & Mandigo et al., 2017). In *bocks*^{DP01391} larvae, the distribution of microtubules around each nucleus was polarized along the dorsal/ventral axis of the muscle compared with control larvae, in which the microtubules were evenly distributed around each nucleus. In *Amph*^{26} larvae, when microtubules emanate from each nucleus, they are distributed evenly, as in controls. However, not all nuclei have associated microtubules.

Together these data suggest a role for the microtubule cytoskeleton in mediating the balance between nucleus-nucleus interactions.

RNAi experiments were used to demonstrate that the effects of these genes on nuclear position in muscle were muscle autonomous and suggested that some functions are temporally restricted. With respect to each RNAi, continued depletion of the protein by expression of the RNAi under the control of the *DMef2-GAL4* driver did not exaggerate the general evenness of nuclear distribution compared with the more acute depletion driven by *twist-GAL4* (compare Fig. 2.1 to Fig. 2.2). In fact, with regard to one factor, *mtm*, the phenotype was less dramatic, suggesting that it primarily functions early in development. More broadly, these data suggest that each of these genes contributes to nuclear position by several mechanisms that may be separated by developmental time.

Despite the general disruption of nuclear positioning across all genotypes analyzed, there were some notable differences in the severity of phenotypes produced between proteins associated with EDMD. Although both are considered *Drosophila* homologues of emerin, depletion of *bocksbeutel* more strongly disrupted nuclear positioning than depletion of *Otefin*. These differences may suggest that *bocks* and *Ote* may have distinct functions and regulatory roles in the process of nuclear positioning. This would not be the first indication that *bocks* and *Ote* have distinct functions. With respect to fertility, *Drosophila* are more sensitive to the loss of *Ote* than they are to the loss of *bocks* (Barton et al., 2014). Because we find the opposite effect with respect to nuclear position in muscle, these data together suggest that *bocksbeutel* and *Otefin* may have specific roles in different tissues.

Our conclusion that EDMD- and CNM-linked genes disrupt nuclear position by distinct mechanisms is further supported by the differences in their genetic interactions. Whereas *bocks* genetically interacts with the microtubule motors dynein and kinesin, *Amph* does not. These data suggest that *bocks* regulates nuclear movement via the described microtubule-dependent pathways (Folker et al., 2012; Folker et al., 2014; Metzger et al., 2012). The mechanism by which *Amph* regulates nuclear movement and nucleus-nucleus interactions is not clear. Recent data from cell culture suggest that this may be an actin-dependent process (Falcone et al., 2014; D'Alessandro et al., 2015). However, we have shown that *Amph* is necessary for proper microtubule organization at the nucleus, suggesting that nucleus-nucleus interactions may be microtubule dependent (Collins & Mandigo et al., 2017).

Taken all together, these data demonstrate that although mispositioned nuclei are a phenotype common to CNM and EDMD, the underlying mechanism is different in each disease. That genes linked to distinct muscle diseases affect nuclear position by different genetic mechanisms is critical to understanding the effect of nuclear position on muscle health. These conclusions dictate that the mechanisms that underlie mispositioned nuclei in each muscle disease must be individually identified and not considered collectively. However, these data also indicate that there may be a web of genetic pathways that have counteracting and balancing effects. Future studies addressing this possibility will be important for understanding muscle disease pathologies and for the development of viable methods to improve nuclear distribution, either genetically or pharmacologically.

2.5 MATERIAL & METHODS

2.5.1 *Drosophila* genetics

All stocks were grown under standard conditions at 25°C. Stocks used were apRed (Richardson et al., 2007), *bocks*^{DP01391} (21846; Bloomington *Drosophila* Stock Center), *klar*^{1} (3256; Bloomington *Drosophila* Stock Center), *Amph*^{26} (6498; Bloomington *Drosophila* Stock Center), UAS-bocks RNAi (38349; Bloomington *Drosophila* Stock Center), UAS-klar RNAi (36721; Bloomington *Drosophila* Stock Center), UAS-koi RNAi (40924; Bloomington *Drosophila* Stock Center), UAS-Ote RNAi (39009; Bloomington *Drosophila* Stock Center), UAS-mtm RNAi (31552; Bloomington *Drosophila* Stock Center), UAS-Amph RNAi (53971; Bloomington *Drosophila* Stock Center), *Dhc64C*$^{4-19}$ (Gepner et al., 1996), and *Khc*^{8} (Brendza et al., 1999). Mutants were balanced and identified using *CyO*, *DGY* and *TM6b*, *DGY*. UAS-RNAi constructs were driven specifically in the mesoderm using *twist-GAL4*, *apRed* or specifically in the muscle using *DMef2-GAL4*, *apRed*. Regarding *apRed* specifically, this fly expresses a nuclear localization signal fused to the fluorescent protein DsRed downstream of the *apterous* mesodermal enhancer. This results in the specific labeling of the nuclei within the lateral transverse muscles of the *Drosophila* embryo (Richardson et al., 2007). The *twist-GAL4*, *apRed*, *DMef2-GAL4*, *apRed Drosophila* lines were made by recombining the *apRed* promoter and the specific *GAL4* driver. In the case of *twist-GAL4*, *apRed*, both elements are on the second chromosome. In the case of *DMef2-GAL4*, *apRed*, both elements are on the third chromosome. There are slight variations between the two genotypes, so each was used as a control in all experiments.

2.5.2 Immunohistochemistry

Embryos were collected at 25°C and washed in 50% bleach to remove the outer membrane, washed with water, and then fixed in 50% formalin (HT501128; Sigma-Aldrich) diluted in 1:1 heptane for 20 min to allow permeabilization. In all cases, embryos were devitellinized by vortexing in a 1:1 methanol:heptane solution.

Antibodies for embryo staining were used at the following final dilutions: rabbit anti-dsRed, 1:400 (632496; Clontech); rat anti-tropomyosin, 1:200 (ab50567; Abcam), and mouse anti–green fluorescent protein, 1:50 (GFP-G1; Developmental Studies Hybridoma Bank). Conjugated fluorescent secondary antibodies used were Alexa Fluor 555 donkey anti-rabbit (1:200), Alexa Fluor 488 donkey anti-rat (1:200), and Alexa Fluor 647 donkey anti-mouse (1:200; all Life Technologies). Embryos were mounted in ProLong Gold (P36930; Life Technologies) and imaged on a Zeiss 700 LSM with a Plan-Apochromat 40×, 1.4 numerical aperture (NA) oil objective at a 1.0× optical zoom.

2.5.3 Analysis of nuclear position in *Drosophila* embryos

Embryos were imaged at stage 16 based on overall embryo shape, the intensity of the apRed and tropomyosin signals, gut morphology, and the morphology of the trachea as previously described (Folker et al., 2012). Images were processed as maximum intensity projections of confocal z-stacks and oriented such that top is dorsal, bottom is ventral, left is anterior, and right is posterior. Measurements were acquired using the line function of ImageJ software. Dorsal and ventral end distances were taken from each LT muscle by measuring the distance between the closest group of nuclei to the dorsal or ventral muscle pole, respectively. All four LT muscles were measured in four hemisegments from each

embryo. A total of 20 embryos were measured for each genotype taken from independent experiments. Statistical analysis was performed with Prism 4.0 (GraphPad). Student's t-test was used to assess the statistical significance of differences in measurements between experimental genotypes to controls.

For qualitative nuclear phenotype analysis, embryos were scored on how nuclei positioned themselves within the first three LT muscles of each hemisegment. LT 4 was excluded for this analysis due to its variable muscle morphology. Nuclei were categorized as "separated, equal distribution" (nuclei properly segregated into two distinct, even clusters with a dorsal/ventral cluster size ratio ≥ 0.85 and ≤ 1.15); "separated, unequal distribution" (nuclei that segregated into two disproportionate clusters); "central" (a nucleus or a small cluster of nuclei located in the middle of the myofiber that is not associated with either the dorsal or ventral group); "clustered" (nuclei remained in a single cluster toward the ventral end of the myofiber); or "spread" (nuclei are distributed through the myofiber with no distinct dorsal or ventral clusters). Linescans of dsRed intensity were performed on 10 LT muscles for each nuclear phenotype and averaged to determine the typical distribution of nuclei in each genotype.

2.5.4 Analysis of nuclear cluster area in *Drosophila* embryos

Dorsal and ventral areas were taken from each LT muscle by measuring the area of each cluster of nuclei near the dorsal or ventral muscle pole, respectively. All four LT muscles were measured in four hemisegments from each embryo using ImageJ. A total of 20 embryos were measured for each genotype taken from independent experiments. Total area of nuclear clusters in each LT muscle was calculated by adding the dorsal and ventral areas. The nuclear distribution ratio was calculated by dividing the dorsal area by the

ventral area. Statistical analysis was performed with Prism 4.0. Student's t-test was used to assess the statistical significance of differences in measurements between experimental genotypes and controls.

2.5.5 Live-embryo imaging

Embryos were collected at 25°C and washed in 50% bleach to remove the outer membrane, washed with water, and mounted with halocarbon oil (H8898; Sigma-Aldrich). Stage 15 embryos were selected for imaging based on gut morphology, the position of nuclei, and the intensity of the apRed signal, as previously described (Folker et al., 2012). Time-lapse images were taken at an acquisition rate of 2 min/stack for 2 h on a Zeiss 700 LSM with a Plan-Apochromat 40×, 1.4 numerical aperture (NA) oil objective at a 1.0× optical zoom.

Movies were processed as maximum intensity projections of confocal z-stacks and oriented such that top is dorsal, bottom is ventral, left is anterior, and right is posterior. Measurements were acquired using the line function in ImageJ. The separation speed of nuclei was taken by measuring the distance between dorsal and ventral nuclear clusters at time 0 and again at time 2 h. Statistical analysis was performed with Prism 4.0. Student's t-test was used to assess the statistical significance of differences in measurements between experimental genotypes to controls.

2.5.6 RNA isolation, construction of cDNA library, and reverse transcription PCR

RNAi knockdown efficiency was measured in single embryos. Because muscle composes a small portion of the total mass of the embryo, RNAi was expressed ubiquitously to test efficiency using the *Tubulin-GAL4* driver. Embryos were washed in

50% bleach to remove the outer membrane and then washed with water. Single embryos of each genotype (*Tubulin-GAL4*, UAS-Ote RNAi, UAS-bocks RNAi, UAS-koi RNAi, UAS-klar RNAi, UAS-mtm RNAi, UAS-Amph RNAi) were selected at stage 17 of embryo development using the morphology of the gut and appearance of the trachea as previously described (Beckett & Baylies, 2007). To extract and isolate RNA, individual embryos were then crushed in an Eppendorf tube in 1 mL of TRIzol according to manufacturer's instructions (15596026; Invitrogen). RNA integrity and concentration were determined using the NanoDrop2000 system (Thermo Fisher Scientific). The cDNA library was established by performing reverse transcription using the SuperScript VILO cDNA Synthesis Kit (11-754-050; Invitrogen), according to manufacturer's protocol. Purified RNA was incubated with SuperScript III reverse transcriptase at 42°C for 2 h, and then reactions were terminated at 85°C for 5 min. RT-PCR was set up after inactivation of reverse transcription using the GoTaq Flexi DNA Polymerase (M8291; Promega). Primers were designed to amplify a ~120–base pair sequence within each targeted mRNA and a 315–base pair sequence within *RP49* as a control. The denaturing temperature was 95°C, the annealing temperature was 49°C, the extension temperature was 72°C, and 40 amplification cycles were run. The primers used were *RP49* forward, 5′-TACAGGCCCAA GATCGTGAA-3′; *RP49* reverse, 5′-GACAATCTCCTTGCGCTTCT-3′; *Ote* forward, 5′-AGCCCAAGGCTATGTGACTG-3′; *Ote* reverse, 5'-GATTCCTGGCAAATGTGCTT-3′; *bocks* forward, 5′-TTACACACGCGAAGTTGACC-3′; *bocks* reverse, 5′-GTGGCTCG TATGTGGGAAGT-3′; *koi* forward, 5′-CTCAGAACTGTCCCCTCACC-3′; *koi* reverse, 5′-GTGGCTCGTATGTGGGAAGT-3′; *klar* forward, 5′-CCCTCCATATCAACCAGGA C-3′; *klar* reverse, 5′-GGCAAGACTTTCGTCGAACT-3′; *mtm* forward, 5′-CAAAGTGG

CAGACGGCTATT-3′; *mtm* reverse, 5′-GAACTACGACGGAGGTGCTC-3′; *Amph* forward, 5′-GGAAGGCAAAAGTGCATCTC-3′; and *Amph* reverse, 5′-GAACAGATTT GGCCAGCATT-3′. PCR products were run on a 2% agarose gel and visualized with ethidium bromide. Gels were imaged using Typhoon FLA 9500 (GE Healthcare Life Sciences). Band intensities were quantified using ImageQuant. Values are normalized to expression of RP49 and displayed with control expression normalized to 1.

CHAPTER 3

CENTRONUCLEAR MYOPATHY-LINKED GENES REGULATE NUCLEAR INTERACTIONS AND POSITIONING DURING EMBRYONIC MUSCLE DEVELOPMENT

The content in this chapter was adapted from the following manuscript:

Collins, M.A., Coon, A.L., Shu, T., Thomas, R., Singh, A., and Folker, E.S. Centronuclear myopathy-linked genes regulate nuclear interactions and positioning during embryonic muscle development. *In preparation*.

3.1 INTRODUCTION

Centronuclear myopathy is a genetically heterogeneous group of inherited muscle disorders characterized by the classic clinical features of a congenital myopathy. As the name of the disease implies, the most prominent histopathological feature of CNM is an increased abundance of centrally mispositioned nuclei. Originally described by Dr. Spiro in 1966 (Spiro et al., 1966), central nuclei have been routinely used as a pathological marker for differentiating and diagnosing muscle diseases from neurological disorders for over 50 years. Advances in genetic screening have helped identify a number of genes associated with CNM. The most common forms of CNM have been attributed to X-linked recessive mutations in the *MTM1* gene (encoding myotubularin), autosomal-dominant mutations in the *DNM2* gene (encoding dynamin-2) and the *BIN1* gene (encoding amphiphysin-2; also known as bridging integrator-1), as well as autosomal-recessive mutations in *BIN1* and the *RYR1* gene (encoding the ryanodine receptor).

Because the proteins encoded by these genes are involved in various aspects of membrane formation, shaping, and remodeling of membrane structure, like the transverse-tubule network and sarcoplasmic reticulum, CNM has been traditionally classified as a "T-tubule disease" (Dowling et al., 2009; Al-Qusairi et al., 2009; Toussaint et al., 2011; Fugier et al., 2011; Durieux et al., 2010; Chin et al., 2015). Defects in membrane trafficking have emerged as a key pathogenic mechanisms, with aberrant T-tubule formation, abnormalities in triad assembly, and disturbance of the excitation-contraction machinery. However, mispositioned nuclei are the most obvious and common phenotype in patients afflicted with not only CNM but other muscular dystrophies as well. Yet this defining feature has

remained largely ignored. As a result, the genetic mechanisms of how genes linked to CNM regulate the dynamic process of nuclear positioning remain unknown.

Although there has been little investigation into the role of CNM associated proteins in the context of nuclear positioning, myotubularin, amphiphysin-2, and dynamin-2 have been shown to interact with various cytoskeletal elements including microtubules (Shpetner & Vallee, 1992; Maeda et al., 1992; Hnia et al., 2012) and actin filaments (Mooren et al., 2009; Gu et al., 2010; Suetsugu & Gautreau, 2012). Such interactions suggest a role for each of these protein in regulating cytoskeletal dynamics and potentially nuclear dynamics as well since nuclear movement is dependent on the cytoskeletal proteins. To support this, work done using cultured myofibers reported that amphiphysin-2 interacts with and activates the actin nucleation promoting factor, N-WASP (Falcone et al., 2014). This regulatory function was a prerequisite for triad formation and was necessary for proper movement of nuclei to the periphery. Additionally, amphiphysin-2 was also demonstrated to biochemically interact with the MT plus-end protein, CLIP-170, as well as actin via nesprin in *C. elegans* and mammalian cell culture (D'Alessandro et al., 2015), suggesting it may have a conserved role in contributing to the attachment between the nucleus and the cytoskeleton. Together, these data suggest that the combined actions of amphiphysin, and perhaps other CNM-linked genes, along with the LINC complex and cytoskeleton may interact to coordinate the position of nuclei. Thus, the proteins linked to CNM pose as novel regulators of myonuclear positioning.

3.2 RESULTS

3.2.1 Muscle-specific depletion of CNM-linked genes disrupt myonuclear position in the *Drosophila* embryo

We previously demonstrated that GAL4/UAS disruption of two genes that have been linked to CNM, *Amph* and *mtm*, had muscle autonomous effects on nuclear positioning during *Drosophila* muscle development (Fig 2.1 and Fig. 2.2). To determine whether the other CNM-associated genes also contribute to active nuclear positioning, we investigated the function of *RyR* (*Drosophila* Ryanodine receptor) and *shibire* (*Drosophila* dynamin) as well as the dynamin-related protein 1, *Drp1*. Similar to the CNM genes Drp1 is a member of the dynamin family of large GTPases and is critical for mitochondrial fission. Despite its similarity to dynamin, there are no reports of *Drp1*-related CNM mutations. Each gene was depleted using UAS-RNAi expression under the control of the mesoderm-specific *twist-GAL4* driver (Fig. 3.1).

In control embryos, the nuclei in 95% of LT muscle were positioned in two separate clusters, with one near the dorsal end of the muscle and the other near the ventral end of the muscle (Fig. 3.1 A and B). Since the predominant phenotype observed in CNM patients as well as *Drosophila* embryo muscles is centrally mispositioned nuclei, the frequency of nuclear phenotypes was counted (Fig. 3.1 B). In embryos, *twist-GAL4* depletion of *RyR*, *shi,* or *Drp1* caused little to no increase in the number of centrally located nuclei compared to controls. The position of nuclei relative to each muscle end was also measured. Since depletion of *RyR*, *shi,* or *Drp1* resulted in shorter muscles (Fig. 3.1 C), all measurements were normalized to the muscle length. Across the entire population, depletion of *RyR* or *shi* did not affect impact on the position of nuclei relative to either the dorsal or the

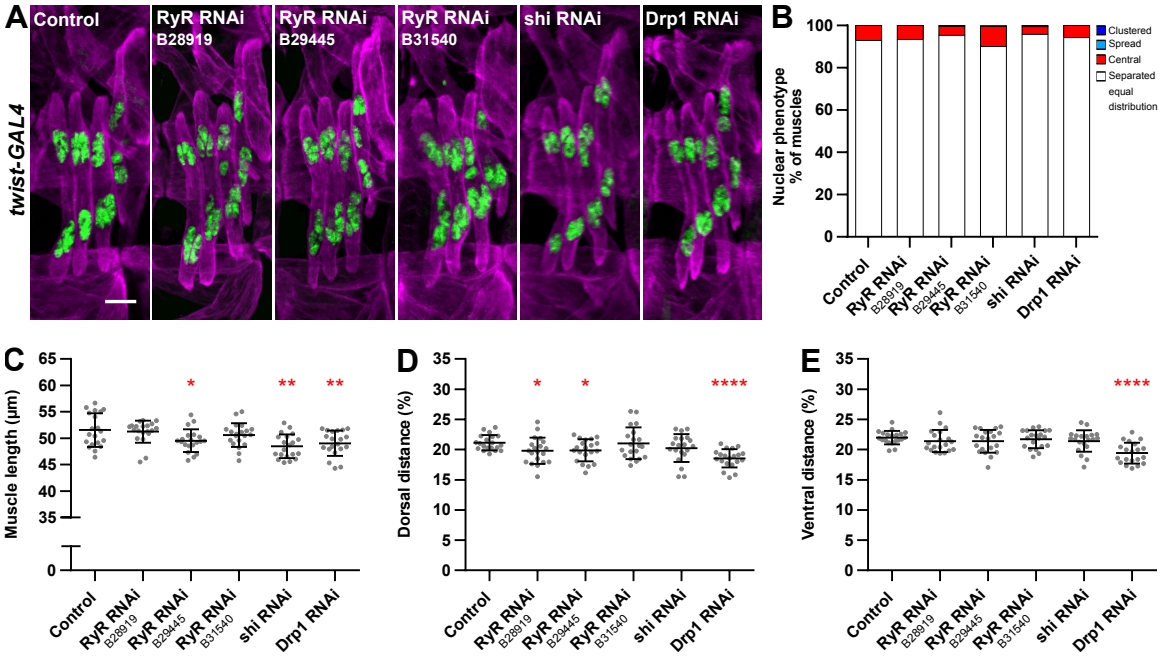

Figure 3.1: Mesoderm-specific knockdown of the CNM-linked genes, *RyR* and *shi*, and *Drp1* in *Drosophila* embryos. (**A**) Immunofluorescence images of the LT muscles in one hemisegment from stage 16 (16 hours AEL) embryos that expressed the indicated UAS-RNAi constructs under the control of *twist-GAL4.* Muscles in magenta, myonuclei in green. Scale bar, 10 µm. (**B**) The frequency at which each nuclear positioning phenotype was observed in each of the indicated UAS-RNAi constructs. (**C–E**) Graphs indicating the average LT muscle length (**C**), the distance between the dorsal end of the muscle and the nearest nucleus (**D**), and the distance between the ventral end of the muscle and the nearest nucleus (**E**). All distances were normalized to the muscle length. For (C–E), each data point indicates the average distance within a single embryo. Error bars indicate SD from 20 embryos. Student's t-test was used for comparison to controls. *P < 0.05, **P < 0.005, ****P < 0.00005.

ventral ends of the muscle (Fig. 3.1 D and E). However, nuclei in *Drp1*-depleted embryos were statistically closer to both ends of the muscle. This data indicates a possible role for dynamin-related protein in regulating nuclear positioning in muscle, despite no known association to CNM or any other muscle disease.

Likewise, each gene was also depleted in embryos under the control of the muscle-specific *DMef2-GAL4* driver. Nuclei in embryos expressing the control RNAi under *DMef2-GAL4* expression were positioned in two separate clusters at opposite ends of the muscle, similar to *twist-GAL4* controls (Fig. 3.2 A). Conversely, there was a dramatic increase in the number of centrally positioned nuclei observed in *RyR*-, *shi*-, and *Drp1*-depleted embryos (Fig 3.2 B). Specifically, 18%, and 25% of *shi*- and *Drp1*-muscles

contained at least one nucleus mispositioned within the center that was not associated with either the dorsal or ventral cluster of nuclei, compared to 6% in controls. This increase in mispositioned nuclei is consistent with prior work, which reported that *DMef2-GAL4* depletion of *Amph* and *mtm* resulted in stronger phenotypes compared to *twist-GAL4* depletion (Collins & Mandigo et al., 2017). Additionally, central nuclei are suggestive of a disruption in the attractive interactions that exist between nuclei. Thus, *RyR*, *shi*, and *Drp1* may also be critical for maintaining nuclei within their clusters as they migrate to the muscle poles. However, *DMef2-GAL4* depletion of *RyR* or *shi* had no impact on nuclear positioning, while *DMef2-GAL4* depletion of *Drp1* had a diminished impact on nuclear positioning relative to either end of the muscle (Fig. 3.2 D and E). Together, these data suggest that *shi* and *Drp1* regulate the associations between nuclei in a muscle- and temporally-specific manner during muscle development.

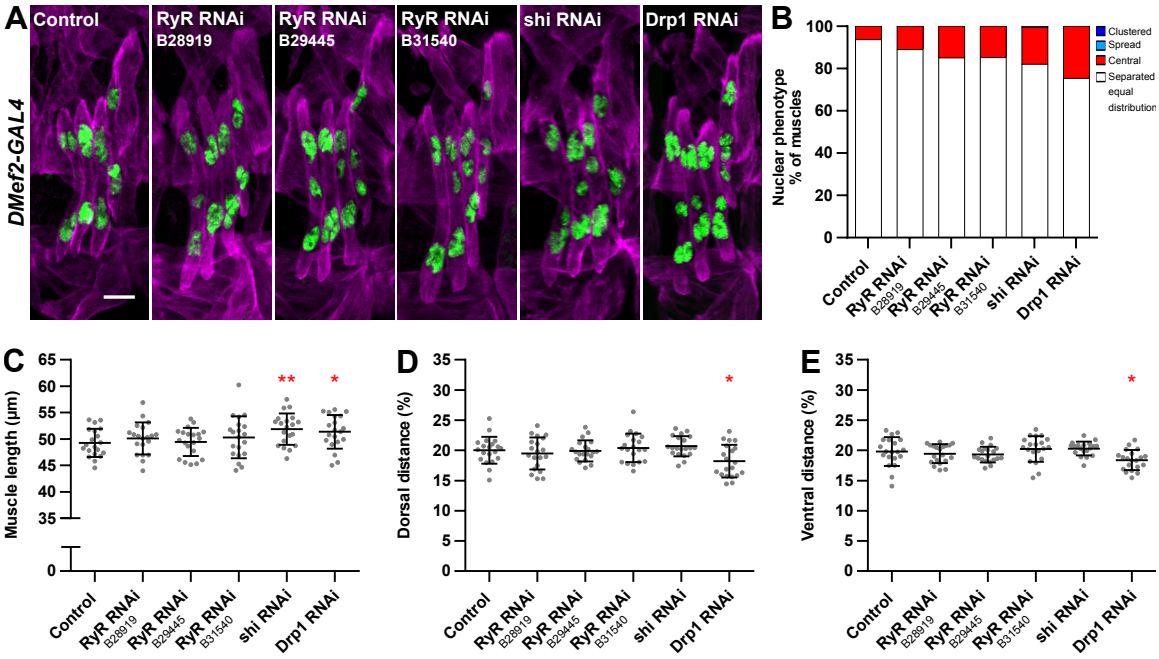

Figure 3.2: Muscle-specific knockdown of the CNM-linked genes, *RyR* and *shi*, and *Drp1* in *Drosophila* embryos. (**A**) Immunofluorescence images of the LT muscles in one hemisegment from stage 16 (16 hours AEL) embryos that expressed the indicated UAS-RNAi constructs under the control of *DMef2-GAL4.* Muscles in magenta, myonuclei in green. Scale bar, 10 µm. (**B**) The frequency at which each nuclear positioning

phenotype was observed in each of the indicated UAS-RNAi constructs. (**C–E**) Graphs indicating the average LT muscle length (**C**), the distance between the dorsal end of the muscle and the nearest nucleus (**D**), and the distance between the ventral end of the muscle and the nearest nucleus (**E**). All distances were normalized to the muscle length. For (C–E), each data point indicates the average distance within a single embryo. Error bars indicate SD from 20 embryos. Student's t-test was used for comparison to controls. *P < 0.05, **P < 0.005.

3.2.2 The CNM-linked genes, *Amphiphysin*, *myotubularin*, and *Ryanodine receptor* affect embryonic myonuclear position

To support previous RNAi experiments and identify disease-causing alleles for genetic network analysis, we tested embryos that were homozygous for either the $Amph^{26}$ null allele (Zelhof et al., 2001), the $mtm^{\Delta 77}$ null allele (Velichkova et al., 2010), or the RyR^{16} hypomorph allele (Sullivan et al., 2000) and analyzed the position of nuclei (Fig. 3.3 A). Previously, we demonstrated a role for Amphiphysin in maintaining the attractive interactions between neighboring nuclei for their necessary association into clusters (Collins & Mandigo et al., 2017). Consistent with this published data, there was an increase in the number of mispositioned nuclei (22%) within the center of the muscle in $Amph^{26}$ embryos (Fig. 3.3 B). However, the frequency of central nuclei in both $mtm^{\Delta 77}$ or RyR^{16} embryos was similar when compared to controls. Yet, all three mutants resulted in significantly shorter muscles (Fig. 3.3 C), consistent with each of their roles in T-tubule formation and triad assembly (Jungbluth & Gautel, 2014). Furthermore, nuclear positioning was disrupted in $Amph^{26}$ and $mtm^{\Delta 77}$ embryos. Compared to controls, nuclei were closer to the dorsal end of the muscle (Fig. 3.3 D) yet further away from the ventral end of the muscle (Fig. 3.3 E). Furthermore, the distance between the dorsal and ventral nuclear clusters was significantly shorter in both $Amph^{26}$ and $mtm^{\Delta 77}$ embryos, indicating that the two clusters of nuclei were closer together than clusters in control muscles.

Together, these data suggest a role for both *Amphiphysin* and *myotubularin* in regulating the position of nuclei during embryonic muscle development.

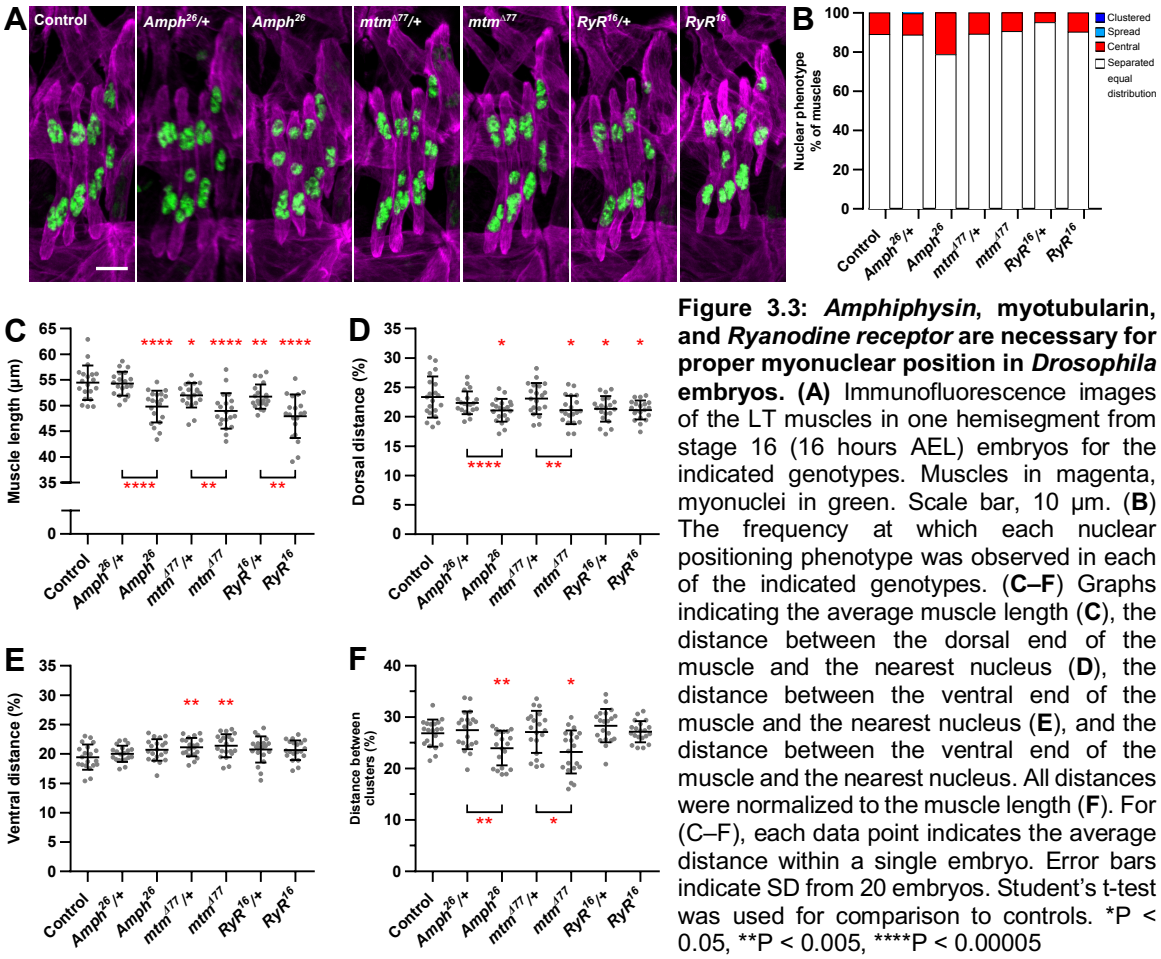

Figure 3.3: *Amphiphysin*, myotubularin, and *Ryanodine receptor* are necessary for proper myonuclear position in *Drosophila* embryos. (A) Immunofluorescence images of the LT muscles in one hemisegment from stage 16 (16 hours AEL) embryos for the indicated genotypes. Muscles in magenta, myonuclei in green. Scale bar, 10 µm. (**B**) The frequency at which each nuclear positioning phenotype was observed in each of the indicated genotypes. (**C–F**) Graphs indicating the average muscle length (**C**), the distance between the dorsal end of the muscle and the nearest nucleus (**D**), the distance between the ventral end of the muscle and the nearest nucleus (**E**), and the distance between the ventral end of the muscle and the nearest nucleus. All distances were normalized to the muscle length (**F**). For (C–F), each data point indicates the average distance within a single embryo. Error bars indicate SD from 20 embryos. Student's t-test was used for comparison to controls. *P < 0.05, **P < 0.005, ****P < 0.00005

3.2.3 *Amphiphysin* genetically interacts with the cytoskeletal factors *ensconsin*, *CLIP-190*, and *singed* to regulate embryonic myonuclear positioning

Of all the CNM-associated genes tested, depletion of *Amphiphysin* had the strongest effect on myonuclear positioning. Recent studies have identified a few interactions between Amphiphysin and some known regulators of nuclear movement. In *in vitro* myofibers, N-WASP interacts with amphiphysin-2 to regulate peripheral nuclear positioning and triad organization during myofiber formation (Falcone et al., 2014).

Furthermore, Amphiphysin can also bind to actin as well as the microtubule plus-end binding protein CLIP170 (D'Alessandro et al., 2015). However, Amphiphysin does not interact with either of the microtubule motors, kinesin or dynein, to regulate nuclear positioning in *Drosophila* embryos (Collins & Mandigo et al., 2017). Therefore, to determine whether *Amph* is regulating nuclear movement in a cytoskeleton-dependent manner, we tested for genetic interactions between *Amphiphysin* and *ensconsin* (*Drosophila* MAP7), *CLIP-190* (*Drosophila* CLIP-170), as well as the actin bundler, *singed* (*Drosophila* fascin). We performed double-heterozygote experiments to evaluate the genetic interactions between $Amph^{26}$ to each cytoskeletal factor, ens^{swo} (Fig. 3.4), $CLIP\text{-}190^{KG06490}$ (Fig. 3.5), and sn^{28} (Fig. 3.6).

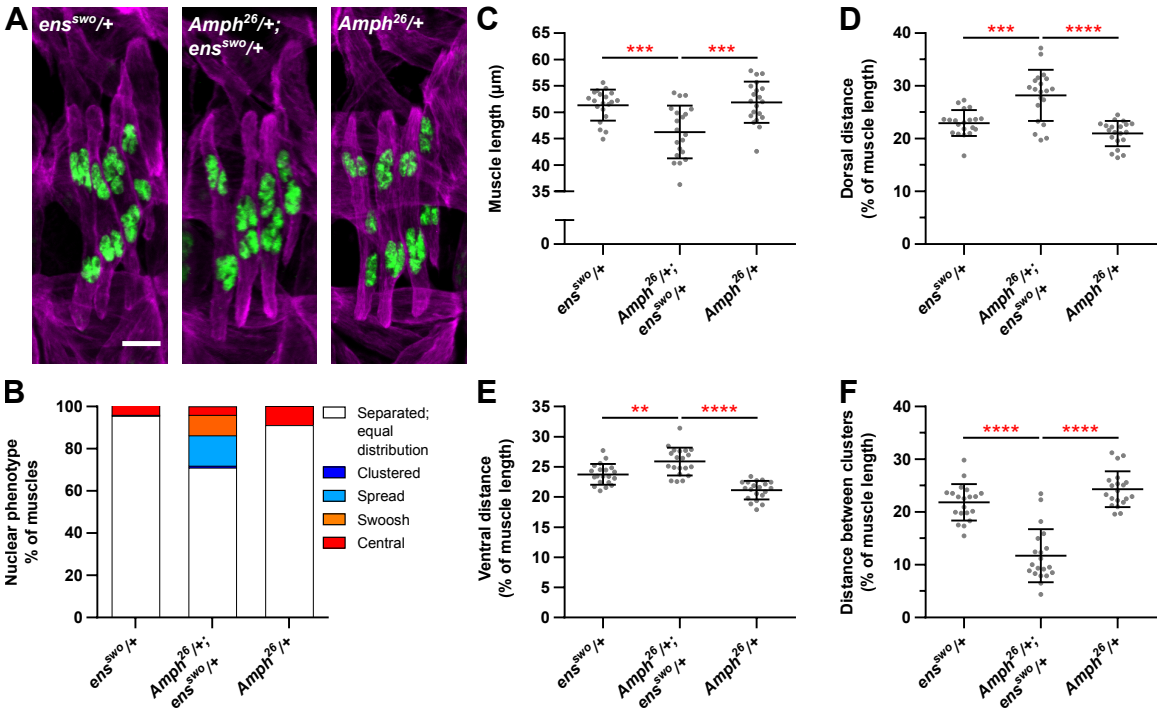

Figure 3.4: *Amphiphysin* genetically interacts with *ensconsin* to regulate nuclear interactions and positioning in *Drosophila* embryonic muscles. (**A**) Immunofluorescence images of the LT muscles in one hemisegment from stage 16 (16 hours AEL) embryos for the indicated genotypes. Muscles in magenta, myonuclei in green. Scale bar, 10 µm. (**B**) The frequency at which each nuclear positioning phenotype was observed in each of the indicated genotypes. (**C–E**) Graphs indicating the average LT muscle length (**C**), the distance between the dorsal end of the muscle and the nearest nucleus (**D**), and the distance between the ventral end of the muscle and the nearest nucleus (**E**) in the indicated genotypes. All distances were normalized to the muscle length. For (C–E), each data point indicates the average distance within a single

embryo. Error bars indicate SD from 20 embryos. Student's t-test was used for comparison to controls. **P < 0.005, ***P < 0.0005, ****P < 0.00005.

Starting with the microtubule-associated protein ensconsin, the position of myonuclei in embryos that were *Amph*^{26}/+; *ens*^{swo}/+ double heterozygotes was different from that with each individual heterozygote (Fig. 3.4 A-D). Nuclei were positioned further away from both ends of the muscles (Fig 3.4 D and E), with respect to muscle length which was also significantly shorter (Fig. 3.4 C). In addition, the distance between the dorsal cluster and ventral cluster of nuclei was significantly shorter in the *Amph*^{26}/+; *ens*^{swo}/+ double heterozygotes, indicating that nuclei failed to fully separate into distinct clusters. As a result, 25% of muscles contained a single group of nuclei, with no distinct dorsal or ventral clusters (Fig. 3.4 B). This severe disruption in nuclear positioning strongly suggests that *Amphiphysin* genetically interacts with *ensconsin* to regulate both the position of nuclei as well as the interactions between nuclei during muscle development.

The same approach was used to determine whether Amphiphysin also genetically interacts with the microtubule plus-end protein CLIP-190 to regulate myonuclear positioning. Similarly, the position of myonuclei was evaluated in embryos that were double heterozygotes for *CLIP-190*^{KG06490}/+, *Amph*^{26}/+ (Fig 3.5 A). No genetic interaction was observed between *Amph* and *CLIP-190* myonuclear position with respect to the dorsal muscle end, ventral muscle end, or distance between the nuclear clusters (Fig. 3.5 C-F). However, there was a significant increase in the number of nuclei mispositioned within the center of the myofibers in *CLIP-190*^{KG06490}/+, *Amph*^{26}/+ double heterozygotes compared to either the *CLIP-190*^{KG06490}/+ or *Amph*^{26}/+ single heterozygotes (Fig. 3.5 B). These data suggest that while the position or separation of nuclear clusters is not affected by the loss

of *Amph* and *CLIP-190*, both factors genetically interact to maintain the attractive interactions between nuclei so that they remain associated within their respective cluster.

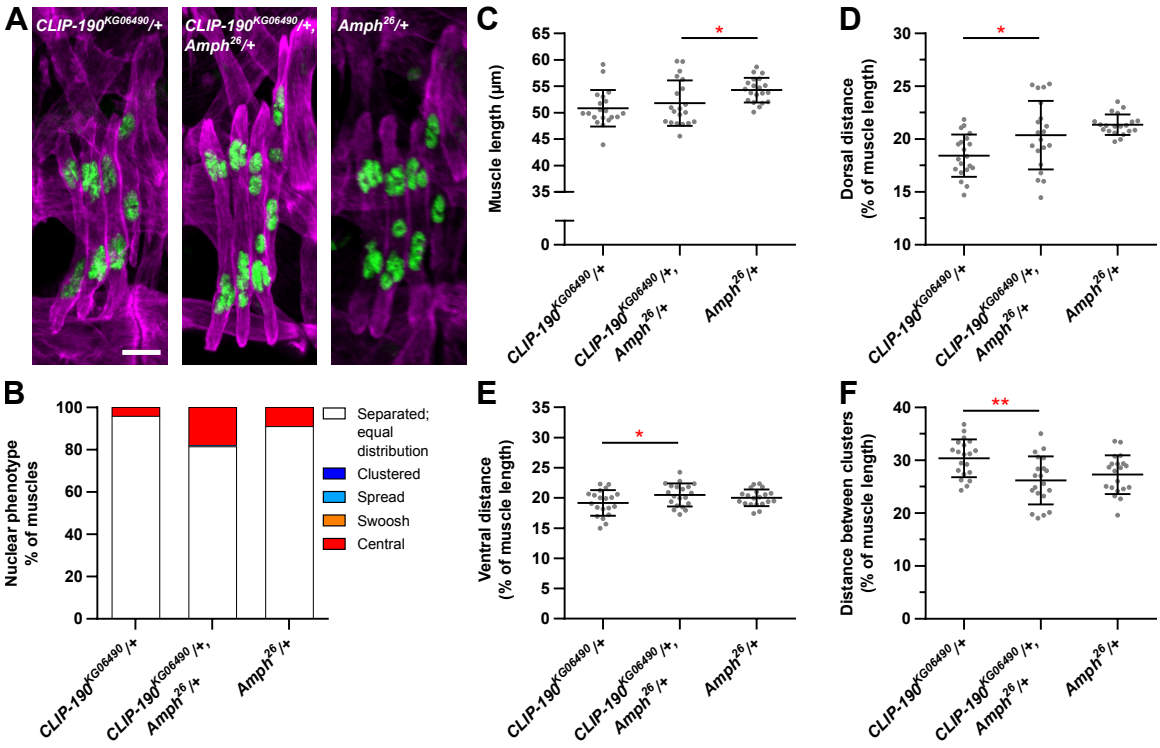

Figure 3.5: *Amphiphysin* genetically interacts with *CLIP-190* to regulate attractive nuclear interactions in *Drosophila* embryonic muscles. (**A**) Immunofluorescence images of the LT muscles in one hemisegment from stage 16 (16 hours AEL) embryos for the indicated genotypes. Muscles in magenta, myonuclei in green. Scale bar, 10 µm. (**B**) The frequency at which each nuclear positioning phenotype was observed in each of the indicated genotypes. (**C–E**) Graphs indicating the average LT muscle length (**C**), the distance between the dorsal end of the muscle and the nearest nucleus (**D**), and the distance between the ventral end of the muscle and the nearest nucleus (**E**) in the indicated genotypes. All distances were normalized to the muscle length. For (C–E), each data point indicates the average distance within a single embryo. Error bars indicate SD from 20 embryos. Student's t-test was used for comparison to controls. *P < 0.05, **P < 0.005.

Lastly, we examined embryos that were double heterozygotes for sn^{28}/+; $Amph^{26}$/+ for a potential genetic interaction between Amphiphysin and the actin-bundler, singed (Fig. 3.6 A). Although the average muscle length was significantly decreased in the double heterozygotes (Fig. 3.6 C), the position of nuclei was not disrupted with respect to either the dorsal or ventral muscle ends (Fig. D and E). Instead, the distance between the dorsal and ventral nuclear clusters was significantly decreased in the sn^{28}/+; $Amph^{26}$/+ double

heterozygotes compared to either of the single heterozygotes (Fig. 3.6 F). However, the majority of nuclei still separated into distinct clusters (Fig. 3.6 B). Altogether, these data indicate that Amphiphysin genetically interacts with both the microtubule and actin cytoskeleton to regulate the position of nuclei and nuclear interactions during embryonic muscle development.

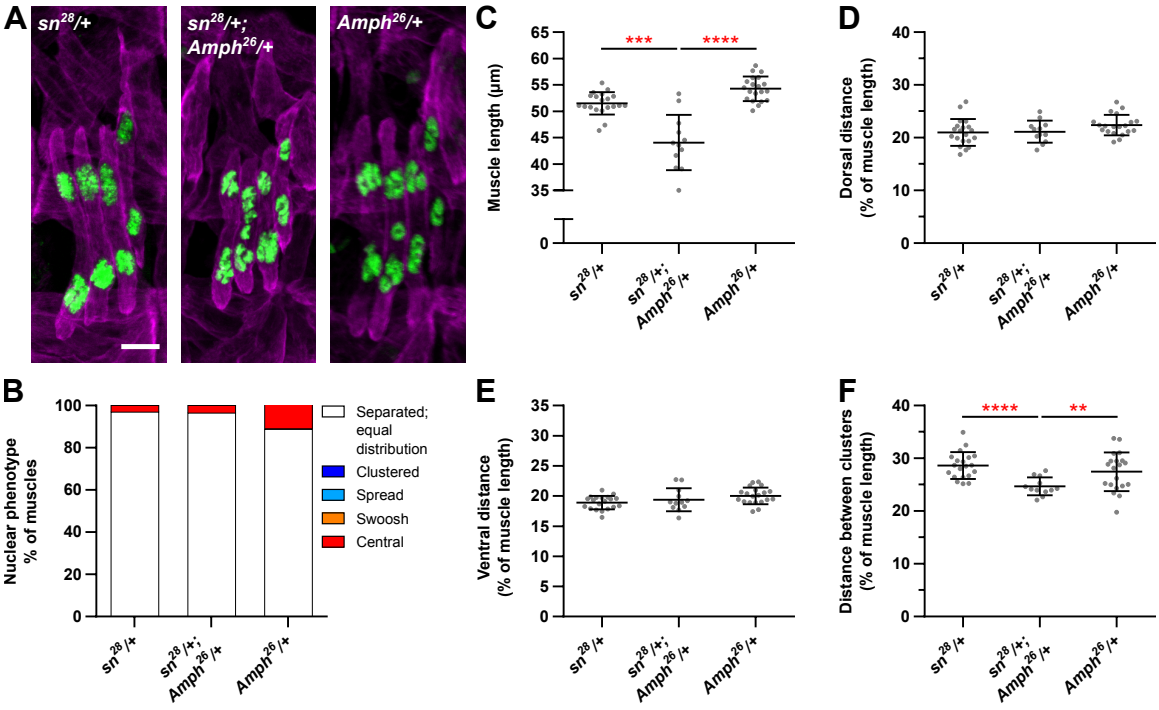

Figure 3.6: *Amphiphysin* genetically interacts with *singed* to regulate the distance between nuclear clusters in *Drosophila* embryonic muscles. (**A**) Immunofluorescence images of the LT muscles in one hemisegment from stage 16 (16 hours AEL) embryos for the indicated genotypes. Muscles in magenta, myonuclei in green. Scale bar, 10 µm. (**B**) The frequency at which each nuclear positioning phenotype was observed in each of the indicated genotypes. (**C–E**) Graphs indicating the average LT muscle length (**C**), the distance between the dorsal end of the muscle and the nearest nucleus (**D**), and the distance between the ventral end of the muscle and the nearest nucleus (**E**) in the indicated genotypes. All distances were normalized to the muscle length. For (C–E), each data point indicates the average distance within a single embryo. Error bars indicate SD from 20 embryos. Student's t-test was used for comparison to controls. **P < 0.005, ***P < 0.0005, ****P < 0.00005.

3.3 DISCUSSION

Centronuclear myopathy has been recognized and diagnosed for over 50 years, yet despite knowing the genetic cause and clinical features that result, the underlying pathology

of CNM remains poorly understood. In recent years, several mechanisms have been proposed involving the "MAD" pathway and their role in the formation, shaping, and remodeling of membrane structures that are critical for endocytosis, the formation of muscle-specific structures, as well as the generation of muscle contractions. Although such mechanisms can at least partially explain the resulting muscle weakness and atrophy observed in patients afflicted with CNM, how disruptions in the "MAD" pathway genes cause other disease features, namely the abundance of central nuclei, still remain unknown.

We used *Drosophila* musculature to investigate whether the genes associated with CNM actively regulate the position of nuclei during embryonic muscle development. First, mesoderm- and muscle-specific depletion of *RyR*, *shi*, and *Drp1* had varying effects on nuclear positioning. Of the three, depletion of *Drp1* disrupted nuclear positioning relative to the muscle ends (Fig. 3.1 and 3.2). However, muscle-specific depletion of *Drp1* and *shi* both caused an increase in the number nuclei found in the center of the muscle, indicating that nuclei are prematurely dissociating from their original cluster (Fig 3.2 B). These data suggest that there may be a general role for GTPases in regulating how nuclei interact with one another. More generally, these data may also indicate that different mechanisms regulate the position of nuclei separately from those that maintain nucleus-nucleus interactions.

To expand upon work that characterized the $Amph^{26}$ null allele (Collins & Mandigo et al., 2017), we also examined $mtm^{\Delta 77}$ and RyR^{16} embryos for nuclear positioning phenotypes. Consistent with previous data, 21% of muscles in $Amph^{26}$ mutants had a nucleus within the center of the myofiber (Fig. 3.3 B), supporting Amphiphysin's role in maintaining attractive nucleus-nucleus interactions. However, the frequency of central

nuclei was about the same in $mtm^{\Delta 77}$ nor RyR^{16} muscles compared to controls. One possible explanation for this relatively low abundance could be that nuclear dynamics are disrupted. For example, *in vivo* time-lapse movies of $Amph^{26}$ embryos demonstrated that nuclei move significantly faster. Thus, such movies of nuclear movements in $mtm^{\Delta 77}$ and RyR^{16} embryos would be useful in determining whether or not either gene regulates nuclear-nuclear interactions. Despite the lack of central nuclei, the position of nuclei in $mtm^{\Delta 77}$ embryos, with respect to the muscle ends, was significantly disrupted (Fig 3.3 D and E). These data further support our conclusion that nuclear interactions and nuclear positioning may be regulated by distinct mechanisms during embryonic development.

Finally, to gain more of a mechanistic understanding of how *Amph* regulates both nuclear interactions and positioning, we investigated potential genetic interactions between Amphiphysin and three cytoskeletal factors. *Amph* was shown to genetically interact with *ensconsin*, *CLIP-190*, and *singed*, yet the resulting phenotype of each interaction differed from one another. *Amph* interacts with both *ens* and *CLIP-190* to maintain nuclear interactions, as 20-30% of nuclei failed to separate into two clusters of equal size (Fig. 3.4 B and Fig. 3.5 B). These data are consistent with previous work that has proposed a similar MT-dependent mechanisms for holding nuclei together (Folker et al., 2012). However, *Amph* also interacts with both *ens* and *sn* to regulate nuclear positioning, as the position of nuclei within the muscle was disrupted (Fig 3.4 D-F and Fig. 3.6 F). Hence, these data support recent work demonstrating that Amphiphysin interacts with both the microtubule and actin cytoskeletons (Falcone et al., 2014; D'Alessandro et al., 2015).

Taken all together, these data strongly support the conclusion that genes association with CNM play an important role in regulating nuclei as they move during embryonic

muscle development. Additionally, these data also demonstrate that proper nuclear positioning depends on the presence of nuclear interactions in addition to the molecular machinery that physically move nuclei within the muscle. Further investigation of the connection between CNM-linked genes and mispositioned nuclei will help advance our understanding of the intricate interaction between the nucleus and the microtubule and actin cytoskeletons as well as demonstrate the importance of the nucleus, and its position, on muscle cell development and function.

3.4 MATERIAL & METHODS

3.4.1 *Drosophila* genetics

All stocks were grown under standard conditions at 25°C. Stocks used were apRed (Richardson et al., 2007), UAS-mCherry RNAi (35785; Bloomington *Drosophila* Stock Center), UAS-RyR RNAi (28919, 29445, 31540; Bloomington *Drosophila* Stock Center), UAS-shi RNAi (36921; Bloomington *Drosophila* Stock Center), UAS-Drp1 RNAi (51483; Bloomington *Drosophila* Stock Center), $Amph^{26}$ (6498; Bloomington *Drosophila* Stock Center), $mtm^{\Delta 77}$ (a gift from Amy Kiger; (Ribeiro et al., 2011)), RyR^{16} (6812; Bloomington *Drosophila* Stock Center), ens^{swo} (Metzger et al., 2012), $CLIP\text{-}190^{KG06490}$ (14493; Bloomington *Drosophila* Stock Center), and sn^{28} (a gift from Tina Tootle). Mutants were balanced and identified using *CyO DGY*, *TM6b DGY,* and *FM7 DGY*. UAS-RNAi constructs were driven specifically in the mesoderm using *twist-GAL4*, *apRed* or specifically in the muscle using *DMef2-GAL4*, *apRed*. Regarding *apRed* specifically, this fly expresses a nuclear localization signal fused to the fluorescent protein DsRed

downstream of the *apterous* mesodermal enhancer. This results in the specific labeling of the nuclei within the lateral transverse muscles of the *Drosophila* embryo (Richardson et al., 2007). The *twist-GAL4*, *apRed*, *DMef2-GAL4*, *apRed Drosophila* lines were made by recombining the *apRed* promoter and the specific *GAL4* driver. In the case of *twist-GAL4*, *apRed*, both elements are on the second chromosome. In the case of *DMef2-GAL4*, *apRed*, both elements are on the third chromosome. There are slight variations between the two genotypes, so each was used as a control in all experiments. For double-heterozygote experiments, single heterozygotic embryos were crossed out to control for differences in genetic backgrounds present in the double heterozygotic embryos.

3.4.2 Immunohistochemistry

Embryos were collected at 25°C and washed in 50% bleach to remove the outer chorion membrane, washed with water, and then fixed in 50% formalin (Sigma, Product # HT501128) diluted in 1:1 heptane for 20 minutes. Embryos were then devitellinized by vortexing in a 1:1 methanol:heptane solution. Primary antibodies for embryo staining were used at the following final dilutions: rabbit anti-DsRed (1:400, Clontech 632496) and rat anti-tropomyosin (1:200, Abcam ab50567). mouse anti-GFP (1:50, Developmental Studies Hybridoma Bank GFP-G1). The conjugated fluorescent secondary antibodies used were Alexa Fluor 555 donkey-anti-rabbit (1:200), Alexa Fluor 488 donkey-anti-rat (1:200), and Alexa Fluor 647 donkey-anti-mouse (1:200) (all Life Technologies). Embryos were mounted in ProLong Gold (Life Technologies, P36930).

3.4.3 Analysis of nuclear position in *Drosophila* embryos

Embryos were imaged at stage 16 based on overall embryo shape, the intensity of the apRed and tropomyosin signals, gut morphology, and the morphology of the trachea as previously described (Folker et al., 2012; Collins & Mandigo et al., 2017). Confocal z-stacks of fixed embryos were acquired on a Zeiss 700 LSM using a Plan-Apochromat 40×, 1.4 NA oil objective with a 1.0× optical zoom. Images were processed as maximum intensity projections and oriented such that top is dorsal, bottom is ventral, left is anterior, and right is posterior. Measurements were made using the Segmented Line tool in Fiji software (Schindelin et al., 2012). Muscle length measurements were taken starting from the dorsal tip and following through the center of each LT muscle, down to the ventral tip. Dorsal and ventral end distances were taken from each LT muscle by measuring the distance between the closest group of nuclei to the dorsal or ventral muscle pole, respectively. Internuclear distances were taken by measuring the shortest distance in between the dorsal and ventral clusters of nuclei within each LT muscle. Internuclear distances were also plotted according to relative frequency. All three measurements are reported as distances normalized to the muscle length (Fig. 3.1) and as raw values (Fig. 3.2). Statistical analysis was performed with Prism 4.0 (GraphPad). Student's t-test was used to assess the statistical significance of differences in measurements between experimental genotypes to controls.

For qualitative nuclear phenotype analysis, embryos were scored on how nuclei positioned themselves within the first three LT muscles of each hemisegment. LT 4 was excluded for this analysis due to its variable muscle morphology. Nuclei were categorized as "separated, equal distribution" (nuclei properly segregated into two distinct, even

clusters); “central” (a nucleus that is not associated with either the dorsal or ventral group located in the middle of the myofiber), “clustered” (nuclei remained in a single cluster toward the ventral end of the myofiber), “spread” (nuclei are distributed through the myofiber with no distinct dorsal or ventral clusters) or “swoosh” (nuclei remained in a single cluster within the middle of the myofiber). phenotype and averaged to determine the typical distribution of nuclei in each genotype.

CHAPTER 4

MICROTUBULE NUMBER AND NUCLEUS-NUCLEUS INTERACTIONS UNIQUELY REGULATE NUCLEAR MOVEMENT IN MUSCLE

The content in this chapter was adapted from the following manuscript:

Collins, M.A., Coon, A.L., Thomas, R., Mandigo, T.R., Wynn, E., and Folker, E.S. (2019) Microtubule number and nucleus-nucleus interactions uniquely regulate nuclear movement in muscle. *Under revision at Nature Communications*.

4.1 ABSTRACT

Nuclear movement is a fundamental process of eukaryotic cell biology. Skeletal muscle presents an intriguing model to study nuclear movement because its development requires the precise positioning of multiple nuclei within a single cytoplasm. Furthermore, there is a high correlation between aberrant nuclear positioning and poor muscle function. Although many genes that regulate nuclear movement have been identified, the mechanisms by which these genes act is not known. Using *Drosophila melanogaster* muscle development as a model system, and a combination of live-embryo microscopy and laser ablation of nuclei, we have found that phenotypically similar mutants are based in different molecular disruptions. Specifically, *ensconsin* (*Drosophila* MAP7) regulates the number of growing microtubules that are used to move nuclei whereas *bocksbeutel* (*Drosophila* emerin) and *klarsicht* (*Drosophila* KASH-protein) regulate interactions between nuclei.

4.2 INTRODUCTION

Since the identification of the Linker of Nucleoskeleton and Cytoskeleton (LINC) complex (Crisp et al., 2006; Starr & Fridolfsson, 2010; Tapley & Starr, 2013), the question of how nuclei move has been a pressing question in biology. The process of moving this heavy organelle is conserved throughout evolution in all cell types (Mosley-Bishop et al., 1999; Tran et al., 2001; Starr et al., 2001; Lee et al., 2002; Starr & Han, 2002; Del Bene et al., 2008; Zhang et al., 2009b; Yu et al., 2011), thus magnifying the importance of understanding the underlying mechanism. Although many mechanisms have been

described for mononucleated cells (Gundersen & Worman, 2013), how nuclei are moved in a syncytium has remained a mystery. Many genes that regulate nuclear position in syncytial skeletal muscle cells have been identified (Roman & Gomes, 2018), but how these genes contribute to nuclear movement and whether these genes regulate nuclear positioning through a single mechanism is not known. The limited mechanistic understanding is in part driven by the complexity that many nuclei in a single cytoplasm creates. Furthermore, while many studies investigating myonuclear movement have been done in cell culture (Cadot et al., 2012; Wilson & Holzbaur, 2012), such *in vitro* systems lack the complex signaling cascades that provide directionality cues to nuclei as they translocate, highlighting the importance of studying nuclear movement in an organismal context (Folker et al., 2014). Consequently, most work has relied on describing nuclei as mispositioned with little, if any, distinction between phenotypes (Metzger et al., 2012; Collins & Mandigo et al., 2017; Folker et al., 2012; Elhanany-Tamir et al., 2012). To better understand the mechanisms by which each gene regulates nuclear movement, it is critical to establish methods that can characterize nuclear phenotypes *in vivo* and distinguish between those that appear similar by a basic phenotypic scoring system.

4.3 RESULTS

4.3.1 Disruption of *bocksbeutel* and *klarsicht* have distinct effects on myonuclear positioning compared to *ensconsin* in the *Drosophila* embryo

As a first approach, we have investigated the contributions of *bocksbeutel* (*Drosophila* emerin), *klarsicht* (*Drosophila* KASH-protein), and *ensconsin* (*Drosophila*

MAP7). Each gene was zygotically removed in *Drosophila* embryos with the respective *bocks*^{DP01391} null (Collins & Mandigo et al., 2017), *klar*^{1} null (Welte et al., 1998), or *ens*^{swo} nonsense mutation (Metzger et al., 2012) alleles. Fixed images of *Drosophila* embryos show that in controls, nuclei were in two clusters positioned at either end of the lateral transverse (LT) muscle whereas in *bocks*^{DP01391} and *klar*^{1} embryos, most of the nuclei were clustered together in a single group near the ventral end of the muscle (Fig. 4.1 A), as previously shown (Collins & Mandigo et al., 2017). Qualitatively this clustering phenotype

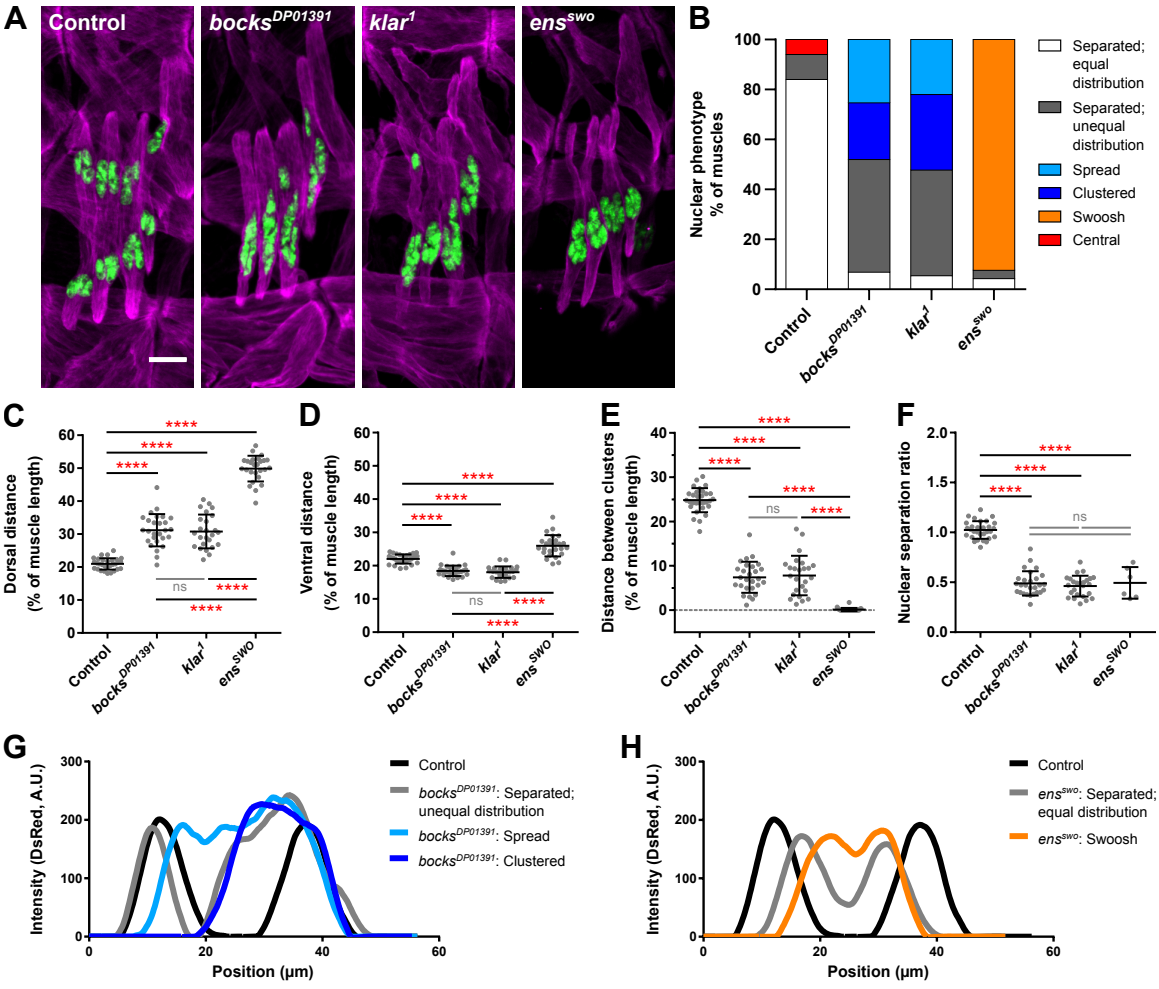

Figure 4.1: *Bocksbeutel*, *klarsicht*, and *ensconsin* regulate myonuclear position in *Drosophila* embryos. (**A**) Immunofluorescence images of the lateral transverse (LT) muscles in one hemisegment from stage 16 (16 hours AEL, after egg lay) embryos for the indicated genotypes. Muscles in magenta, myonuclei in green. Scale bar, 10 µm. (**B**) The frequency at which each nuclear positioning phenotype was observed in each of the indicated genotypes. (**C–F**) Graphs indicating the distance between the dorsal end of the muscle and the nearest nucleus (**C**), the distance between the ventral end of the muscle and the nearest nucleus (**D**), and the distance between the dorsal and ventral clusters of nuclei (**E**). All distances were normalized to the

muscle length. (**F**) The relative size of the dorsal cluster of nuclei compared to the ventral cluster of nuclei. It is important to note that in 21 out of the 27 *ens*^{swo} embryos, there was only one cluster present. Thus, the nuclear separation ratio was only calculated for the 6 embryos that had two distinct clusters. Data points in (C–F) correspond to the average value within a single embryo. Error bars indicate the s.d. from ≥25 embryos for each genotype taken from at least three independent experiments. One-way ANOVA with Tukey HSD post hoc test was used to assess the statistical significance of differences in measurements between all experimental groups. (**G–H**) Averaged linescans of DsRed intensity for each nuclear phenotype observed in *bocks*^{DP01391} mutants (**G**) and *ens*^{swo} mutants (**H**) compared to controls. Position correlates to the length of the muscle. Dorsal end position corresponds to 0 µm.

was similar to nuclear positioning defects observed in *ens*^{swo} embryos in which nuclei also failed to separate into distinct groups, as previously described (Metzger et al., 2012). To quantitatively evaluate myonuclear position, the distance of each nuclear cluster with respect to the dorsal and ventral muscle poles was measured. Since the LT muscles in all three mutants were significantly shorter (Fig. 4.2 A, statistics summarized in Table 4.1, end of Results), we measured the raw distance (Fig. 4.2) and the distance as percent of muscle length (Fig. 4.1). Compared to controls, nuclei in *bocks*^{DP01391} and *klar*^{1} embryos were positioned further from the dorsal muscle pole (Fig. 4.1 C and Fig. 4.2 B) yet closer to the ventral muscle pole (Fig. 4.1 D and Fig. 4.2 C), as previously described (Collins & Mandigo et al., 2017). However, nuclei in *ens*^{swo} embryos were positioned significantly further from both muscle poles when compared to controls or *bocks*^{DP01391} and *klar*^{1} embryos. Additionally, the distance between dorsal and ventral clusters was measured (Fig. 4.1 E and Fig. 4.2 D). The distance between clusters was significantly decreased in *bocks*^{DP01391} and *klar*^{1} embryos because distinct clusters of nuclei formed in only a small fraction of muscles (Fig. 4.2 E). In contrast, since nuclei failed to separate in nearly all *ens*^{swo} muscles, this distance was almost 0 µm. Finally, we measured the area of dorsal and ventral clusters to compare the distribution of nuclei as previously described (Collins & Mandigo et al., 2017). In controls, nuclei were evenly distributed between the two clusters, whereas more nuclei remained associated within the ventral cluster in *bocks*^{DP01391} and

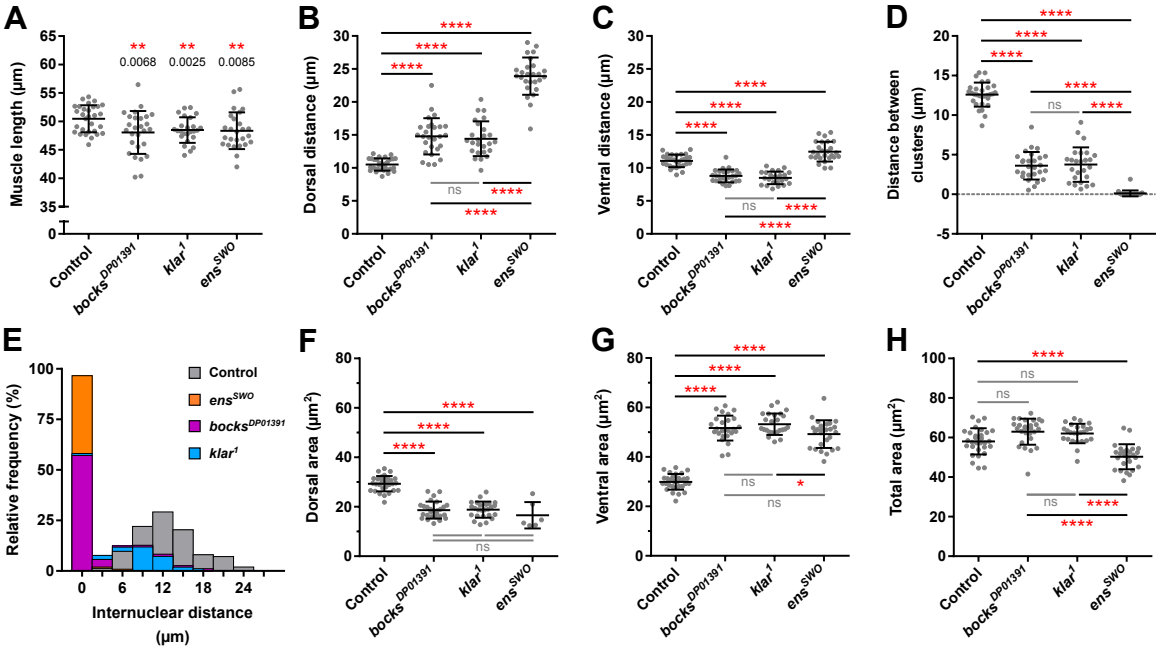

Figure 4.2: *Bocksbeutel*, *klarsicht*, and *ensconsin* are necessary for proper muscle length and myonuclear position in *Drosophila* embryos. (**A**) The average length of the LT muscle for the indicated genotypes. (**B–D**) Graphs indicating the raw distance between the dorsal end of the muscle and the nearest nucleus (**B**), the raw distance between the ventral end of the muscle and the nearest nucleus (**C**), and the raw distance between the dorsal and ventral nuclear clusters (**D**). (**E**) The relative distribution of all internuclear distances measured, represented as raw values. (**F–H**) Graphs indicating the area of nuclei located near the dorsal end of the muscle (**F**), the area of nuclei located near the ventral end of the muscle (**G**), and the total area of all myonuclei present within the muscle (**H**). In 21 out of the 27 *ens*^{swo} embryos, there was only one cluster present. Thus, the dorsal cluster area was only measured in the 6 embryos that had two distinct clusters. Data points in (A–D) and (F–H) correspond to the average value within a single embryo. Error bars indicate the s.d. from ≥25 embryos for each genotype taken from at least three independent experiments. For (**A**) Student's t-test with Welsh's correction was used to assess the statistical significance of differences in measurements between experimental genotypes to controls. For (B–D) and (F–H) One-way ANOVA with Tukey HSD post hoc test was used to assess the statistical significance of differences in measurements between all experimental groups.

klar^{1} embryos, thus significantly decreasing the nuclear separation ratio (Fig. 4.1 F), as previously described (Collins & Mandigo et al., 2017). Similarly, in the rare case in which nuclei separated in *ens*^{swo} embryos, there were more nuclei in the ventral cluster compared to the dorsal cluster. Although the total area occupied by nuclei was similar between controls, *bocks*^{DP01391} and *klar*^{1}, it was significantly reduced in *ens*^{swo} embryos (Fig. 4.2 H). However, the number of nuclei was the same between controls and *ens*^{swo} embryos, indicating that fusion is not affected (Fig. 4.3 A and B). Additionally, the total volume occupied by nuclei is the same in both genotypes (Fig. 4.3 A-C and Supp. Movie 5 and 6).

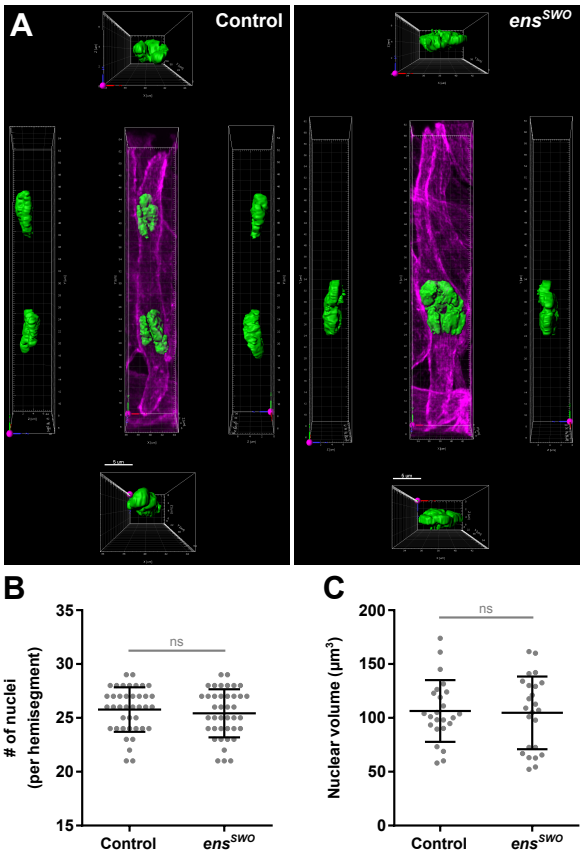

Figure 4.3: Total nuclear volume and number of nuclei are not disrupted in *ensconsin*-depleted embryos. (**A**) Three-dimensional volumetric renderings of nuclear clusters created from Airyscan images of a single LT muscle from stage 16 (16 hours AEL) control and *ens*^{swo} embryos. Muscles in magenta, myonuclei in green. Scale bar, 5 µm. Each rendering showing just the nuclei have been rotated -90° (left) and +90° (right) along the y-axis as well as -90° (bottom) and +90° (top) along the x-axis, relative to the center image. (**B**) The total volume of nuclei within a single LT muscle. Data points correspond to the total volume of nuclei within a single LT muscle. Error bars indicate the s.d. from 24 LT muscles for each genotype measured from six different embryos. Student's t-test with Welsh's correction was used to assess the statistical significance of differences in nuclear volume between *ens*^{swo} embryos and controls. (**C**) The number of nuclei per hemisegment counted from live stage 17 (17 hours AEL) control and *ens*^{swo} embryos. Data points correspond to the total number of nuclei counted within a single hemisegment. Error bars indicate the s.d. from 40 hemisegments for each genotype taken from 10 different embryos. Student's t-test with Welsh's correction was used to assess the statistical significance of differences in the number of nuclei counted from *ens*^{swo} embryos and controls.

Thus, the reduced area is due to nuclei occupying a greater depth in the *ens*^{swo} embryos. Based on these measurements, the most dominant phenotype observed in control embryos was nuclei that separated into two distinct groups of equal size. In *bocks*^{DP01391} and *klar*^{1} embryos, nuclei either remained as a single cluster positioned near the ventral end of the muscle (Fig. 4.1 B and G, "clustered" and "spread") or in two clusters in which the dorsal group was much smaller than the ventral group (Fig. 4.1 B and G, "separated: unequal distribution"). Finally, the most dominant phenotype observed in *ens*^{swo} embryos was single clusters positioned near the center of the muscle (Fig. 4.1 B and H, "swoosh"). In total, these data indicate that while *bocksbeutel*, *klarsicht*, and *ensconsin* are all required for proper nuclear movement, the disruption of *ens* causes a distinct type of nuclear

positioning defect compared to the disruption of *bocks* and *klar* and suggest that these genes may regulate distinct aspects of nuclear movement.

4.3.2 *Ensconsin* is necessary for directional nuclear movement whereas *bocksbeutel and klarsicht* are necessary to separate nuclei

To investigate these phenotypes further, the position of nuclear clusters within the LT muscles was tracked over the course of 2 hours. In control muscles, once all the nuclei separated into two distinct clusters, these clusters migrated toward opposite muscle ends, steadily increasing the distance between themselves (Fig. 4.4 A and Supp. Movie 7, left panel). However, 100% of all nuclei observed in ens^{swo} muscles failed to separate over the time course (Fig. 4.4 A, yellow brackets and Supp. Movie 10, left panel), significantly reducing the separation speed to 0 μm/hr (Fig. 4.4 B and C). Similarly, nuclei that remained associated together in $bocks^{DP01391}$ and $klar^{1}$ muscles also failed to separate (Fig. 4.4 B, blue data points and Supp. Movie 8 and 9, left panels). However, this non-separation phenotype was only observed in about 50% of muscles (Fig. 4.4 C). In the other 50% of muscles, a single nucleus separated and migrated towards the dorsal end of the muscle (Fig. 4.4 A, yellow arrows), at a rate slightly faster than control nuclei (Fig. 4.4 B, gray data points). Furthermore, the morphology of the single clusters was different in $bocks^{DP01391}$ and $klar^{1}$ compared to ens^{swo}. In ens^{swo} clustered nuclei were spherical, whereas nuclear clusters in $bocks^{DP01391}$ and $klar^{1}$ embryos were significantly elongated (Fig. 4.4 D). The trajectory of individual myonuclei within each cluster was also tracked over the 2-hour time course (Fig. 4.4 E). Surprisingly, the displacement of nuclei in $bocks^{DP01391}$ and $klar^{1}$ embryos was similar to nuclei in controls, including those that remain in ventral cluster where more nuclei were present (Fig. 4.4 F and Supp. Movie 7-10, right panels). The

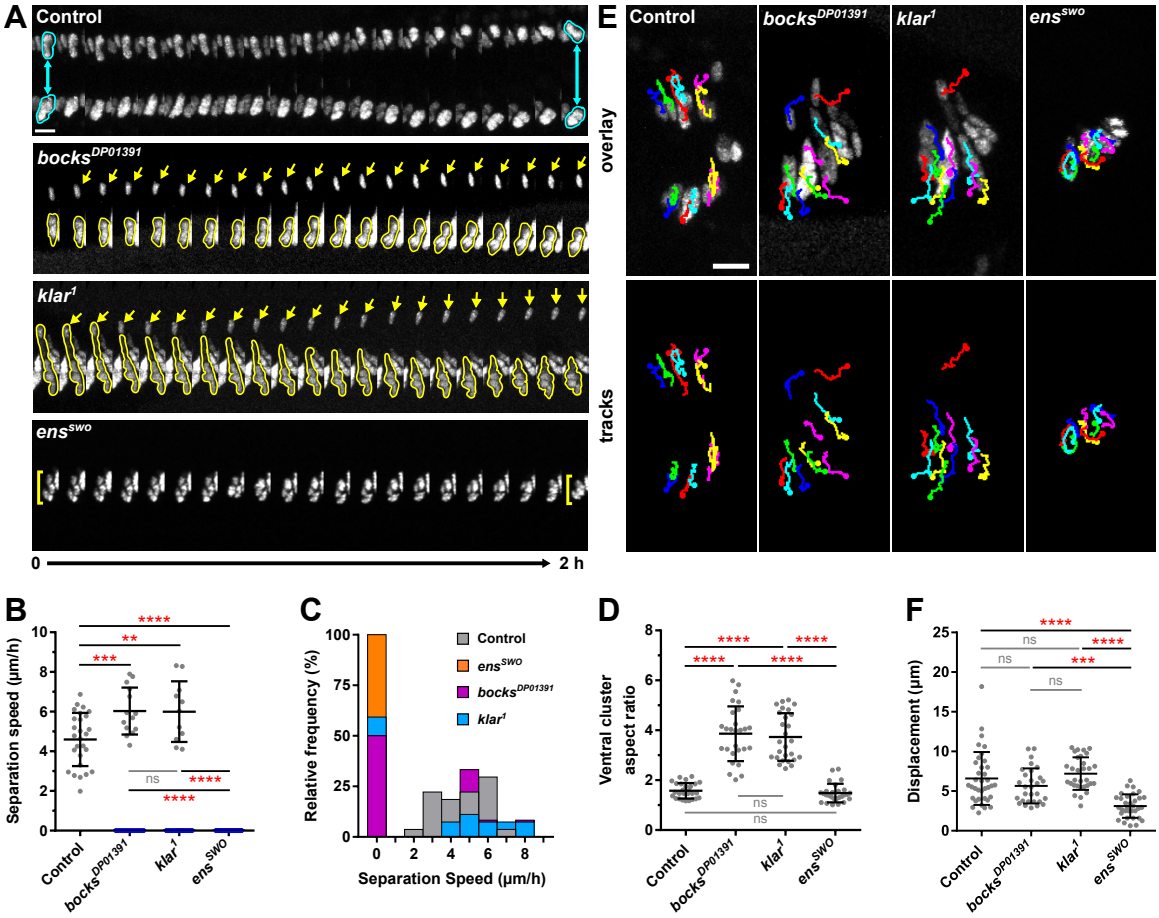

Figure 4.4: *Bocksbeutel*, *klarsicht*, and *ensconsin* are necessary for the proper separation of myonuclei in *Drosophila* embryos. (**A**) Montages from time-lapse acquisitions showing the separation of the dorsal cluster from the ventral cluster of nuclei within a single LT muscle of a stage 15 (15 hours AEL) embryo for the indicated genotypes. Nuclei outlined in cyan indicate the proper separation of nuclei into two distinct clusters (control). Yellow arrows indicate an escaper nucleus that separates from the ventral group in either *bocks*^{DP01391} or *klar*^{1} mutant embryos. Yellow brackets indicate nuclei that fail to separate and remain associated as a single cluster in *ens*^{SWO} mutant embryos. Scale bar, 10 μm. (**B**) The separation speed of nuclear clusters. Data points correspond to the speed measured from a single LT muscle. Gray data points indicate the speed at which the dorsal and ventral clusters of nuclei separate from one another, whereas blue data points indicate nuclei that failed to separate (speed = 0 μm/h). Error bars indicate the s.d. from ≥25 LT muscles for each genotype taken from independent experiments. (**C**) The relative distribution of nuclear separation speeds. (**D**) The aspect ratio of the ventral nuclear cluster measured at 0 h. Data points correspond to the ventral nuclear cluster within a single LT muscle. Error bars indicate the s.d. from ≥25 LT muscles for each genotype taken from independent experiments. (**E**) Tracks following the movement of individual nuclei within four LT muscles over the course of two hours, superimposed over the first frame (t = 0 h). Scale bar, 10 μm. (**F**) The displacement of individual nuclei. Data points correspond to the displacement of a single nucleus. Error bars indicate the s.d. from 36 nuclei for each genotype taken from three independent experiments. For (B), (D), and (F), One-way ANOVA with Tukey HSD post hoc test was used to assess the statistical significance of differences in measurements between all experimental groups.

resulting trajectories of *bocks*^{DP01391} and *klar*^{1} ventral nuclei demonstrate that directional nuclear movement is the same between nuclei that separate from the ventral cluster and migrate dorsally compared to nuclei that fail to separate and remain clustered together.

Conversely, the displacement of nuclei in *ens*^{swo} embryos was significantly decreased, as nuclei rotated within in the cluster but did not translocate. Together these data suggest that in *ens*^{swo} mutants, the ability of the cell to exert force on nuclei is reduced. However, the movement of the nuclei in the *bocks*^{DP01391} and *klar*^{1} suggests that force production is normal and that instead nuclei are being held together in a single cluster. This further suggests that nuclei in the *bocks*^{DP01391} and *klar*^{1} mutants are under tension whereas those in *ens*^{swo} mutants are not.

4.3.3 Laser ablation of myonuclei demonstrates that the application of mechanical tension onto nuclei is *ensconsin*-dependent.

To test whether nuclei were under tension in *bocks*^{DP01391} and *klar*^{1} muscles but not *ens*^{swo}, we used 2-photon laser ablation to remove individual nuclei and measure the response of the neighboring nuclei within the syncytium (Fig. 4.5 A). When a nucleus was ablated in controls (1 s, yellow circle and Supp. Movie 11), the remaining nuclei within the cluster moved away from the ablation site, toward the center of the muscle fiber (Fig. 4.5 D, 2–5 s). Nuclei in the opposite cluster also moved towards the muscle center. However, the nuclei in the neighboring LT muscles did not respond to the ablation. Furthermore, ablation did not affect the health of the muscle or the animal. Three hours after ablation, nuclei returned to their proper position adjacent to the muscle end. Ablation did not affect viability as embryos were able to developmentally progress to stage 17, initiate muscle contraction and hatching (Fig. 4.5 E), and crawl out of the field of view.

We then ablated nuclei in muscles of animals where nuclei had failed to separate into distinct clusters (Fig. 4.6 A). When compared to controls, the area of the ventral

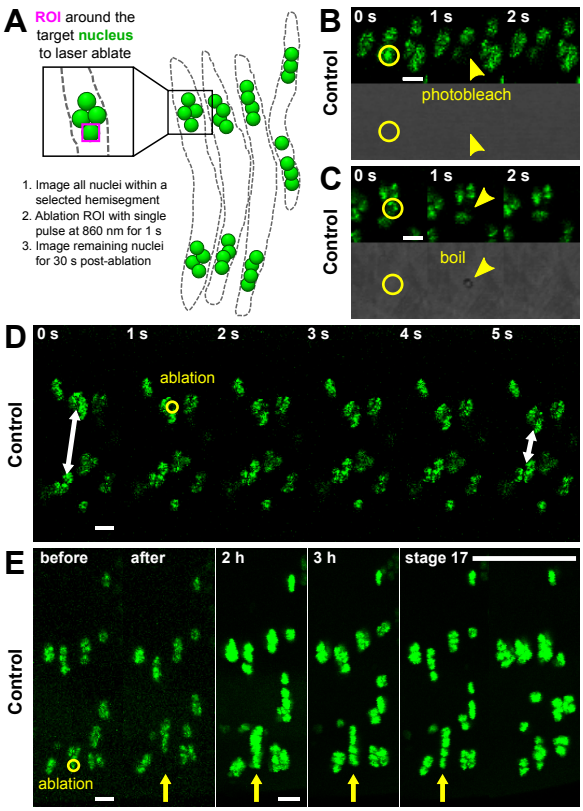

Figure 4.5: *In vivo* 2-photon laser ablation of myonuclei. (**A**) Schematic illustrating how myonuclei are ablated in the LT muscles of a living stage 16 (16 hours AEL) control embryo. Nuclei (green) in the LT muscles (dotted grey outline) are identified by the expression of DsRed. Before ablation, all nuclei within a hemisegment are imaged. The nucleus to be ablated is selected by a region of interest (magenta ROI) and then ablated using a pulsed 2-photon laser at 860 nm for 1 s. The remaining nuclei are then imaged every second for 30 s to observe the post-ablation response. (**B–C**) Montages from time-lapse images showing failed ablation attempts. Nuclei in green, transmitted light in gray. Photobleached nuclei were characterized by just the loss of fluorescence with no subsequent response (**B**) while embryos that were boiled were identified by a hole burned through the membrane (**C**, arrowhead). Scale bar, 5 µm. (**D**) Montage from a time-lapse image showing the ablation of a single nucleus within the LT muscles of a stage 16 control embryo. The first frame shows all the nuclei before the ablation event (0 s). The next frame (1 s) shows the ablation of a single nucleus (yellow circle), followed by the subsequent response of the remaining nuclei present within the cluster after the ablation event (white arrows). (**E**) Still images from a stage 16 embryo that was followed from the time of ablation until stage 17 (last embryonic stage) to demonstrate that ablation does not affect embryonic development or viability. Scale bar, 10 µm.

clusters in *bocks*^{DP01391} (Supp. Movie 12) and *klar*^{1} (Supp. Movie 13) embryos before ablation was significantly larger (Fig. 4.6 B, before). After ablation, the remaining nuclei moved away from the ablation site and showed a 43% reduction in size in both genotypes (Fig. 4.6 B and B' after). The dramatic decrease in size suggests that the stretching of nuclei, in addition to the greater number of nuclei present, contributed to the difference in the size of the clusters. In contrast, nuclei in *ens*^{swo} embryos (Supp. Movie 14) moved only slightly after ablation (Fig. 4.6 A) and their size was reduced by only 10%, a value consistent with the removal of 1 out of 6-7 nuclei (Fig. 4.6 B and B'). In addition, after ablation, clusters in *bocks*^{DP01391} and *klar*^{1} embryos traveled a greater distance compared to controls while clusters in *ens*^{swo} embryos traveled less (Fig. 4.6 C and C'). Similarly, the clusters in *bocks*^{DP01391} and *klar*^{1} had a greater initial velocity compared to controls whereas nuclei in *ens*^{swo} embryos had a reduced initial velocity (Fig. 4.6 D and D'). Together, these

data demonstrate that nuclei in *bocks*^{DP01391} and *klar*^{1} embryos are under more tension than nuclei in controls, while nuclei in *ens*^{swo} embryos are under less tension.

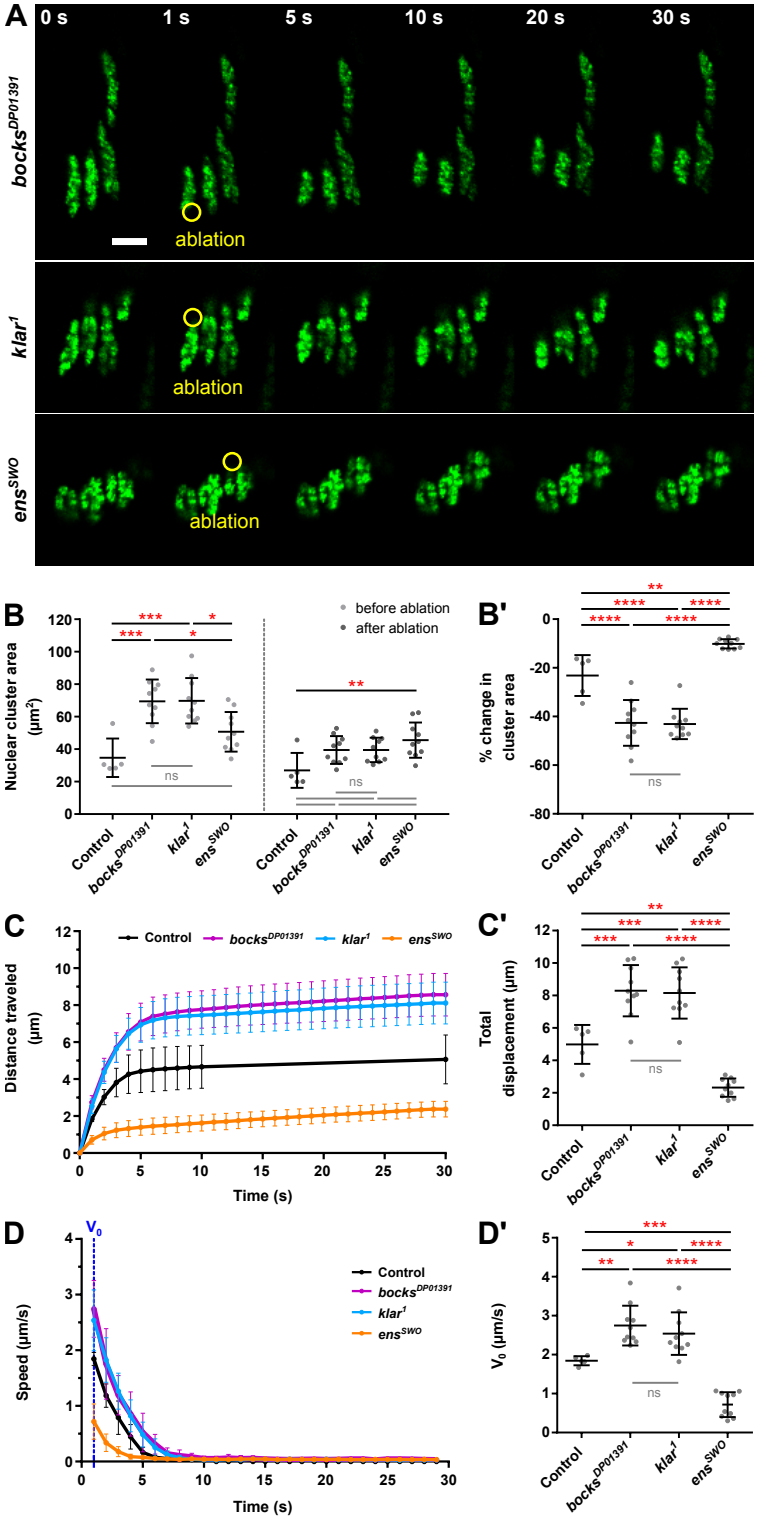

Figure 4.6: Nuclei in *bocksbeutel* and *klarsicht* mutants are under more tension than nuclei in *ensconsin* mutants. (**A**) Montages from time-lapse acquisitions showing the ablation of a myonucleus within the LT muscles of a stage 16 (16 hours AEL) embryo for the indicated genotypes. The first frame shows the nuclei before ablation (0 s). The next frame (1 s) shows the ablation of a single nucleus (yellow circle), followed by the subsequent response of the remaining nuclei after ablation (5-30 s). Scale bar, 10 µm. (**B**) The average area of nuclear clusters before and after ablation. (**B'**) The same data in (B) represented as a percent change in cluster area. A negative change in area indicates that the size of the nuclear cluster decreased after the ablation. (**C**) The average displacement of nuclear clusters after ablation as a function of time. (**C'**) The average total displacement of nuclear clusters after ablation. (**D**) The average change in speed of nuclear clusters after ablation as a function of time. (**D'**) The average initial speed (V0) of nuclear clusters the first second after ablation. Data points in (B–D') correspond to an individual ablation event. Error bars indicate the s.d. from ≥5 ablation events performed in different embryos for each genotype. One-way ANOVA with Tukey HSD post hoc test was used to assess the statistical significance of differences in measurements between all experimental genotypes to controls.

4.3.4 Loss *bocks* and *klar* reorganize MTs while loss of *ens* completely disrupts MT organization and the number of dynamic MTs

Since myonuclei are physically linked to the microtubule cytoskeleton (Tassin et al., 1985; Espigat-Georger et al., 2016), ensconsin is a microtubule binding protein (Bulinski & Bossler, 1994; Gallaud et al., 2014), and nuclear envelope proteins have been demonstrated to impact microtubule organization (Hale et al., 2008; Bugnard et al., 2005; Starr & Fridolfsson, 2010; Gimpel et al., 2017), we hypothesized that the differences in nuclear behaviors may be linked to variations in microtubule organization. We therefore evaluated the organization of the microtubule network in the ventral longitudinal muscle 3 (VL3) of stage L3 larvae (Fig. 4.7 A), which are a large, flat, rectangular muscle group that contain two distinct regions of microtubules that are uniquely organized. The first region pertained to areas of the muscle, distant from nuclei, where microtubules intersect to form a lattice (Fig. 4.7 A, yellow box, and B) while the second region consisted of microtubules that emanate directly from the nuclei and form arrays around the nuclear periphery (Fig. 4.7 A, cyan box, and C). As previously reported (Collins et al., 2017; Elhanany-Tamir et al., 2012), nuclei in $bocks^{DP01391}$ and $klar^{1}$ larvae were mispositioned in a single row along the anterior-posterior axis of the muscle compared to nuclei in controls, which were evenly distributed in two parallel lines. Analysis of the lattice network of microtubules (Fig. 4.7 B) was performed using the Texture Detection Technique (TeDT), which detects the angles at which neighboring microtubules intersect (Liu & Ralston, 2014). In controls, the dominant intersection angles were parallel (0°, 180°, 360°) to the anterior-posterior axis of the muscle (Fig. 4.7 D, average in D'). Microtubules in $bocks^{DP01391}$, $klar^{1}$, and ens^{swo} larval

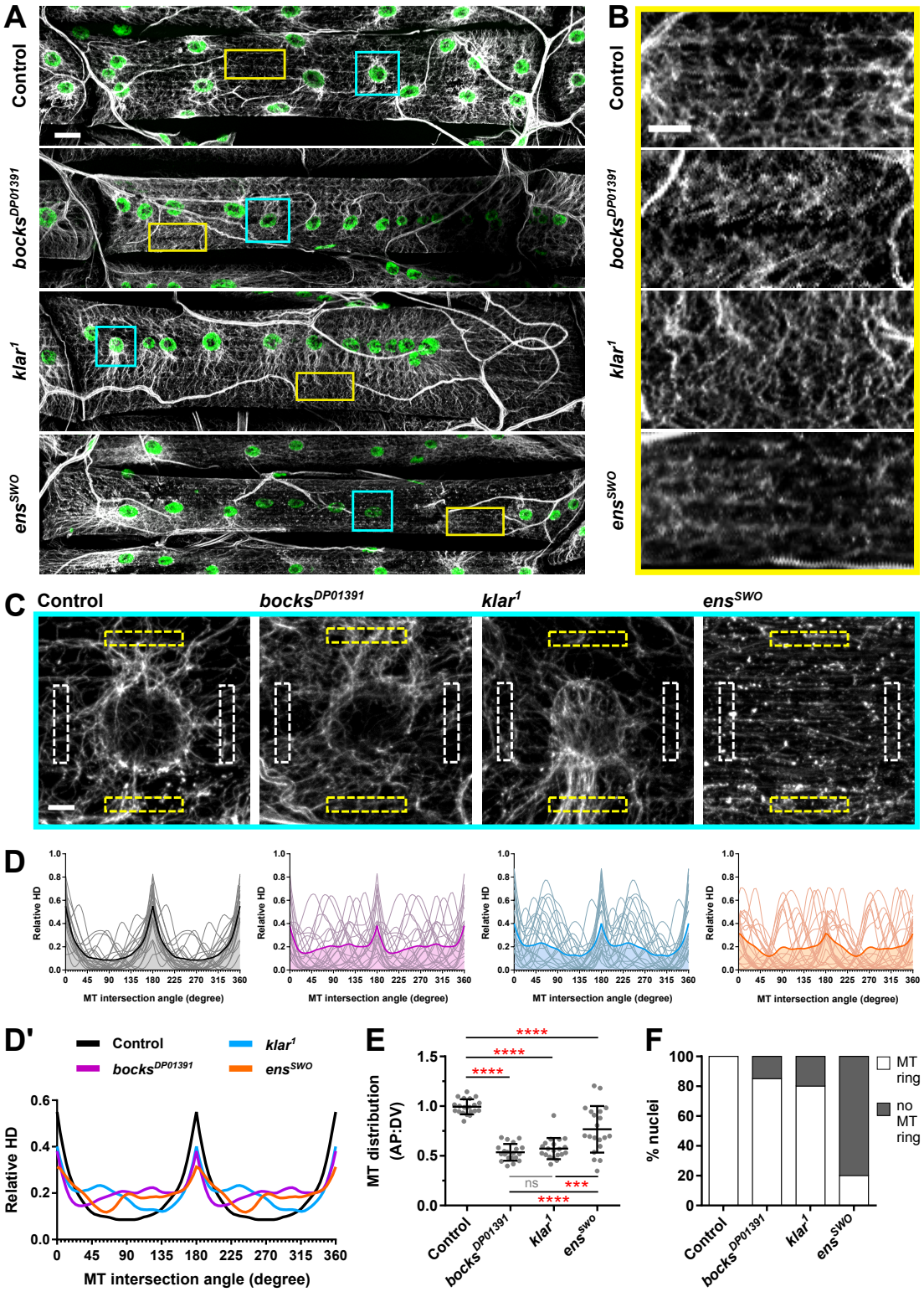

Figure 4.7: *Bocksbeutel*, *klarsicht*, and *ensconsin* disrupt microtubule organization in *Drosophila* larval skeletal muscle. (**A**) Immunofluorescence images of ventral longitudinal muscle 3 (VL3) from stage L3 larvae for the indicated genotypes. Microtubules (α-tubulin) in gray, myonuclei in green. Scale bar, 25 μm. (**B**) Magnified regions of the microtubule lattice taken from the images shown in (A), as indicated by the yellow box. Scale bar, 10 μm. (**C**) Magnified regions of microtubules emanating from myonuclei taken from the images

shown in (A), as indicated by the cyan box. White dotted boxes indicate the location of anterior and posterior fluorescence intensity measurements while yellow dotted boxes indicate the location of dorsal and ventral fluorescence intensity measurements for microtubule polarity analysis. Scale bar, 5 μm. (**D**) TeDT analysis of microtubule lattice regions. Intersection angles are represented as directional histograms (HD) from 0° to 360°. Thin lines indicate TeDT analysis for individual MT lattice regions, while the thick color line indicates the average of 20 MT lattice regions for each genotype. (**D'**) The average TeDT analysis from 20 MT lattice regions as shown in (D) for *bocks*^{DP01391} (purple), *klar*^{1} (blue), and *ens*^{swo} (orange) compared to controls (black). (**E**) The polarity of microtubules around myonuclei, represented as the microtubule distribution ratio for each nucleus. Data points correspond to the microtubule distribution ratio of a single nucleus. Error bars indicate the s.d. from 20 nuclei for each genotype from ≥10 VL3 muscles. One-way ANOVA with Tukey HSD post hoc test was used to assess the statistical significance of differences in measurements between all experimental groups. (**F**) The frequency in which microtubule rings were observed around nuclei in each of the indicated genotypes. A total of 20 nuclei were analyzed for each genotype from ≥10 VL3 muscles.

muscles were highly disorganized, with an overall reduction in the frequency of microtubules intersecting at every 180° (Fig. 4.7 D').

To evaluate the organization of microtubules that extend off of nuclei, we counted the percentage of nuclei that have a dense ring of microtubules on the nuclear periphery (Fig. 4.7 F) and measured the proportion of microtubules on the dorsal-ventral axis of the muscle versus the anterior-posterior axis (Fig. 4.7 E). In controls, all nuclei had a ring of microtubules and the distribution ratio was close to 1.0, indicating that microtubules are uniformly emanating from nuclei. 85% of *bocks*^{DP01391} and 80% of *klar*^{1} nuclei had a ring of microtubules (Fig. 4.7 F) and the distribution ratio was reduced to 0.535 and 0.572 in *bocks*^{DP01391} and *klar*^{1} larvae respectively (Fig. 4.7 E), indicating that more microtubules are extending along the dorsal-ventral axis compared to the anterior-posterior axis. Only 20% of nuclei in *ens*^{swo} mutants had rings and there was a wide distribution in the proportion of microtubules on the dorsal-ventral and anterior-posterior axes compared to both controls, *bocks*^{DP01391} and *klar*^{1} mutants. Together, these data indicate that although *bocksbeutel*, *klarsicht*, and *ensconsin* are necessary to maintain the link between myonuclei and microtubules, the disruption of *bocks* or *klar* results in the reorganization of microtubules around mispositioned nuclei whereas the loss of *ens* completely disrupts the general organization of microtubules throughout the muscle.

Our finding that microtubule organization is dependent on ensconsin differs from previous studies that suggested that the function of ensconsin was only to activate Kinesin (Barlan et al., 2013). To determine whether the disruption in microtubule organization was a consequence of mispositioned nuclei or a contributor to nuclear movement, we examined the behavior of EB1 during embryonic muscle development when nuclei are actively moving. EB1 comets were tracked for 1 minute in the LT muscles (Supp. Movie 15 and 16) and the dorsal oblique (DO) muscles (Supp. Movie 17 and 18), a set of broad, flat muscles, which make them more amenable to fast, live-embryo imaging (Fig. 4.8 A). The

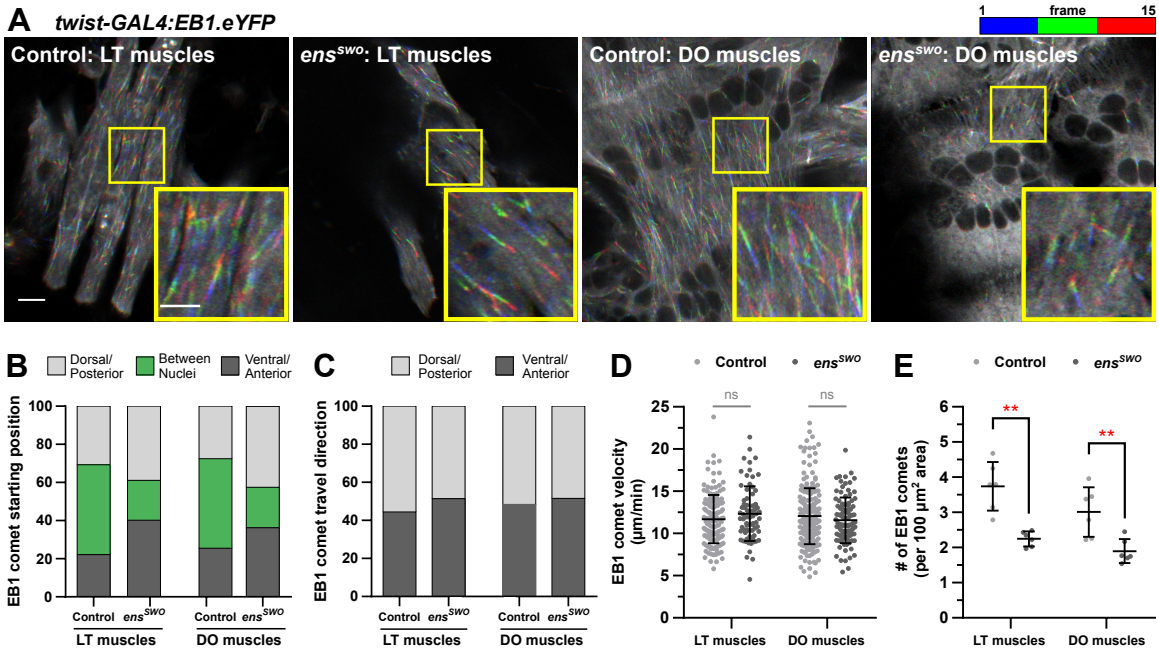

Figure 4.8: Depletion of *ensconsin* decreases the number of EB1 comets in *Drosophila* embryonic muscles. (**A**) Temporal overlays tracking EB1 comets for 15 s in the lateral transverse (LT) muscles and dorsal oblique (DO) muscles of stage 16 control and ensswo embryos. Scale bar, 5 μm. (inset in yellow box) Magnified regions of the temporal overlays tracking EB1 comets for 15 s. Scale bar, 3 μm. (**B**) The frequency of EB1 comets observed in controls and ensswo muscles starting in the dorsal/posterior muscle pole region, ventral/anterior muscle pole region, or the region between nuclei. (**C**) The frequency of EB1 comets observed in controls and ensswo muscles traveling either toward the dorsal/posterior muscle pole or the ventral/anterior muscle pole. (**D**) The average velocity of EB1 comets in controls and ensswo muscles. Data points correspond to the velocity measured from a single EB1 comet. Error bars indicate the s.d. from EB1 comets measured from 6 different embryos for each muscle group taken from independent experiments. (**E**) The average number of EB1 comets counted in controls and ensswo muscles, normalized to the muscle area. Data points correspond to the total number of EB1 comets counted from a single embryo. Error bars indicate the s.d. from 6 different embryos for each muscle group taken from independent experiments. For (D) and (E), Student's t-test with Welsh's correction was used to assess the statistical significance of differences in measurements between ensconsin-depleted embryos and controls for each muscle group.

location from which EB1 emerged, their direction of travel, and their speed was the same in controls and *ens*^{swo} embryos in both muscle types (Fig. 4.8 B-D). However, the number of EB1 comets was significantly decreased in both LT and DO muscles of *ens*^{swo} embryos (Fig. 4.8 E). Because most microtubules emanate from the nuclei in *Drosophila* larval muscles, the decrease in microtubule number (Fig. 4.8 E) is consistent with the decreased percentage of nuclei with microtubule rings (Fig. 4.8 F) and a role for ensconsin in maintaining the general organization of microtubules within skeletal muscles.

	Genotype Comparisons					
Statistical Analysis	**control vs. *bocks*^{DP01391}**	**control vs. *klar*^{1}**	**control vs. *ens*^{SWO}**	***bocks*^{DP01391} vs. *klar*^{1}**	***bocks*^{DP01391} vs. *ens*^{SWO}**	***klar*^{1} vs. *ens*^{SWO}**
Figure 4.1 (One-way ANOVA with Tukey HSD post hoc test)						
4.1 C: Dorsal distance (%)	**< 0.0001**	**< 0.0001**	**< 0.0001**	0.9858	**< 0.0001**	**< 0.0001**
4.1 D: Ventral distance (%)	**< 0.0001**	**< 0.0001**	**< 0.0001**	0.8985	**< 0.0001**	**< 0.0001**
4.1 E: Internuclear distance (%)	**< 0.0001**	**< 0.0001**	**< 0.0001**	0.9685	**< 0.0001**	**< 0.0001**
4.1 F: Nuclear separation ratio	**< 0.0001**	**< 0.0001**	**< 0.0001**	0.8120	0.9995	0.9142
Figure 4.2 (*Student's t-test with Welsh's correction; One-way ANOVA with Tukey HSD post hoc test)						
4.2 A: Muscle length*	**0.0068**	**0.0024**	**0.0085**	N/A	N/A	N/A
4.2 B: Dorsal distance (µm)	**< 0.0001**	**< 0.0001**	**< 0.0001**	0.9462	**< 0.0001**	**< 0.0001**
4.2 C: Ventral distance (µm)	**< 0.0001**	**< 0.0001**	**< 0.0001**	0.7650	**< 0.0001**	**< 0.0001**
4.2 D: Internuclear distance (µm)	**< 0.0001**	**< 0.0001**	**< 0.0001**	0.9878	**< 0.0001**	**< 0.0001**
4.2 F: Dorsal area	**< 0.0001**	**< 0.0001**	**< 0.0001**	0.9980	0.5315	0.4700
4.2 G: Ventral area	**< 0.0001**	**< 0.0001**	**< 0.0001**	0.6108	0.2171	**0.0123**
4.2 H: Total area	0.0519	0.0888	**< 0.0001**	0.9477	**< 0.0001**	**< 0.0001**
Figure 4.3 (Student's t-test with Welsh's correction)						
4.3 B: # of nuclei	N/A	N/A	0.4689	N/A	N/A	N/A
4.3 C: Nuclear volume	N/A	N/A	0.8487	N/A	N/A	N/A
Figure 4.4 (One-way ANOVA with Tukey HSD post hoc test)						
4.4 B: Separation speed	**0.0003**	**0.0029**	**< 0.0001**	0.9957	**< 0.0001**	**< 0.0001**
4.4 D: Ventral cluster aspect ratio	**< 0.0001**	**< 0.0001**	0.9728	0.9200	**< 0.0001**	**< 0.0001**
4.4 F: Displacement	0.3952	0.7351	**< 0.0001**	0.0655	**< 0.0001**	**< 0.0001**
Figure 4.6 (One-way ANOVA with Tukey HSD post hoc test)						
4.6 B: Nuclear cluster area (before)	**0.0002**	**0.0002**	0.1347	>0.9999	**0.0155**	**0.0134**
4.6 B: Nuclear cluster area (after)	0.0861	0.0851	**0.0050**	>0.9999	0.4740	0.4783
4.6 B': % change in cluster area	**<0.0001**	**<0.0001**	**0.0081**	0.9989	**<0.0001**	**<0.0001**
4.6 C': Total cluster displacement	**0.0004**	**0.0006**	**0.0044**	0.9954	**<0.0001**	**<0.0001**
4.6 D': Initial velocity (V_0)	**0.0039**	**0.0342**	**0.0003**	0.7175	**<0.0001**	**<0.0001**
Figure 4.7 (One-way ANOVA with Tukey HSD post hoc test)						
4.7 E: MT Distribution (AP:DV)	**< 0.0001**	**< 0.0001**	**< 0.0001**	0.8361	**<0.0001**	**0.0002**
Figure 4.8 (Student's t-test with Welsh's correction)						
4.8 D: EB1 comet velocity (LT muscles)	N/A	N/A	0.4296	N/A	N/A	N/A
4.8 D: EB1 comet velocity (DO muscles)	N/A	N/A	0.5967	N/A	N/A	N/A
4.8 E: # of EB1 comets (LT muscles)	N/A	N/A	**0.0024**	N/A	N/A	N/A
4.8 E: # of EB1 comets (DO muscles)	N/A	N/A	**0.0094**	N/A	N/A	N/A

Table 4.1: Summary of P-values. The following scale was used to determine statistical significance: not significant (ns) ≥ 0.05, *P<0.05, **P<0.01, ***P<0.001, ****P<0.0001, N/A not applicable.

4.4 DISCUSSION

All together, these data demonstrate that nuclear movement in a muscle syncytium requires both the transmission of force from the cytoskeleton to the nucleus and the separation of nuclei from their neighbors (Fig. 4.9). Disruption of these two separate processes produces superficially similar nuclear positioning phenotypes, but careful analysis of the precise position, shape, and movement of nuclei clearly indicates that there are distinct molecular underpinnings. Consistent with this, we found that loss of ensconsin contributes to the application of force to nuclei by regulating the number of growing microtubules. Surprisingly, force was applied to nuclei in the absence of the KASH-domain protein klarsicht or the emerin homolog bocksbeutel. Consequently, nuclei moved a similar total distance to those nuclei in control embryos. However, nuclei remained attached rather

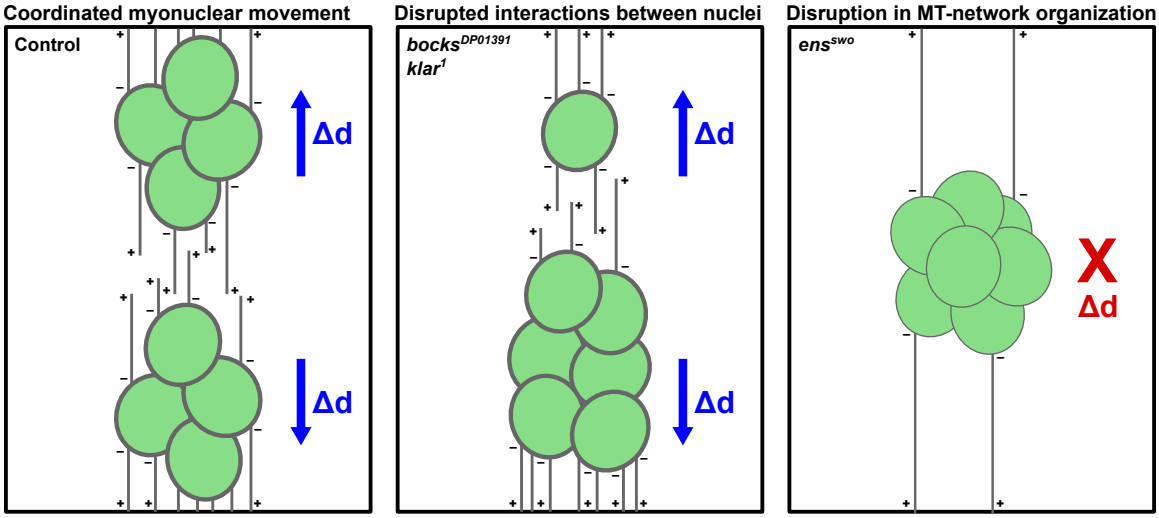

Figure 4.9: Model of myonuclear movement during *Drosophila* embryonic muscle development. In skeletal muscle, the active translocation of myonuclei (green) is dependent on the integrity of the nuclear envelope and the organization of the microtubule cytoskeleton. To achieve proper nuclear positioning, the two nuclear envelope proteins, bocksbeutel and klarsicht, facilitate the separation and distribution of nuclei into two distinct clusters of equal size by relieving associative interactions between neighboring nuclei. Since each myonucleus acts as a local microtubule organizing center, microtubules (gray) nucleate from the nuclear periphery (minus ends, −) and extend out (plus ends, +) to the cell cortex. These microtubules are able to generate force to pull their attached nuclei via ensconsin, which maintains the organization of the MT-network and promotes the sliding of adjacent microtubules. As a result of the coordinated actions of these proteins, nuclei are pull to the end of the muscle before achieving their final position. Blue arrows denote the direction of net displacement (Δd) of nuclei.

than separating and therefore were all moved toward the ventral end of the muscle. Interestingly in *bocks*^{DP01391} and *klar*^{1} mutants, nuclei did rarely separate from the single cluster and move as individuals to the dorsal end of the muscle. This observation is consistent with the phenotype being based in aberrant associations between nuclei and not a disruption of directional cues. Finally, we use laser ablation of individual nuclei to demonstrate that nuclei in *bocks*^{DP01391} and *klar*^{1} mutants are under increased tension compared to controls whereas those in *ens*^{swo} mutants are under decreased tension compared to controls to confirm that force is applied to nuclei in *bocks*^{DP01391} and *klar*^{1} mutants but not in *ens*^{swo} mutants. More broadly, these data present the first direct evidence that regulation of interactions between nuclei is a critical determinant of nuclear movement and that nucleus-nucleus interactions are LINC complex-dependent. Thus, these data raise the possibility that aligned nuclei in the center of a developing or regenerating muscle are physically linked and that this linkage is critical for nuclear functions.

4.5 MATERIAL & METHODS

4.5.1 *Drosophila* genetics

All stocks were grown under standard conditions at 25°C. Stocks used were apRed (Richardson et al., 2007), *bocks*^{DP01391} (Bloomington *Drosophila* Stock Center, 21846), *klar*^{1} (Bloomington *Drosophila* Stock Center, 3256), *ens*^{swo} (Metzger et al., 2012), and UAS-EB1.eYFP (Rogers et al., 2008). Mutants were balanced and identified using *TM6b*, *DGY*. The UAS-EB1.eYFP construct was specifically expressed in the mesoderm using the *twist-GAL4, apRed* driver. Flies carrying *apRed* express a nuclear localization signal (NLS)

fused to the fluorescent protein DsRed downstream of the *apterous* mesodermal enhancer. This results in the specific labeling of the myonuclei within the lateral transverse muscles of the *Drosophila* embryo (Richardson et al., 2007). Thus, only nuclei within the LT muscles are labeled using this reporter. The *twist-GAL4, apRed Drosophila* line was made by recombining the *apRed* promoter and the specific GAL4 driver, with both elements on the second chromosome.

4.5.2 Immunohistochemistry

Embryos were collected at 25°C and washed in 50% bleach to remove the outer chorion membrane, washed with water, and then fixed in 50% formalin (Sigma, Product # HT501128) diluted in 1:1 heptane for 20 minutes. Embryos were then devitellinized by vortexing in a 1:1 methanol:heptane solution. Primary antibodies for embryo staining were used at the following final dilutions: rabbit anti-DsRed (1:400, Clontech 632496), rat anti-tropomyosin (1:200, Abcam ab50567), mouse anti-GFP (1:50, Developmental Studies Hybridoma Bank GFP-G1). The conjugated fluorescent secondary antibodies used were Alexa Fluor 555 donkey-anti-rabbit (1:200), Alexa Fluor 488 donkey-anti-rat (1:200), and Alexa Fluor 647 donkey-anti-mouse (1:200) (all Life Technologies). Larvae at stage L3 were dissected as previously described (Collins & Mandigo et al., 2017; Auld et al., 2018). In brief, larvae were dissected in ice-cold PIPES dissection buffer containing 100 mM PIPES (Sigma-Aldrich, P6757), 115 mM D-Sucrose (Fisher Scientific, BP220-1), 5 mM Trehalose (Acros Organics, 182550250), 10 mM Sodium Bicarbonate (Fisher Scientific, BP328-500), 75 mM Potassium Chloride (Fisher Scientific, P333-500), 4 mM Magnesium Chloride (Sigma-Aldrich, M1028) and 1 mM EGTA (Fisher Scientific, 28-071-G), then fixed with 10% formalin (Sigma-Aldrich, HT501128). For larval staining, mouse anti-

αTubulin (1:200, Sigma-Aldrich T6199) was used. Acti-stain 555 phalloidin (1:400, Cytoskeleton PHDH1-A) and Hoechst 33342 (1 μg/ml) were added with the fluorescent secondary antibody Alexa Fluor 488 donkey-anti-mouse (1:200, Life Technologies). Both embryos and larvae were mounted in ProLong Gold (Life Technologies, P36930).

4.5.3 Analysis of nuclear position in *Drosophila* embryos

Embryos at stage 16 were selected to be imaged based on overall embryo shape, the intensity of the apRed and tropomyosin signals, gut morphology, and the morphology of the trachea as previously described (Folker et al., 2012; Collins & Mandigo et al., 2017; Auld et al., 2018). Confocal z-stacks of fixed embryos were acquired on a Zeiss 700 LSM using a Plan-Apochromat 40×, 1.4 NA oil objective with a 1.0× optical zoom. Images were processed as maximum intensity projections and oriented such that top is dorsal, bottom is ventral, left is anterior, and right is posterior. Muscle length measurements were taken starting from the dorsal tip and following through the center of each LT muscle, down to the ventral tip. Dorsal and ventral end distances were taken from each LT muscle by measuring the distance between the closest group of nuclei to the dorsal or ventral muscle pole, respectively. Internuclear distances were taken by measuring the shortest distance in between the dorsal and ventral clusters of nuclei within each LT muscle. Internuclear distances were also plotted according to relative frequency. All three measurements are reported as distances normalized to the muscle length (Fig. 4.1) and as raw values (Fig. 4.2). All four LT muscles were measured in four hemisegments from each embryo. Statistical analysis was performed with Prism 4.0 (GraphPad).

4.5.4 Analysis of nuclear cluster area in *Drosophila* embryos

Area of nuclear clusters were measured in fixed stage 16 embryos as previously described (Collins & Mandigo et al., 2017). In brief, the area of each cluster of nuclei near either the dorsal or ventral muscle pole was measured in Fiji (Schindelin et al., 2012). Total area of nuclear clusters in each LT muscle was calculated by adding the dorsal and ventral areas. The nuclear separation ratio was calculated by dividing the area of the dorsal cluster by the area of the ventral cluster. Nuclear clusters from all four LT muscles were measured in four hemisegments from each embryo. Statistical analysis was performed with Prism 4.0 (GraphPad).

For qualitative nuclear phenotype analysis, embryos were scored on how nuclei were positioned within the first three LT muscles of each hemisegment. LT 4 was excluded for this analysis due to its variable muscle morphology. Nuclear phenotypes were categorized as either "separated; equal distribution" (nuclei properly segregated into two distinct, even clusters with a nuclear separation ratio ≥ 0.85 and ≤ 1.15), "separated; unequal distribution" (nuclei that segregated into two disproportionate clusters with a nuclear separation ratio < 0.85 or > 1.15), "central" (a nucleus that is not associated with either the dorsal or ventral group located in the middle of the myofiber), "clustered" (nuclei remained in a single cluster toward the ventral end of the myofiber), "spread" (nuclei are distributed through the myofiber with no distinct dorsal or ventral clusters) or "swoosh" (nuclei remained in a single cluster within the middle of the myofiber). Linescans of DsRed intensity were performed on 10 LT muscles for each nuclear phenotype and averaged to determine the typical distribution of nuclei in $bocks^{DP01391}$ and ens^{swo} genotypes compared to controls.

4.5.5 Volumetric imaging and analysis of nuclear clusters

Fixed stage 16 embryos were imaged on a Zeiss LSM 880 with Airyscan (super resolution acquisition, 2x Nyquist sampling) using a Plan-Apochromat 40×, 1.3 NA oil objective at a 1.0× optical zoom and 0.15 µm step size interval through the entire depth of the muscle. Post processing of Airyscan images was completed in ZEN Blue 2016 software. Quantitative volumetric analysis was performed in Imaris version 9.2.1 (Bitplane AG). Images were first processed as maximum intensity projections of confocal z-stacks and oriented such that top is dorsal, bottom is ventral, left is anterior, and right is posterior. A volumetric rendering of each nuclear cluster was created using the Surface Visualization tool of the DsRed channel. Volume measurements were automatically computed from the Surface renderings by Imaris. Statistical analysis was performed with Prism 4.0 (GraphPad).

4.5.6 Live-embryo imaging and analysis

Movies were processed in Fiji (Schindelin et al., 2012) as maximum intensity projections of confocal z-stacks and corrected for drift using the Correct 3D drift plugin. To calculate the separation speed of nuclei, the Line tool was used to measure the distance between dorsal and ventral nuclear clusters at time 0 h and again at time 2 h. Separation speeds were also plotted according to relative frequency. The aspect ratio of ventral clusters was measured at time 0 h using the Shape Descriptors plugin, which calculates aspect ratio of an ellipse by dividing the major axis of the ellipse by its minor axis. An aspect ratio value closer to 1 indicates a more spherical cluster. Tracks following the movement of individual nuclei within clusters were generated using the Manual Tracking plugin. The

displacement of each nucleus was calculated as the difference between the final and initial position. Statistical analysis was performed with Prism 4.0 (GraphPad).

To assess for potential fusion defects, the number of nuclei in the LT muscles was counted from live stage 17 embryos when nuclei have separated and maximized their distance from their neighbors. Nuclei within the LT muscles were identified by expression of DsRed. The number of nuclei were counted from all 4 LT muscles within a single hemisegment, with a total of 4 hemisegments analyzed for each embryo.

4.5.7 2-photon ablation of nuclei

Embryos were collected at 25°C and were washed in 50% bleach to remove the outer membrane, washed with water, and mounted with halocarbon oil (Sigma, Product # H8898). Stage 16 embryos were selected for ablation based on gut morphology, the position of nuclei, and the intensity of the apRed signal as previously described (Folker et al., 2012; Collins & Mandigo et al., 2017; Auld et al., 2018). Time-lapse images of embryos before, during, and after ablation were acquired on a Zeiss 710 LSM using a Plan-Apochromat 40×, 1.1 NA water objective with a 1.0× optical zoom. Ablation was performed using the Coherent Chameleon Ultra II femtosecond pulsed-IR laser at 860 nm with 15-17% laser power. As shown in Figure 4.5, a nucleus was selected for ablation by drawing a region of interest (ROI) in ZEN Black 2012 software. For each ablation time-lapse, the first frame (time = 0 s) was taken before the ablation event. The next frame (time = 1 s), shows the ablation of the targeted nucleus, followed by the subsequent response of the remaining nuclei present. Since no muscle marker is present, imaging with transmitted light was used to ensure that ablation did not destroy the surrounding tissue. An ablation was considered successful by the loss of the DsRed signal accompanied by the movement

of nuclei. Nuclei that were simply photobleached were characterized by just the loss of DsRed fluorescence without any subsequent response from the embryo (Fig. 4.5 B). A failed ablation attempt that resulted in boiling of the embryo was identified by a hole burned through the membrane (Fig. 4.5 C, arrowhead), as seen through the transmitted light channel.

Movies were processed in Fiji (Schindelin et al., 2012) as single confocal slices and oriented such that top is dorsal, bottom is ventral, left is anterior, and right is posterior. The area of clusters in which a nucleus was ablated was measured before and after the ablation event. The area of nuclear clusters before and after ablation were plotted as a percentage change. The displacement and velocity of nuclear clusters were measured using the centroid measurement, which calculates the center point of a cluster based on the average x and y coordinates of all pixels in the cluster. The total displacement of each cluster was calculated as the cumulative distance traveled over the 30 s after ablation. The initial velocity was defined as the speed a cluster traveled the first second after ablation. Statistical analysis was performed with Prism 4.0 (GraphPad).

4.5.8 Analysis of microtubule organization in *Drosophila* larvae

Confocal z-stacks of dissected stage L3 larvae were acquired on a Zeiss 700 LSM using a Plan-Apochromat 40×, 1.4 NA oil objective lens at a 0.5× optical zoom for whole muscle images and at a 2.0× optical zoom for regions around myonuclei. Images were processed as maximum intensity projections and oriented such that top is dorsal, bottom is ventral, left is anterior, and right is posterior. Microtubule organization was assessed in two distinct regions of interest within the ventral longitudinal muscle 3 (VL3). The first region consists of microtubules that intersect at regions between nuclei to form a lattice. For these

regions, the Texture Detection Technique (TeDT) was used (Liu & Ralston, 2014). TeDT is a robust tool that can assess the orientation of the microtubule network by detecting the dominant angles at which microtubules intersect one another. For TeDT analysis, 200 x 100 square pixel regions of the microtubule lattice that excluded nuclei were cropped from whole muscle images. TeDT analysis on cropped regions was performed in MATLAB (MathWorks) which presented the resulting intersection angles detected as directional histograms (HD) from 0° to 360°.

The second region of interest were microtubules emanating directly from the myonuclei. Polarity of these microtubules was analyzed as previously described (Collins & Mandigo et al., 2017). The fluorescence intensity was measured from a 10 μm x 2 μm region positioned 15 μm anteriorly and 15 μm posteriorly from the center of the nucleus, using the Plot Profile tool in Fiji (Schindelin et al., 2012). Similarly, the fluorescence intensity was also measured from a 2 μm x 10 μm region positioned 15 μm dorsally and 15 μm ventrally from the center of the nucleus. Average fluorescence intensities were calculated for the anterior/posterior (AP) positions as well as the dorsal/ventral (DV) positions. A ratio between the average AP and DV fluorescence intensities was used to determine the microtubule distribution ratio. A value of 1 indicates a uniform distribution of microtubules around the nucleus. Values >1 indicate there are more microtubules distributed within the anterior/posterior regions relative to the nucleus, while values <1 indicate there are more microtubules distributed within the dorsal/ventral regions relative to the nucleus. Organization of microtubules emanating from nuclei was also qualitatively assessed based on the presence of a dense microtubule ring around the nuclear periphery. Images of nuclei were blindly scored for the presence or absence of a microtubule ring. A

nucleus was considered to have a microtubule ring based on the contiguous presence of α-tubulin intensity around the perimeter of the nucleus. Statistical analysis was performed with Prism 4.0 (GraphPad).

4.5.9 Analysis of microtubule dynamics in *Drosophila* embryos

Embryos for live imaging of EB1 comets were collected and prepared similarly. Stage 16 embryos were selected for imaging based on gut morphology, the position of nuclei, and the intensity of the apRed signal as previously described (Folker et al., 2012; Collins & Mandigo et al., 2017; Auld et al., 2018). Time-lapse images of EB1-eYFP were acquired on a Zeiss LSM 880 with Airyscan Fast mode (super resolution acquisition, 2x Nyquist sampling) using a Plan-Apochromat 40×, 1.3 NA oil objective at a 4.0× optical zoom at an acquisition rate of 1 s/frame for 1 min. Post processing of Airyscan Fast images was done in ZEN Blue 2016 software. EB1 comets were imaged within the LT muscles as well as the dorsal oblique (DO) muscles, which are a flatter muscle group, ideal for imaging quick dynamics. Movies were processed as single confocal slices in Fiji (Schindelin et al., 2012). Time-lapse images taken in the LT muscles were oriented such that top is dorsal, bottom is ventral, left is anterior, and right is posterior. Time-lapse images taken in the DO muscles were oriented such that top is posterior, bottom is anterior, left is dorsal, and right is ventral. Trajectories of EB1 comets were made from time-lapse images using the Temporal-Color Code plugin, which sums up the first 15 consecutive frames (1 s each), and then overlays the resulting image to a blue-green-red color sequence, with each color representing a total of 5 seconds. All quantifications of EB1 dynamics was performed on temporal overlays by hand. Only comets that were visible for the full 15 seconds were used in this analysis. The starting position of each comet was categorized within the LT muscles

as either starting within the dorsal pole region, ventral pole region, or between nuclei. Similarly, the starting position of each comet was categorized within the DO muscles as either starting within the anterior pole region, posterior pole region, or between nuclei. The direction of EB1 comets was also determined as either traveling dorsally/posteriorly or ventrally/anteriorly and whether the comets move toward or away from the nearest myotendinous junction. The length of EB1 trajectories over the 15 s timeframe was measured to calculate EB1 comet velocity over the 1 min time-lapse. The number of EB1 comets was counted and normalized to the muscle area. Statistical analysis was performed with Prism 4.0 (GraphPad).

CHAPTER 5

DISCUSSION

5.1 SUMMARY & SIGNIFICANCE

The aim of this thesis is to offer novel insights into the mechanisms that regulate myonuclear movement, within the context of muscle development and disease. Data presented in this thesis not only advances our current understanding about how nuclei move during myogenesis, but also demonstrates the powerful advantages of using *Drosophila* skeletal muscle as an *in vivo* model system to study this dynamic process.

5.1.1 Attractive and repulsive nucleus-nucleus interactions are regulated by disease-specific mechanisms

Chapter 2 investigates the different mechanisms by which nuclear positioning is disrupted in two muscle diseases, Emery-Dreifuss muscular dystrophy and Centronuclear myopathy. First, we show that genes linked to EDMD and CNM do regulate nuclear positioning in *Drosophila* embryonic muscles. Of all the genes tested, the position of nuclei becomes severely aberrant when either *Amphiphysin* (a CNM-linked gene) or *bocksbeutel*, and *klarsicht* (two EDMD-linked genes) are disrupted. However, we go on to demonstrate that the resulting nuclear phenotypes differ significantly from one another. Disruption in *Amph* causes nuclei to be mispositioned within the center of myofibers. Conversely, disruptions in either *bocks* or *klar* blocks the separation of nuclei into two distinct and evenly-sized clusters. From this data, we proposed that there are attractive and repulsive

interactions that exist between myonuclei. Our hypothesis is supported by live-embryo time-lapse microscopy, which clearly demonstrates these two types of interactions. While most nuclei remain stuck within a single cluster due to the lack of *bocks*, nuclei dissociate prematurely from clusters at a much higher frequency due to the lack of *Amph*. Taken together, this study is the first to demonstrate that nuclei interact with one another and such nucleus-nucleus interactions are necessary to regulate the association and dissociation of nuclei as they migrate throughout the myofiber.

5.1.2 A role for Centronuclear Myopathy-linked genes in regulating nuclear positioning and nuclear interactions during muscle development

Expanding upon our initial study, Chapter 3 investigates the potential role and subsequent mechanisms by which CNM-associated genes regulate nuclear movement during embryonic muscle development. Despite the abundance of central nuclei present in CNM-afflicted muscles, the link between mispositioned nuclei and the "MAD" pathway remains unclear. We demonstrate that disruption of *myotubularin*, *shibire*, or *dynamin-related protein 1*, along with *Amphiphysin*, affects the position of myonuclei. Yet these data indicate that there are at least two different mechanisms through which these CNM genes may be regulating nuclear positioning: one that maintains attractive interactions between nuclei, while the other regulates the machinery required to position nuclei throughout the muscle cell.

This conclusion is supported by evidence gained from double heterozygote experiments which demonstrate that Amphiphysin genetically interacts with three separate cytoskeletal proteins to regulate specific aspects of nuclear movement. *Amph* works with actin and microtubules, through *sn* and *ens* respectively, to position nuclear clusters within

their proper regions of the muscle. Additionally, *Amph* also maintains attractive interactions between nuclei through two microtubule proteins, *ens* and *CLIP-190*. Together, these data increase our mechanistic understanding of the molecular pathways through which *Amph* regulates both nuclear interactions and positioning. As the majority of myonuclear movements are microtubule-driven, evidence supporting a genetic interaction between *Amphiphysin* and *singed* adds to the small but growing list of actin-dependent mechanisms that move nuclei within muscle. Additionally, these data are consistent with other reports that identified CLIP-170 and actin as Amphiphysin binding-partners in both mammalian cell culture and *C. elegans*, confirming such interactions are not only necessary for nuclear movement but are conserved mechanisms.

5.1.3 Similar nuclear phenotypes are based in distinct physical mechanisms that are regulated by the nuclear envelope and the microtubule cytoskeleton

The work presented in Chapter 4 extends the regulatory pathways identified thus far, a step beyond the genetic mechanisms detailed in Chapters 2 and 3. This chapter focuses on comparing the nuclear phenotypes in three different mutants: the two nuclear envelope proteins, bocksbeutel and klarsicht, compared to the microtubule-associated protein, ensconsin. Despite localizing to different parts of the cells, each of these genes cause the similar clustering of nuclei within the muscle, as described by their respective papers (Metzger et al., 2012; Collins & Mandigo et al., 2017)(Metzger et al., 2012; Collins et al., 2017). By using a combination of genetic and biophysical approaches along with various microscopy methods, we extensively characterize the precise position, shape, distribution, and movement of nuclei within each mutant. Our analyses provide evidence that these similar

nuclear positioning phenotypes are actually based in distinct molecular underpinnings. Specifically, we found that loss of *ens* effects the application of force to nuclei by regulating the number of growing microtubules that pull nuclei as they translocate. Conversely, the loss of *bocks* or *klar* disrupts the associations between nuclei and their subsequent separation, yet does not affect the presence of directional cues nor transmission of force.

In addition, the data presented in Chapter 4 also clarify some misconceptions and assumptions regarding myonuclear movement during muscle development. As previously mentioned, our data does not support the claim that the resulting nuclear phenotypes produced by *bocks*, *klar*, and *ens* are the same. More specifically, our analyses determined that the single clusters of nuclei in *ens*-depleted muscles are positioned within the center of the myofiber, not towards the ventral end as described by Metzger et al. (2012). This conclusion also suggests that fusion of myoblasts during muscle development occurs at the center of the growing myotube, rather than towards the ventral end as previously assumed. Data from this chapter provide the first direct evidence that regulation of nucleus-nucleus interactions mediated by the LINC Complex components, bocksbeutel and klarsicht, is a critical determinant of nuclear movement. However, neither factor is necessary for the application of force to nuclei, as mechanical tension was not affected by loss of *bock* or *klar*. More broadly, these data demonstrate that nuclear movement in a muscle syncytium requires both the separation of nuclei from their one another as well as the transmission of force, generated by the microtubule cytoskeleton, to the nucleus.

5.2 BROADER IMPACT & FUTURE DIRECTIONS

5.2.1 Identification of attractive and repulsive nucleus-nucleus interactions

In Chapter 2, we proposed the existence of attractive and repulsive interactions between myonuclei. But how nuclei communicate and coordinate their position relative to one another and whether they share information beyond their respective positions remains poorly studied. It is evident that the association and disassociation of nuclei is critical for their proper movement at specific developmental timepoints. Thus, the idea of inter-nuclear communication is of particular interest with respect to skeletal muscle. In contrast to other cell types that use mechano-sensing and -transduction strategies to relay information past the cell membrane, myonuclei may use different or additional mechanisms to interact with each other. We propose that the nuclear envelope proteins, bocksbeutel and klarsicht, are necessary to relieve interactions between nuclei. We speculate that since *bocks* and *klar* are necessary for the organization of microtubules, loss of either gene can partially disrupt the MT-machinery needed to pull nuclei apart from one another and nuclei remain associated in a single cluster. Incomplete disruption of the MT-network could support the observation of escaper nuclei. An alternative explanation involves *bocks* or *klar* recruiting other factors, such as dynein or kinesin, to the nuclear envelope to separate nuclei. We also proposed that Amphiphysin is necessary in maintain nucleus-nucleus interactions, through a mechanisms that also seems to be microtubule-dependent. Nevertheless, these hypotheses regarding the molecular details of attractive and repulsive nucleus-nucleus interactions need to be examined in greater detail.

5.2.2 A novel *in vivo* approach for studying the impact of biophysical forces on nuclear movement during muscle development

In Chapter 4, we integrated several novel techniques to probe how nuclei generate and transduce force. We developed a new ablation assay that physically disrupts an individual nucleus within a *Drosophila* embryo to induce precise subcellular changes to the internal environment of the muscle cell. This approach allows us to directly test the impact of mechanical forces on nuclear movement. Using this technique, we determined that the application of mechanical tension onto nuclei was dependent on the force-generating capacity of the microtubule-network, mediated through ensconsin. We also incorporated *in vivo* super-resolution imaging of EB1 dynamics. By visualizing the interplay between the myonuclei and the microtubule cytoskeleton, we demonstrated that ensconsin regulates the number of growing microtubules and the general organization of the microtubule cytoskeleton that is necessary to pull nuclei apart. Both of these techniques have extended the imaging capabilities of our system from beyond just the nucleus. Furthermore, these methods were instrumental in characterizing the differences between superficially similar nuclear positioning phenotypes. In the future, these approaches will continue to be effective to identify the molecular underpinnings driving different nuclear phenotypes.

5.3 CONCLUDING REMARKS

Over the last few decades, the phenomenon of nuclear positioning has rapidly gained interest. Recent advances have identified many of the regulatory mechanisms

involved in positioning nuclei and the consequences such movements have on various cellular processes and signaling pathways. This thesis provides a significant contribution to our understanding of nuclear movement within muscle and offers new insights into the correlation between mispositioned nuclei and muscles disease. We establish *Drosophila* musculature as a biologically- and clinically-relevant model to study myonuclear positioning that replicates mispositioning phenotypes observed in diseased muscles. Using this *in vivo* system, we determine that there are distinct mechanisms that regulate several aspects of myonuclei including their position, shape, distribution, and movement during muscle development. Therefore, disruptions in nuclear positioning may arise from the dysregulation of one or more of these different regulatory pathways. This conclusion is supported by our evidence that not all muscle diseases produce the same mispositioning phenotypes, reinforcing the importance of studying the impact of disease-associated genes on nuclear movement and muscle health. In total, the research described here provides a new perspective and novel approaches for studying the intricacies of nuclear movement, not just within skeletal muscle, but in all eukaryotic cells alike.

APPENDIX

A1 CHAPTER 2 – SUPPLEMENTAL MOVIE FIGURE LEGENDS

Supplemental Movie 1: Nuclear migration in the lateral transverse muscle of a control *Drosophila* embryo. Time-lapse acquisition showing the migration of myonuclei within four LT muscles of a control embryo. Time-lapse starts at stage 15 (15 hours AEL, t = 0 min), when nuclei have already separated into two distinct clusters. Each LT muscle has one dorsal cluster and one ventral cluster that migrate directionally to opposite ends of the muscle. At stage 16 (16 hours AEL), the dorsal and ventral clusters have reached their respective muscle pole, maximizing the distance between them. Time-lapse movies shown as maximum projections. Z-stacks were acquired at a rate of 2 min/stack. Movie plays at 6 frames/s. Scale bar, 10 µm.

Supplemental Movie 2: Altered nuclear migration in the lateral transverse muscle of a *bocks*^{DP01391} mutant embryo. Time-lapse acquisition showing the migration of myonuclei within four LT muscles of a *bocks*^{DP01391} mutant embryo. Time-lapse starts at stage 15 (15 hours AEL, t = 0 min), where a majority of nuclei failed to separate and remain clustered together in the ventral end of the muscle. Only an escaper nucleus separates from the ventral cluster and migrates directionally toward the dorsal muscle pole. Time-lapse movies shown as maximum projections. Z-stacks were acquired at a rate of 2 min/stack. Movie plays at 6 frames/s. Scale bar, 10 µm.

Supplemental Movie 3: Altered nuclear migration in the lateral transverse muscle of an *Amph^{26}* mutant embryo. Time-lapse acquisition showing the migration of myonuclei within four LT muscles of an *Amph^{26}* mutant embryo. Time-lapse starts at stage 15 (15 hours AEL, t = 0 min), when nuclei have already separated into two distinct clusters. A dorsal nucleus prematurely dissociates from its cluster and migrates towards the ventral pole before moving back and re-associating with its original cluster. Time-lapse movies shown as maximum projections. Z-stacks were acquired at a rate of 2 min/stack. Movie plays at 6 frames/s. Scale bar, 10 μm.

Supplemental Movie 4: Altered nuclear migration in the lateral transverse muscle of an *Amph^{26}* mutant embryo. Time-lapse acquisition showing the migration of myonuclei within four LT muscles of an *Amph^{26}* mutant embryo. Time-lapse starts at stage 15 (15 hours AEL, t = 0 min), when nuclei have already separated into two distinct clusters. A ventral nucleus prematurely dissociates from its original cluster, migrates towards the opposite cluster, and remains associated with the other dorsal nuclei. Time-lapse movies shown as maximum projections. Z-stacks were acquired at a rate of 2 min/stack. Movie plays at 6 frames/s. Scale bar, 10 μm.

A2 CHAPTER 4 – SUPPLEMENTAL MOVIE FIGURE LEGENDS

Supplemental Movie 5: Volumetric imaging of myonuclei in the lateral transverse muscle of a control *Drosophila* embryo. Movie of a three-dimensional volumetric rendering of the dorsal and ventral nuclear clusters within a single LT muscle from a stage 16 (16 hours AEL) control embryo. Muscles in magenta, myonuclei in green. Scale bar, 5 μm. The LT muscle is rotated 360° along the x-axis and 360° along the y-axis.

Supplemental Movie 6: Volumetric imaging of myonuclei in the lateral transverse muscle of an *ens^{swo}* mutant embryo. Movie of a three-dimensional volumetric rendering of the nuclear cluster within a single LT muscle from a stage 16 (16 hours AEL, *ens^{swo}* embryo. Muscles in magenta, myonuclei in green. Scale bar, 5 μm. The LT muscle is rotated 360° along the x-axis and 360° along the y-axis.

Supplemental Movie 7: Nuclear migration in the lateral transverse muscle of a control *Drosophila* embryo. Time-lapse acquisition showing the migration of myonuclei within four LT muscles of a control embryo. Tracks correspond to the movement of individual nuclei within each cluster over the course of two hours. Time-lapse starts at stage 15 (15 hours AEL, t = 0 min), when nuclei have already separated into two distinct clusters. Each LT muscle has one dorsal cluster and one ventral cluster that migrate directionally to opposite ends of the muscle. At stage 16 (16 hours AEL), the dorsal and ventral clusters have reached their respective muscle pole, maximizing the distance between them. Time-lapse movies shown as maximum projections. Z-stacks were acquired at a rate of 1 min/stack. Movie plays at 10 frames/s. Scale bar, 10 μm.

Supplemental Movie 8: Altered nuclear migration in the lateral transverse muscle of a *bocks*^{DP01391} mutant embryo. Time-lapse acquisition showing the migration of myonuclei within four LT muscles of a *bocks*^{DP01391} mutant embryo. Tracks correspond to the movement of individual nuclei over the course of two hours. Time-lapse starts at stage 15 (15 hours AEL, t = 0 min), where a majority of nuclei failed to separate and remain clustered together in the ventral end of the muscle. Only two escaper nuclei separate from the ventral cluster and migrate directionally toward the dorsal muscle pole. Time-lapse movies shown as maximum projections. Z-stacks were acquired at a rate of 1 min/stack. Movie plays at 10 frames/s. Scale bar, 10 µm.

Supplemental Movie 9: Altered nuclear migration in the lateral transverse muscle of a *klar*^{1} mutant embryo. Time-lapse acquisition showing the migration of myonuclei within four LT muscles of a *klar*^{1} mutant embryo. Tracks correspond to the movement of individual nuclei over the course of two hours. Time-lapse starts at stage 15 (15 hours AEL, t = 0 min), where a majority of nuclei failed to separate and remain clustered together in the ventral end of the muscle. Only one escaper nucleus separates from the ventral cluster and migrates directionally toward the dorsal muscle pole. Time-lapse movies shown as maximum projections. Z-stacks were acquired at a rate of 1 min/stack. Movie plays at 10 frames/s. Scale bar, 10 µm.

Supplemental Movie 10: Altered nuclear migration in the lateral transverse muscle of an *ens*^{swo} mutant embryo. Time-lapse acquisition showing the migration of myonuclei within four LT muscles of an *ens*^{swo} mutant embryo. Tracks correspond to the movement of individual nuclei over the course of two hours. Time-lapse starts at stage 15 (15 hours AEL, after egg lay, t = 0 min). In each LT muscle, none of the nuclei separate

and remain within a single cluster. Time-lapse movies shown as maximum projections. Z-stacks were acquired at a rate of 1 min/stack. Movie plays at 10 frames/s. Scale bar, 10 μm.

Supplemental Movie 11: *In vivo* 2-photon laser ablation of myonuclei in a control *Drosophila* embryo. Time-lapse acquisition showing the ablation of a myonucleus within the LT muscles of a stage 16 (16 hours AEL) control embryo. The first frame shows the nuclei before ablation (0 s). The next frame (1 s) shows the ablation of a single nucleus (yellow circle), followed by the subsequent response of the remaining nuclei after ablation (2-5 s). Myonuclei in green, transmitted light in gray. Time-lapse movies were acquired at a rate of 1 s/frame. Movie plays at 7 frames/s. Scale bar, 10 μm.

Supplemental Movie 12: *In vivo* 2-photon laser ablation of myonuclei in a *bocks*^{DP01391} mutant embryo. Time-lapse acquisition showing the ablation of a myonucleus within the LT muscles of a stage 16 (16 hours AEL) *bocks*^{DP01391} mutant embryo. The first frame shows the nuclei before ablation (0 s). The next frame (1 s) shows the ablation of a single nucleus (yellow circle), followed by the subsequent response of the remaining nuclei after ablation (5-30 s). Myonuclei in green, transmitted light in gray. Time-lapse movies were acquired at a rate of 1 s/frame. Movie plays at 7 frames/s. Scale bar, 10 μm.

Supplemental Movie 13: *In vivo* 2-photon laser ablation of myonuclei in a *klar*^{1} mutant embryo. Time-lapse acquisition showing the ablation of a myonucleus within the LT muscles of a stage 16 (16 hours AEL) *klar*^{1} mutant embryo. The first frame shows the nuclei before ablation (0 s). The next frame (1 s) shows the ablation of a single nucleus (yellow circle), followed by the subsequent response of the remaining nuclei after ablation

(5-30 s). Myonuclei in green, transmitted light in gray. Time-lapse movies were acquired at a rate of 1 s/frame. Movie plays at 7 frames/s. Scale bar, 10 μm.

Supplemental Movie 14: *In vivo* 2-photon laser ablation of myonuclei in an *ens^{swo}* mutant embryo. Time-lapse acquisition showing the ablation of a myonucleus within the LT muscles of a stage 16 (16 hours AEL) *ens^{swo}* mutant embryo. The first frame shows the nuclei before ablation (0 s). The next frame (1 s) shows the ablation of a single nucleus (yellow circle), followed by the subsequent response of the remaining nuclei after ablation (5-30 s). Myonuclei in green, transmitted light in gray. Time-lapse movies were acquired at a rate of 1 s/frame. Movie plays at 7 frames/s. Scale bar, 10 μm.

Supplemental Movie 15: *In vivo* imaging of EB1 comet dynamics in the lateral transverse muscles of a control *Drosophila* embryo. Time-lapse acquisition of the LT muscles in a stage 16 (16 hours AEL) control embryo expressing EB1.eYFP. Time-lapse movies were acquired at a rate of 1 s/frame over a time course of 60 s. Movie plays at 7 frames/s. Scale bar, 5 μm.

Supplemental Movie 16: *In vivo* imaging of EB1 comet dynamics in the lateral transverse muscles of an *ens^{swo}* mutant embryo. Time-lapse acquisition of the LT muscles in a stage 16 (16 hours AEL) ensswo mutant embryo expressing EB1.eYFP. Time-lapse movies were acquired at a rate of 1 s/frame over a time course of 60 s. Movie plays at 7 frames/s. Scale bar, 5 μm.

Supplemental Movie 17: *In vivo* imaging of EB1 comet dynamics in the dorsal oblique muscles of a control *Drosophila* embryo. Time-lapse acquisition of the DO muscles in a stage 16 (16 hours AEL) control embryo expressing EB1.eYFP. Time-lapse

movies were acquired at a rate of 1 s/frame over a time course of 60 s. Movie plays at 7 frames/s. Scale bar, 5 μm.

Supplemental Movie 18: *In vivo* imaging of EB1 comet dynamics in the dorsal oblique muscles of an *ens^{swo}* mutant embryo. Time-lapse acquisition of the DO muscles in a stage 16 (16 hours AEL) *ens^{swo}* mutant embryo expressing EB1.eYFP. Time-lapse movies were acquired at a rate of 1 s/frame over a time course of 60 s. Movie plays at 7 frames/s. Scale bar, 5 μm.

A3 ADDITIONAL EXPERIMENTS & NEGATIVE RESULTS

credit: Strange Planet by Nathan Pyle [Twitter: @nathanwpyle]

A3.1 Muscle-specific RNAi depletion at 29°C

The GAL4-UAS system was used to deplete genes linked to EDMD and CNM specifically from the muscle using either the mesoderm-specific *twist-GAL4* driver or the muscle-specific *DMef2-GAL4* driver (Chapter 2). When comparing RNAi depletion to zygotic removal of each gene, only 20% of embryos under the control of the *DMef2-GAL4* driver phenocopied nuclear positioning defects observed in $bocks^{DP01391}$ and $klar^{1}$ mutants (compare Fig. 2.1, Fig. 2.2, and Fig. 2.3). To increase *twist-GAL4* expression and subsequent RNAi efficiency, each RNAi listed in Section 2.5.1 was raised at 29°C. Embryos were fixed, stained, mounted, and imaged as described in Section 2.5.2. The position of nuclei and the area of nuclear clusters were analyzed in stage 16 embryos as described in Section 2.5.3. In short, the dorsal and ventral end distances were taken from each LT muscle by measuring the distance between the closest group of nuclei to the dorsal or ventral muscle pole, respectively. Dorsal and ventral areas were also measured from each LT muscle by measuring the area of each cluster of nuclei near the dorsal or ventral muscle pole, respectively. Total area of nuclear clusters in each LT muscle was calculated by adding the dorsal and ventral areas. The nuclear distribution ratio was calculated by dividing the dorsal area by the ventral area. For qualitative nuclear phenotype analysis, embryos were scored on how nuclei positioned themselves within the first three LT muscles of each hemisegment. Nuclei were categorized as "separated, equal distribution" (nuclei properly segregated into two distinct, even clusters with a dorsal/ventral cluster size ratio ≥ 0.85 and ≤ 1.15; "separated, unequal distribution" (nuclei that segregated into two disproportionate clusters); "central" (a nucleus or a small cluster of nuclei located in the middle of the myofiber that is not associated with either the dorsal or ventral group);

"clustered" (nuclei remained in a single cluster toward the ventral end of the myofiber); or "spread" (nuclei are distributed through the myofiber with no distinct dorsal or ventral clusters). Statistical analysis was performed with Prism 4.0 (GraphPad). Student's t-test was used to assess the statistical significance of differences in measurements between experimental genotypes to controls.

In control embryos, the nuclei in each LT muscle were positioned in two separate clusters, with one near the dorsal end of the muscle and the other near the ventral end of the muscle (Fig. A.1 A). Both dorsal and ventral nuclear distances where comparable to those measured in controls embryos raised at a standard 25°C (Fig. A.1 C and D). In contrast, *twist*-driven expression of koi RNAi resulted in a mild disruption in nuclear position while depletion of *Ote*, *mtm*, and *Amph* caused only a mispositioning of the nuclei relative to the ventral end of the muscle (Fig. A.1 C and D).

In addition, the ratio of the dorsal nuclear cluster size compared to the size of the ventral nuclear clusters was measured. Similar to control embryos raised at 25°C, the average nuclear separation ratio for controls at 29°C was ~1. In contrast, the nuclei near the ventral end of the muscle was on average twice as large as the cluster near the dorsal end in *klar* RNAi embryos, similar to what was observed in $klar^{1}$ mutants (Fig. A.1 H). However, *twist*-driven expression of *Amph* and *bocks* RNAi resulted in an increased nuclear separation ratio, which differed from what was observed in $bocks^{DP01391}$ and $Amph^{26}$ null embryos. Furthermore, there was an increase in the number of centrally positioned nuclei in each RNAi (Fig A.1 I). However, there was also a significant increase in the number of hemisegments that contained extra lateral transverse muscles. Typically, each hemisegment consists of 4 LT muscles. However, the frequency of a hemisegment

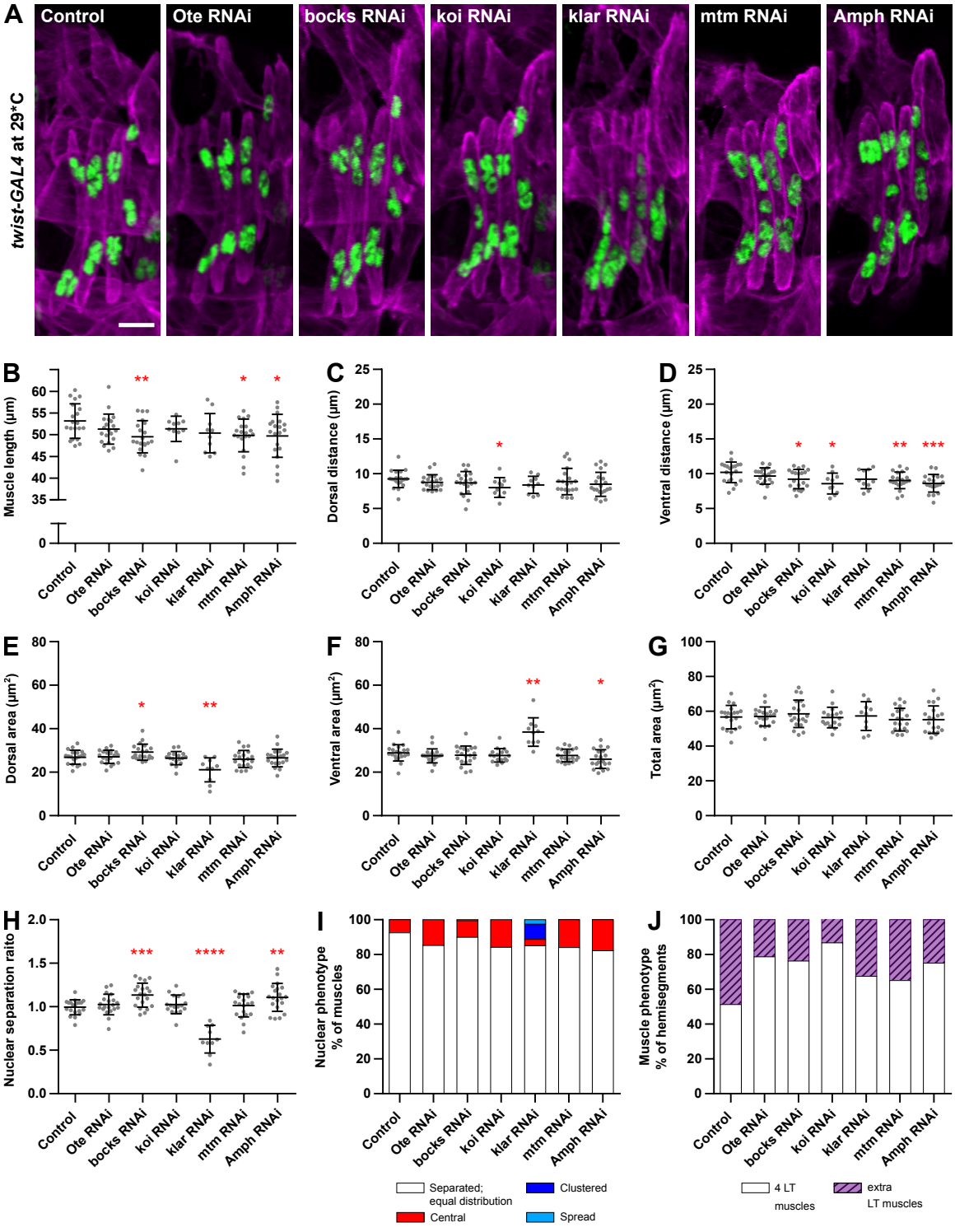

Figure A.1: Mesoderm-specific knockdown of EDMD- and CNM-linked genes at increased temperature effects nuclear positioning and muscle development in *Drosophila* embryos. (**A**) Immunofluorescence images of the LT muscles in one hemisegment from stage 16 (16 hours AEL) embryos that expressed the indicated UAS-RNAi constructs under the control of *twist-GAL4* driven at 29°C. Muscles in magenta, myonuclei in green. Scale bar, 10 µm. (**B–D**) Graphs indicating the average LT muscle length (**B**), the raw distance between the dorsal end of the muscle and the nearest nucleus (**C**), and the raw distance between the ventral end of the muscle and the nearest nucleus (**D**). (**E–G**) Graphs indicating the area of nuclei located

near the dorsal end of the muscle (**E**), the area of nuclei located near the ventral end of the muscle (**F**), and the total area of all myonuclei present within the muscle (**G**). (**H**) The relative size of the dorsal cluster of nuclei compared to the ventral cluster of nuclei. (**I–J**) The frequency at which each nuclear positioning phenotype was observed (**I**) and the frequency at which extra LT muscles were observed (**J**) in each of the indicated UAS-RNAi constructs was driven with *twist-GAL4*. For (B–H), each data point indicates the average distance within a single embryo. Error bars indicate SD from 20 embryos. Student's t-test was used for comparison to controls. *P < 0.05, **P < 0.005, ***P < 0.0005, ****P < 0.00005.

containing 5 or more LT muscles ranged from about 15-50% (Fig. A.1 J). Since it is not possible to determine which of the 4 LT muscles have been duplicated, nuclear positioning was not assessed in hemisegments containing extra muscles. Thus, while the position of nuclei was more strongly affected in some *twist*-depleted embryos, the increased temperature also caused severe defects on muscle development and was not considered a feasible method of increasing RNAi expression.

A3.2 Evaluating microtubule organization in fixed *Drosophila* embryos

Many types of the nuclear movements that occur during myogenesis are microtubule-dependent. Additionally, nuclei are physically linked to the microtubule cytoskeleton and nuclear envelope proteins have been demonstrated to impact microtubule organization. Therefore, we hypothesized that the differences in nuclear behaviors observed may be linked to variations in microtubule organization (Chapter 4). To evaluated the organization of the microtubule network, embryos were fixed, stained, and mounted, as described in Section 4.5.2 with the following modifications. Embryos were fixed with 37% formaldehyde for 10 minutes at room temperature and were then devitellinized by vortexing in a 1:1 methanol:heptane solution. Primary antibodies for embryo staining were used at the following final dilutions: rabbit anti-DsRed (1:400, Clontech 632496), rat anti-tropomyosin (1:200, Abcam ab50567), and mouse anti-αTubulin (1:200, Sigma-Aldrich T6199). The conjugated fluorescent secondary antibodies used were Alexa Fluor 555

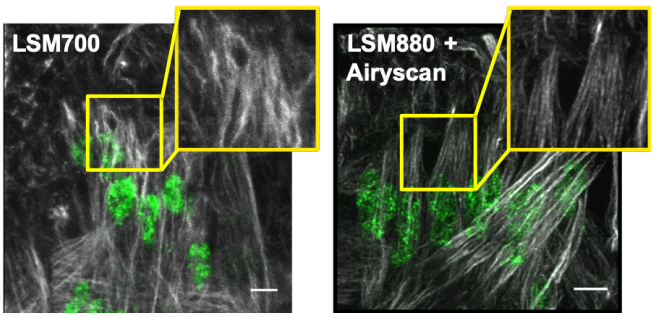

Fig. A.2: Organization of the microtubule network in *Drosophila* embryonic skeletal muscles. Immunofluorescence images of the MT network around the dorsal cluster of nuclei in the LT muscles from stage 16 (16 hours AEL) control embryos. Image taken on a standard LSM system (left) compared to image taken on an LSM system with Airyscan processing. MT (α-tubulin) in gray, myonuclei in green. Scale bar, 5 μm. (inset in yellow box) Magnified regions showing the MT network.

donkey-anti-rabbit (1:200), Alexa Fluor 488 donkey-anti-rat (1:200), and Alexa Fluor 647 donkey-anti-mouse (1:200) (all Life Technologies).

Stage 16 embryos were selected for imaging as described in Section 4.5.3. Confocal images of fixed embryos were first acquired on a Zeiss 700 LSM using a Plan-Apochromat 40×, 1.4 NA oil objective with a 1.0× optical zoom (Fig. A.2, left). While the α-tubulin antibody labeled the microtubules (grey), the resolution was not sufficient enough to quantify changes in the organization of the MT network. To improve resolution, stage 16 embryos were then imaged on a Zeiss LSM 880 with Airyscan (super resolution acquisition, 2× Nyquist sampling) using a Plan-Apochromat 40×, 1.3 NA oil objective at a 1.0× optical zoom (Fig. A.2, right). Post processing of Airyscan images was completed in ZEN Blue 2016 software. When compared to images taken on the standard laser-scanning confocal system, images taken on a similar LSM system with Airyscan processing had dramatically improved resolution of the microtubules, where linear bundles of MTs were detectable. However, microtubules from the neighboring epithelial layer above and below the lateral transverse muscles were also labeled, making it not possible to quantify distinguishable changes in MT organization solely within the musculature. Therefore, MT organization was evaluated in stage L3 larvae (Section 4.3.4 and Fig. 4.7) instead.

A3.3 Screening of fluorescent actin and tubulin reporters for *in vivo* time-lapse imaging of *Drosophila* embryos

Various fluorescent actin and tubulin reporter lines from the Bloomington *Drosophila* Stock Center were screened for potential use in *in vivo* time-lapse imaging experiments (Fig. A.3). Each reporter construct was created by fluorescently tagging each gene through the insertion of a P-element transposon at the N-terminus. All reporter lines were driven specifically in the muscle, under the control of *DMef2-GAL4* from embryonic stage 12 through larval development. Stage 16 embryos were prepared and selected for live-imaging as previously described in Sections 2.5.5 and 4.5.6. Confocal z-stacks of live embryos were acquired on a Zeiss 700 LSM using a Plan-Apochromat 40×, 1.4 NA oil objective with a 1.0× optical zoom using the same laser power and gain. Stocks were scored based on the quality of its fluorescence.

Of the 11 actin.GFP reporters, 4 lines (B9249, B9251, B9256, B9258) had the strongest signal with little to no background noise. Neither of the two actin.mRFP lines (B24778 and B24779) were considered practical options as the nuclear dsRed signal was also visible and the signal was poor compared to the actin.GFP lines. Similarly, none of the tubulin.GFP lines were suitable options for labeling the microtubule network as the signal was either too diffuse (B7373) or too grainy (B7374, B32075, B32076) to observe any define structures. Therefore, microtubule dynamics was evaluated in embryos using an UAS-EB1.eYFP reporter (Section 4.3.4 and Fig. 4.8) instead. An alternate approach would be to use a protein trap, which can be used to detect tubulin (or any protein of interest) that has been fluorescently-tagged at the endogenous locus.

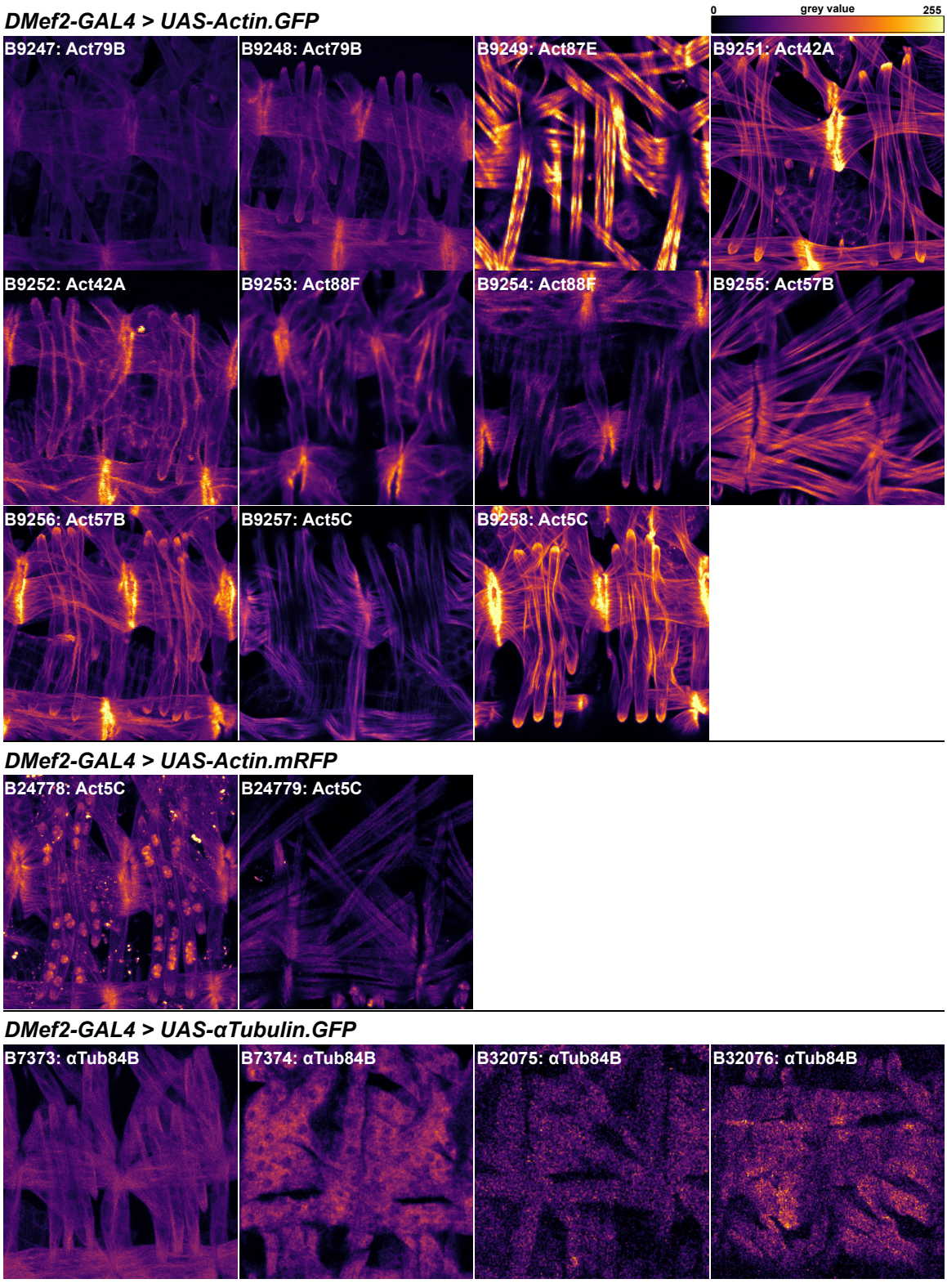

Figure A.3: Expression of UAS-reporter lines for actin and microtubules. Immunofluorescence images of stage 16 (16 hours AEL) embryos expressing the indicated UAS-GFP or UAS-mRFP constructs under the control of *DMef2-GAL4*. The intensity signal is represented as a heat map. All reporter lines are identified by their BDSC stock number and are commercially available through the Bloomington *Drosophila* Stock Center.

REFERENCES

Abmayr, S.M. and Pavlath, G.K. (2012) Myoblast fusion: Lessons from flies and mice. *Development*. **139**:641–656.

Al-Qusairi, L., Weiss, N., Toussaint, A., Berbey, C., Messaddeq, N., Kretz, C., Sanoudou, D., Beggs, A.H., Allard, B., Mandel, J.-L., Laporte, J., Jacquemond, V., and Buj-Bello, A. (2009) T-tubule disorganization and defective excitation-contraction coupling in muscle fibers lacking myotubularin lipid phosphatase. *Proceedings of the National Academy of Sciences*. **106**:18763–18768.

Almonacid, M. and Paoletti, A. (2010) Mechanisms controlling division-plane positioning. *Seminars in Cell and Developmental Biology*. **21**:874–880.

Amoasii, L., Hnia, K., Chicanne, G., Brech, A., Cowling, B.S., Muller, M.M., Schwab, Y., Koebel, P., Ferry, A., Payrastre, B., and Laporte, J. (2013) Myotubularin and PtdIns3P remodel the sarcoplasmic reticulum in muscle in vivo. *Journal of Cell Science*. **126**:1806–1819.

Auld, A.L., Collins, M.A., Mandigo, T.R., and Folker, E.S. (2018) High-Resolution Imaging Methods to Analyze LINC Complex Function During Drosophila Muscle Development. *Methods in Molecular Biology*. **1840**:181–203.

Auld, A.L. and Folker, E.S. (2016) Nucleus-dependent sarcomere assembly is mediated by the LINC complex. *Molecular Biology of the Cell*. **27**:2351–2359.

Bakay, M., Wang, Z., Melcon, G., Schiltz, L., Xuan, J., Zhao, P., Sartorelli, V., Seo, J., Pegoraro, E., Angelini, C., Shneiderman, B., Escolar, D., Chen, Y.W., Winokur, S.T., Pachman, L.M., Fan, C., Mandler, R., Nevo, Y., Gordon, E., Zhu, Y., Dong, Y., Wang, Y., and Hoffman, E.P. (2006) Nuclear envelope dystrophies show a transcriptional fingerprint suggesting disruption of Rb-MyoD pathways in muscle regeneration. *Brain*. **129**:996–1013.

Banerjee, I., Zhang, J., Moore-Morris, T., Pfeiffer, E., Buchholz, K.S., Liu, A., Ouyang, K., Stroud, M.J., Gerace, L., Evans, S.M., McCulloch, A., and Chen, J. (2014) Targeted Ablation of Nesprin 1 and Nesprin 2 from Murine Myocardium Results in Cardiomyopathy, Altered Nuclear Morphology and Inhibition of the Biomechanical Gene Response. *PLoS Genetics*. **10**.

Di Barletta, M.R., Ricci, E., Galluzzi, G., Tonali, P., Mora, M., Morandi, L., Romorini, A., Voit, T., Orstavik, K.H., Merlini, L., Trevisan, C., Biancalana, V., Housmanowa-Petrusewicz, I., Bione, S., Ricotti, R., Schwartz, K., Bonne, G., and Toniolo, D. (2000) Different mutations in the LMNA gene cause autosomal dominant autosomal recessive Emery-Dreifuss muscular dystrophy. *American*

Journal of Human Genetics. **66**:1407–1412.

Barton, L.J., Wilmington, S.R., Martin, M.J., Skopec, H.M., Lovander, K.E., Pinto, B.S., and Geyer, P.K. (2014) Unique and shared functions of nuclear lamina LEM domain proteins in Drosophila. *Genetics*. **197**:653–665.

Baye, L.M. and Link, B.A. (2008) Nuclear migration during retinal development. *Brain Research*. **1192**:29–36.

Beckett, K. and Baylies, M.K. (2007) 3D analysis of founder cell and fusion competent myoblast arrangements outlines a new model of myoblast fusion. *Developmental Biology*. **309**:113–125.

Del Bene, F. (2011) Interkinetic nuclear migration: Cell cycle on the move. *The EMBO Journal*. **30**:1676–1677.

Del Bene, F., Wehman, A.M., Link, B.A., and Baier, H. (2008) Regulation of Neurogenesis by Interkinetic Nuclear Migration through an Apical-Basal Notch Gradient. *Cell*. **134**:1055–1065.

Bertrand, A.T., Ziaei, S., Ehret, C., Duchemin, H., Mamchaoui, K., Bigot, A., Mayer, M., Quijano-Roy, S., Desguerre, I., Lainé, J., Yaou, R. Ben, Bonne, G., and Coirault, C. (2014) Cellular microenvironments reveal defective mechanosensing responses and elevated YAP signaling in LMNA-mutated muscle precursors. *Journal of Cell Science*. **127**:2873–2884.

Bione, S., Maestrini, E., Rivella, S., Mancini, M., Regis, S., Romeo, G., and Toniolo, D. (1994) Identification of a novel X-linked gene responsible for Emery-Dreifuss muscular dystrophy. *Nature Genetics*. **8**:323–327.

Biressi, S., Molinaro, M., and Cossu, G. (2007) Cellular heterogeneity during vertebrate skeletal muscle development. *Developmental Biology*. **308**:281–293.

Bitoun, M., Maugenre, S., Jeannet, P.-Y., Lacène, E., Ferrer, X., Laforêt, P., Martin, J.-J., Laporte, J., Lochmüller, H., Beggs, A.H., Fardeau, M., Eymard, B., Romero, N.B., and Guicheney, P. (2005) Mutations in dynamin 2 cause dominant centronuclear myopathy. *Nature Genetics*. **37**:1207–1209.

Blaveri, K., Heslop, L., Yu, D.S., Rosenblatt, J.D., Gross, J.G., Partridge, T.A., and Morgan, J.E. (1999) Patterns of repair of dystrophic mouse muscle: Studies on isolated fibers. *Developmental Dynamics*. **216**:244–256.

Blondeau, F., Laporte, J., Bodin, S., Superti-Furga, G., Payrastre, B., and Mandel, J.-L. (2000) Myotubularin, a phosphatase deficient in myotubular myopathy, acts on phosphatidylinositol 3-kinase and phosphatidylinositol 3-phosphate pathway. *Human Molecular Genetics*. **9**:2223–2229.

Böhm, J., Biancalana, V., DeChene, E.T., Bitoun, M., Pierson, C.R., Schaefer, E., Karasoy, H., Dempsey, M.A., Klein, F., Dondaine, N., Kretz, C., Haumesser, N., Poirson, C., Toussaint, A., Greenleaf, R.S., Barger, M.A., Mahoney, L.J., Kang, P.B., Zanoteli, E., Vissing, J., Witting, N., Echaniz-Laguna, A., Wallgren-Pettersson, C., Dowling, J., Merlini, L., Oldfors, A., Ousager, L.B., Melki, J., Krause, A., Jern, C., Oliveira, A.S.B., Petit, F., Jacquette, A., Chaussenot, A., Mowat, D., Leheup, B., Cristofano, M., Aldea, J.J.P., Michel, F., Furby, A., Llona, J.E.B., Van Coster, R., Bertini, E., Urtizberea, J.A., Drouin-Garraud, V., Roud, C.B., Prudhon, B., Bedford, M., Mathews, K., Erby, L.A.H., Smith, S.A., Roggenbuck, J., Crowe, C.A., Spitale, A.B., Johal, S.C., Amato, A.A., Demmer, L.A., Jonas, J., Darras, B.T., Bird, T.D., Laurino, M., Welt, S.I., Trotter, C., Guicheney, P., Das, S., Mandel, J.L., Beggs, A.H., and Laporte, J. (2012) Mutation Spectrum in the Large GTPase Dynamin 2, and Genotype–Phenotype Correlation in Autosomal Dominant Centronuclear Myopathy. *Human Mutation*. **33**:949–959.

Böhm, J., Biancalana, V., Malfatti, E., Dondaine, N., Koch, C., Vasli, N., Kress, W., Strittmatter, M., Taratuto, A.L., Gonorazky, H., Laforêt, P., Maisonobe, T., Olivé, M., Gonzalez-Mera, L., Fardeau, M., Carrière, N., Clavelou, P., Eymard, B., Bitoun, M., Rendu, J., Fauré, J., Weis, J., Mandel, J.L., Romero, N.B., and Laporte, J. (2014) Adult-onset autosomal dominant centronuclear myopathy due to BIN1 mutations. *Brain*. **137**:3160–3170.

Bonne, G., Di Barletta, M.R., Varnous, S., Bécane, H.M., Hammouda, E.H., Merlini, L., Muntoni, F., Greenberg, C.R., Gary, F., Urtizberea, J. a., Duboc, D., Fardeau, M., Toniolo, D., and Schwartz, K. (1999) Mutations in the gene encoding lamin A/C cause autosomal dominant Emery-Dreifuss muscular dystrophy. *Nature Genetics*. **21**:285–288.

Bonne, G., Leturcq, F., and Yaou, R. Ben. (2004) Emery-Dreifuss Muscular Dystrophy. *GeneReviews*. 1–31.

Bonne, G., Yaou, R. Ben, Béroud, C., Boriani, G., Brown, S., De Visser, M., Duboc, D., Ellis, J., Hausmanowa-Petrusewicz, I., Lattanzi, G., Merlini, L., Morris, G., Muntoni, F., Opolski, G., Pinto, Y.M., Sangiuolo, F., Toniolo, D., Trembath, R., Van Berlo, J.H., Van Der Kooi, A.J., and Wehnert, M. (2003) 108th ENMC International Workshop, 3rd Workshop of the MYO-CLUSTER project: EUROMEN, 7th International Emery-Dreifuss Muscular Dystrophy (EDMD) Workshop, 13-15 September 2002, Naarden, The Netherlands. *Neuromuscular Disorders*. **13**:508–515.

Brendza, K.M., Rese, D.J., Gilbert, S.P., and Saxton, W.M. (1999) Lethal kinesin mutations reveal amino acids important for ATPase activation and structural coupling. *Journal of Biological Chemistry*. **274**:31506–31514.

Brown, J.H. and Cohen, C. (2005) Regulation of muscle contraction by tropomyosin and troponin: How structure illuminates function. *Advances in Protein Chemistry*. **71**:121–159.

Bruston, F., Delbarre, E., Östlund, C., Worman, H.J., Buendia, B., and Duband-Goulet, I. (2010) Loss of a DNA binding site within the tail of prelamin A contributes to altered heterochromatin anchorage by progerin. *FEBS Letters*. **584**:2999–3004.

Bruusgaard, J.C., Liestøl, K., Ekmark, M., Kollstad, K., and Gundersen, K. (2003) Number and spatial distribution of nuclei in the muscle fibres of normal mice studied in vivo. *Journal of Physiology*. **551**:467–78.

Bruusgaard, J.C., Liestøl, K., and Gundersen, K. (2006) Distribution of myonuclei and microtubules in live muscle fibers of young, middle-aged, and old mice. *Journal of Applied Physiology*. **100**:2024–2030.

Bugnard, E., Zaal, K.J.M., and Ralston, E. (2005) Reorganization of microtubule nucleation during muscle differentiation. *Cell Motility and the Cytoskeleton*. **60**:1–13.

Bulinski, J.C. and Bossler, A. (1994) Purification and characterization of ensconsin, a novel microtubule stabilizing protein. *Journal of Cell Science*. **107**:2839–49.

Butler, M.H., David, C., Ochoa, G.C., Freyberg, Z., Daniell, L., Grabs, D., Cremona, O., and De Camilli, P. (1997) Amphiphysin II (SH3p9; BIN1), a member of the amphiphysin/Rvs family, is concentrated in the cortical cytomatrix of axon initial segments and nodes of ranvier in brain and around T tubules in skeletal muscle. *Journal of Cell Biology*. **137**:1355–1367.

Cadot, B., Gache, V., Vasyutina, E., Falcone, S., Birchmeier, C., and Gomes, E.R. (2012) Nuclear movement during myotube formation is microtubule and dynein dependent and is regulated by Cdc42, Par6 and Par3. *EMBO Reports*. **13**:741–749.

Capers, C.R. (1960) Multinucleation of skeletal muscle in vitro. *The Journal of Biophysical and Biochemical Cytology*. **7**:559–566.

Carlson, B.M. (2003) Muscle regeneration in amphibians and mammals: Passing the torch. *Developmental Dynamics*. **226**:167–181.

Ceyhan-Birsoy, O., Agrawal, P.B., Hidalgo, C., Schmitz-Abe, K., DeChene, E.T., Swanson, L.C., Soemedi, R., Vasli, N., Iannaccone, S.T., Shieh, P.B., Shur, N., Dennison, J.M., Lawlor, M.W., Laporte, J., Markianos, K., Fairbrother, W.G., Granzier, H., and Beggs, A.H. (2013) Recessive truncating titin gene, TTN, mutations presenting as centronuclear myopathy. *Neurology*. **81**:1205–1214.

Chang, W., Folker, E.S., Worman, H.J., and Gundersen, G.G. (2013) Emerin organizes actin flow for nuclear movement and centrosome orientation in migrating fibroblasts. *Molecular Biology of the Cell*. **24**:3869–80.

Chargé, S.B.P. and Rudnicki, M.A. (2004) Cellular and Molecular Regulation of Muscle Regeneration. *Physiological Reviews*. **84**:209–238.

Chen, E.H., Pryce, B.A., Tzeng, J.A., Gonzalez, G.A., and Olson, E.N. (2003) Control of myoblast fusion by a guanine nucleotide exchange factor, loner, and its effector ARF6. *Cell*. **114**:751–762.

Chen, J., Smoyer, C.J., Slaughter, B.D., Unruh, J.R., and Jaspersen, S.L. (2014) The sun protein Mps3 controls Ndc1 distribution and function on the nuclear membrane. *Journal of Cell Biology*. **204**:523–539.

Chin, Y.H., Lee, A., Kan, H.W., Laiman, J., Chuang, M.C., Hsieh, S.T., and Liu, Y.W. (2015) Dynamin-2 mutations associated with centronuclear myopathy are hypermorphic and lead to T-tubule fragmentation. *Human Molecular Genetics*. **24**:5542–5554.

Choudhury, P., Srivastava, S., Li, Z., Ko, K., Albaqumi, M., Narayan, K., Coetzee, W.A., Lemmon, M.A., and Skolnik, E.Y. (2006) Specificity of the myotubularin family of phosphatidylinositol-3- phosphatase is determined by the PH/GRAM domain. *Journal of Biological Chemistry*. **281**:31762–31769.

Collins, M.A., Mandigo, T.R., Camuglia, J.M., Vazquez, G.A., Anderson, A.J., Hudson, C.H., Hanron, J.L., and Folker, E.S. (2017) Emery–Dreifuss muscular dystrophy–linked genes and centronuclear myopathy–linked genes regulate myonuclear movement by distinct mechanisms. *Molecular Biology of the Cell*. **28**:2303–2317.

Colombo, K., Grill, S.W., Kimple, R.J., Willard, F.S., Siderovski, D.P., and Gönczy, P. (2003) Translation of polarity cues into asymmetric spindle positioning in Caenorhabditis elegans embryos. *Science*. **300**:1957–1961.

Crisp, M., Liu, Q., Roux, K., Rattner, J.B., Shanahan, C., Burke, B., Stahl, P.D., and Hodzic, D. (2006) Coupling of the nucleus and cytoplasm: Role of the LINC complex. *Journal of Cell Biology*. **172**:41–53.

D'Alessandro, M., Hnia, K., Gache, V., Koch, C., Gavriilidis, C., Rodriguez, D., Nicot, A.S., Romero, N.B., Schwab, Y., Gomes, E.R., Labouesse, M., and Laporte, J. (2015) Amphiphysin 2 Orchestrates Nucleus Positioning and Shape by Linking the Nuclear Envelope to the Actin and Microtubule Cytoskeleton. *Developmental Cell*. **35**:186–198.

van Dam, E.M. and Stoorvogel, W. (2002) Dynamin-dependent Transferrin Receptor

Recycling by Endosome-derived Clathrin-coated Vesicles. *Molecular Biology of the Cell*. **13**:169–182.

Dechat, T., Pfleghaar, K., Sengupta, K., Shimi, T., Shumaker, D.K., Solimando, L., and Goldman, R.D. (2008) Nuclear lamins: Major factors in the structural organization and function of the nucleus and chromatin. *Genes and Development*. **22**:832–853.

Desai, R.A., Gao, L., Raghavan, S., Liu, W.F., and Chen, C.S. (2009) Cell polarity triggered by cell-cell adhesion via E-cadherin. *Journal of Cell Science*. **122**:905–911.

Dialynas, G., Speese, S., Budnik, V., Geyer, P.K., and Wallrath, L.L. (2010) The role of Drosophila Lamin C in muscle function and gene expression. *Development*. **137**:3067–77.

Dowling, J.J., Vreede, A.P., Low, S.E., Gibbs, E.M., Kuwada, J.Y., Bonnemann, C.G., and Feldman, E.L. (2009) Loss of myotubularin function results in T-tubule disorganization in zebrafish and human myotubular myopathy. *PLoS Genetics*. **5**.

Dubowitz, V., Sewry, C.A., Lane, R., Oldfors, A., and Sewry, C.A. (2007) Muscle Biopsy: A Practical Approach. 4th ed. *Elsevier Limited, Philadephia, PA*. 626 pp.

Dundon, S.E.R., Chang, S.S., Kumar, A., Occhipinti, P., Shroff, H., Roper, M., and Gladfelter, A.S. (2016) Clustered nuclei maintain autonomy and nucleocytoplasmic ratio control in a syncytium. *Molecular Biology of the Cell*. **27**:2000–2007.

Durieux, A.C., Vignaud, A., Prudhon, B., Viou, M.T., Beuvin, M., Vassilopoulos, S., Fraysse, B., Ferry, A., Lainé, J., Romero, N.B., Guicheney, P., and Bitoun, M. (2010) A centronuclear myopathy-dynamin 2 mutation impairs skeletal muscle structure and function in mice. *Human Molecular Genetics*. **19**:4820–4836.

Elhanany-Tamir, H., Yu, Y. V., Shnayder, M., Jain, A., Welte, M., and Volk, T. (2012) Organelle positioning in muscles requires cooperation between two KASH proteins and microtubules. *Journal of Cell Biology*. **198**:833–846.

Emery, A.E.H. (2000) Emery-Dreifuss muscular dystrophy - a 40 year retrospective. *Neuromuscular Disorders*. **10**:228–232.

Emery, A.E.H. and Dreifuss, F.E. (1966) Unusual type of benign X-linked muscular dystrophy. *Journal of Neurology, Neurosurgery and Psychiatry*. **29**:338–342.

Englander, L.L. and Rubin, L.L. (1987) Acetylcholine Receptor Clustering and Nuclear Movement in Muscle Fibers in Culture. *Journal of Cell Biology*. **104**:87–95.

Espigat-Georger, A., Dyachuk, V., Chemin, C., Emorine, L., and Merdes, A. (2016)

Nuclear alignment in myotubes requires centrosome proteins recruited by nesprin-1. *Journal of Cell Science*. **129**:4227–4237.

Etienne-Manneville, S. and Hall, A. (2001) Integrin-Mediated Activation of Cdc42 Controls Cell Polarity in Migrating Astrocytes through PKC. *Cell*. **106**:489–498.

Falcone, S., Roman, W., Hnia, K., Gache, V., Didier, N., Auradé, F., Marty, I., Nishino, I., Charlet-Berguerand, N., Romero, B., Marazzi, G., Sassoon, D., Laporte, J., and Gomes, E.R. (2014) N-WASP is required for Amphiphysin-2/BIN1- dependent nuclear positioning and triad organization in skeletal muscle and is involved in the pathophysiology of centronuclear myopathy. *EMBO Molecular Medicine*. **6**:1455–1476.

Favreau, C., Dubosclard, E., Östlund, C., Vigouroux, C., Capeau, J., Wehnert, M., Higuet, D., Worman, H.J., Courvalin, J.C., and Buendia, B. (2003) Expression of Lamin A mutated in the carboxyl-terminal tail generates an aberrant nuclear phenotype similar to that observed in cells from patients with Dunnigan-type partial lipodystrophy and Emery-Dreifuss muscular dystrophy. *Experimental Cell Research*. **282**:14–23.

Fidzianska, A., Niebrój-Dobosz, I., Madej-Pilarczyk, A., Duong, N.T., and Wehnert, M.S. (2010) X-linked Emery-Dreifuss muscular dystrophy with lamin A deficiency and IBM inclusions. *Clinical Neuropathology*. **29**:78–83.

Flucher, B.E., Takekura, H., and Franzini-Armstrong, C. (1993) Development of the Excitation-Contraction Coupling Apparatus in Skeletal Muscle: Assocaition of Sarcoplasmic Reticulum and Transverse Tubules with Myofibrils. *Developmental Biology*. **160**:135–147.

Folker, E.S. and Baylies, M.K. (2013) Nuclear positioning in muscle development and disease. *Frontiers in Physiology*. **4**:1–10.

Folker, E.S., Schulman, V.K., and Baylies, M.K. (2012) Muscle length and myonuclear position are independently regulated by distinct Dynein pathways. *Development*. **139**:3827–3837.

Folker, E.S., Schulman, V.K., and Baylies, M.K. (2014) Translocating myonuclei have distinct leading and lagging edges that require Kinesin and Dynein. *Development*. **141**:355–66.

Fridolfsson, H.N. and Starr, D.A. (2010) Kinesin-1 and dynein at the nuclear envelope mediate the bidirectional migrations of nuclei. *Journal of Cell Biology*. **191**:115–128.

Frock, R.L., Kudlow, B.A., Evans, A.M., Jameson, S.A., Hauschka, S.D., and Kennedy, B.K. (2006) Lamin A/C and emerin are critical for skeletal muscle

satellite cell differentiation. *Genes and Development*. **20**:486–500.

Frost, A., Unger, V.M., and De Camilli, P. (2009) The BAR Domain Superfamily: Membrane-Molding Macromolecules. *Cell*. **137**:191–196.

Fugier, C., Klein, A.F., Hammer, C., Vassilopoulos, S., Ivarsson, Y., Toussaint, A., Tosch, V., Vignaud, A., Ferry, A., Messaddeq, N., Kokunai, Y., Tsuburaya, R., De La Grange, P., Dembele, D., Francois, V., Precigout, G., Boulade-Ladame, C., Hummel, M.C., De Munain, A.L., Sergeant, N., Laquerrière, A., Thibault, C., Deryckere, F., Auboeuf, D., Garcia, L., Zimmermann, P., Udd, B., Schoser, B., Takahashi, M.P., Nishino, I., Bassez, G., Laporte, J., Furling, D., and Charlet-Berguerand, N. (2011) Misregulated alternative splicing of BIN1 is associated with T tubule alterations and muscle weakness in myotonic dystrophy. *Nature Medicine*. **17**:720–725.

Gache, V., Gomes, E.R., and Cadot, B. (2017) Microtubule motors involved in nuclear movement during skeletal muscle differentiation. *Molecular Biology of the Cell*. **28**:865–874.

Gallaud, E., Caous, R., Pascal, A., Bazile, F., Gagné, J.-P., Huet, S., Poirier, G.G., Chrétien, D., Richard-Parpaillon, L., and Giet, R. (2014) Ensconsin/Map7 promotes microtubule growth and centrosome separation in Drosophila neural stem cells. *Journal of Cell Biology*. **204**:1111–1121.

Gepner, J., Li, M.G., Ludmann, S., Kortas, C., Boylan, K., Iyadurai, S.J.P., McGrail, M., and Hays, T.S. (1996) Cytoplasmic dynein function is essential in Drosophila melanogaster. *Genetics*. **142**:865–878.

Gibeaux, R., Politi, A.Z., Philippsen, P., and Nédélec, F. (2017) Mechanism of nuclear movements in a multinucleated cell. *Molecular Biology of the Cell*. **28**:645–660.

Gimpel, P., Lee, Y.L., Sobota, R.M., Calvi, A., Koullourou, V., Patel, R., Mamchaoui, K., Nédélec, F., Shackleton, S., Schmoranzer, J., Burke, B., Cadot, B., and Gomes, E.R. (2017) Nesprin-1α-Dependent Microtubule Nucleation from the Nuclear Envelope via Akap450 Is Necessary for Nuclear Positioning in Muscle Cells. *Current Biology*. **27**:2999–3009.

Gold, E.S., Underhill, D.M., Morrissette, N.S., Guo, J., McNiven, M.A., and Aderem, A. (1999) Dynamin 2 is required for phagocytosis in macrophages. *Journal of Experimental Medicine*. **190**:1849–1856.

Gomes, E.R., Jani, S., and Gundersen, G.G. (2005) Nuclear movement regulated by Cdc42, MRCK, myosin, and actin flow establishes MTOC polarization in migrating cells. *Cell*. **121**:451–463.

Gonorazky, H.D., Bönnemann, C.G., and Dowling, J.J. (2018) The genetics of

congenital myopathies. *Handbook of Clinical Neurology*. **148**:549–564.

González-Jamett, A.M., Momboisse, F., Haro-Acuña, V., Bevilacqua, J.A., Caviedes, P., and Cárdenas, A.M. (2013) Dynamin-2 function and dysfunction along the secretory pathway. *Frontiers in Endocrinology*. **4**:1–9.

Gu, C., Yaddanapudi, S., Weins, A., Osborn, T., Reiser, J., Pollak, M., Hartwig, J., and Sever, S. (2010) Direct dynamin-actin interactions regulate the actin cytoskeleton. *The EMBO journal*. **29**:3593–3606.

Gundersen, G.G. and Worman, H.J. (2013) Nuclear positioning. *Cell*. **3**:1376–1389.

Hale, C.M., Shrestha, A.L., Khatau, S.B., Stewart-Hutchinson, P.J., Hernandez, L., Stewart, C.L., Hodzic, D., and Wirtz, D. (2008) Dysfunctional connections between the nucleus and the actin and microtubule networks in laminopathic models. *Biophysical Journal*. **95**:5462–5475.

Haque, F., Lloyd, D.J., Smallwood, D.T., Dent, C.L., Shanahan, C.M., Fry, A.M., Trembath, R.C., and Shackleton, S. (2006) SUN1 Interacts with Nuclear Lamin A and Cytoplasmic Nesprins To Provide a Physical Connection between the Nuclear Lamina and the Cytoskeleton. *Molecular and Cellular Biology*. **26**:3738–3751.

Helbling-Leclerc, A., Bonne, G., and Schwartz, K. (2002) Emery-Dreifuss muscular dystrophy. *European Journal of Human Genetics*. **10**:157–161.

Hinshaw, J.E. and Schmid, S.L. (1995) Dynamin self-assembles into rings suggesting a mechanism for coated vesicle budding. *Nature*. **374**:190–192.

Hnia, K., Tronchère, H., Tomczak, K.K., Amoasii, L., Schultz, P., Beggs, A.H., Payrastre, B., Mandel, J.L., and Laporte, J. (2011) Myotubularin controls desmin intermediate filament architecture and mitochondrial dynamics in human and mouse skeletal muscle. *The Journal of Clinical Investigation*. **121**:70–85.

Hnia, K., Vaccari, I., Bolino, A., and Laporte, J. (2012) Myotubularin phosphoinositide phosphatases: Cellular functions and disease pathophysiology. *Trends in Molecular Medicine*. **18**:317–327.

Holaska, J.M. and Wilson, K.L. (2007) An emerin 'proteome': purification of distinct emerin-containing complexes from HeLa cells suggests molecular basis for diverse roles including gene regulation, mRNA splicing, signaling, mechano-sensing and nuclear architecture. *Biochemistry*. **46**:8897–8908.

ten Hoopen, R., Cepeda-García, C., Fernández-Arruti, R., Juanes, M.A., Delgehyr, N., and Segal, M. (2012) Mechanism for astral microtubule capture by cortical Bud6p priming spindle Polarity in S. cerevisiae. *Current Biology*. **22**:1075–1083.

Hutcheson, D.A., Zhao, J., Merrell, A., Haldar, M., and Kardon, G. (2009) Embryonic and fetal limb myogenic cells are derived from developmentally distinct progenitors and have different requirements for β-catenin. *Genes & Development*. **23**:997–1013.

Huxley, A.F. and Niedergerke, R. (1954) Structural changes in muscle during contraction. *Nature*. **4412**:971–973.

Huxley, H. (1953) Electron microscope studies of the organisation of the filaments in striated muscle. *Biochimica et Biophysica Acta*. **12**:387–394.

Huxley, H. (1957) The double array of filaments in cross-striated muscle. *The Journal of Biophysical and Biochemical Cytology*. **3**:571–588.

Huxley, H. (1969) The Mechanism of Muscular Contraction. *Science*. **164**:1356–1366.

Huxley, H. and Hanson, J. (1954) Changes in the Cross-Striations of Muscle during Contraction and Stretch and their Structural Interpretation. *Nature*. **173**:973–976.

Isermann, P. and Lammerding, J. (2013) Nuclear mechanics and mechanotransduction in health and disease. *Current Biology*. **23**:R1113–R1121.

Iyer, S.R., Shah, S.B., Valencia, A.P., Schneider, M.F., Hernández-Ochoa, E.O., Stains, J.P., Blemker, S.S., and Lovering, R.M. (2017) Altered nuclear dynamics in MDX myofibers. *Journal of Applied Physiology*. **122**:470–481.

Jones, S.M., Howell, K.E., Henley, J.R., Cao, H., and McNiven, M.A. (1998) Role of dynamin in the formation of transport vesicles from the trans- Golgi network. *Science*. **279**:573–577.

Jungbluth, H. and Gautel, M. (2014) Pathogenic mechanisms in centronuclear myopathies. *Frontiers in Aging Neuroscience*. **6**:1–11.

Jungbluth, H., Treves, S., Zorzato, F., Sarkozy, A., Ochala, J., Sewry, C., Phadke, R., Gautel, M., and Muntoni, F. (2018) Congenital myopathies: Disorders of excitation-contraction coupling and muscle contraction. *Nature Reviews Neurology*. **14**:151–167.

Jungbluth, H., Wallgren-Pettersson, C., and Laporte, J. (2008) Centronuclear (myotubular) myopathy. *Orphanet Journal of Rare Diseases*. **3**:26.

Jungbluth, H., Wallgren-Pettersson, C., and Laporte, J.F. (2009) 164th ENMC International workshop: 6th workshop on centronuclear (myotubular) myopathies, 16-18th January 2009, Naarden, The Netherlands. *Neuromuscular Disorders*. **19**:721–729.

Jungbluth, H., Zhou, H., Sewry, C.A., Robb, S., Treves, S., Bitoun, M., Guicheney, P., Buj-Bello, A., Bönnemann, C., and Muntoni, F. (2007) Centronuclear myopathy due to a de novo dominant mutation in the skeletal muscle ryanodine receptor (RYR1) gene. *Neuromuscular Disorders*. **17**:338–345.

Kelly, A.M. and Zacks, S.I. (1969) The histogenesis of rat intercostal muscle. *Journal of Cell Biology*. **42**:135–153.

Kim, J.H., Jin, P., Duan, R., and Chen, E.H. (2015) Mechanisms of myoblast fusion during muscle development. *Current Opinion in Genetics and Development*. **32**:162–170.

King, M.C., Drivas, T.G., and Blobel, G. (2008) A Network of Nuclear Envelope Membrane Proteins Linking Centromeres to Microtubules. *Cell*. **134**:427–438.

Koch, A.J. and Holaska, J.M. (2012) Loss of emerin alters myogenic signaling and miRNA expression in mouse myogenic progenitors. *PLoS ONE*. **7**.

Koch, A.J. and Holaska, J.M. (2014) Emerin in health and disease. *Seminars in Cell and Developmental Biology*. **29**:95–106.

Kojima, C., Hashimoto, A., Yabuta, I., Hirose, M., Hashimoto, S., Kanaho, Y., Sumimoto, H., Ikegami, T., and Sabe, H. (2004) Regulation of Bin1 SH3 domain binding by phosphoinositides. *The EMBO Journal*. **23**:4413–22.

Laporte, J., Blondeau, F., Buj-Bello, A., and Mandel, J.L. (2001) The myotubularin family: From genetic disease to phosphoinositide metabolism. *Trends in Genetics*. **17**:221–228.

Laporte, J., Hu, L.J., Kretz, C., Mandel, J.L., Kioschis, P., Coy, J.F., Klauck, S.M., Poustka, A., and Dahl, N. (1996) A gene mutated in X-linked myotubular myopathy defines a new putative tyrosine phosphatase family conserved in yeast. *Nature Genetics*. **13**:175–82.

Lattao, R., Bonaccorsi, S., Guan, X., Wasserman, S.A., and Gatti, M. (2011) Tubby-tagged balancers for the drosophila X and second chromosomes. *Fly*. **5**:369–370.

Lee, K.K., Starr, D.A., Cohen, M., Liu, J., Han, M., Wilson, K.L., and Gruenbaum, Y. (2002) Lamin-dependent Localization of UNC-84, A Protein Required for Nuclear Migration in Caenorhabditis elegans. *Molecular Biology of the Cell*. **13**:892–901.

Lehman, W., Craig, R., and Vibert, P. (1994) Ca2+-induced tropomyosin movement in Limulus thin filaments revealed by three-dimensional reconstruction. *Nature*. **368**:65–67.

Lei, K., Zhang, X., Ding, X., Guo, X., Chen, M., Zhu, B., Xu, T., Zhuang, Y., Xu, R., and Han, M. (2009) SUN1 and SUN2 play critical but partially redundant roles in anchoring nuclei in skeletal muscle cells in mice. *Proceedings of the National Academy of Sciences*. **106**:10207–10212.

Leikina, E., Melikov, K., Sanyal, S., Verma, S.K., Eun, B., Gebert, C., Pfeifer, K., Lizunov, V.A., Kozlov, M.M., and Chernomordik, L. V. (2013) Extracellular annexins and dynamin are important for sequential steps in myoblast fusion. *Journal of Cell Biology*. **200**:109–123.

Liu, W. and Ralston, E. (2014) A new directionality tool for assessing microtubule pattern alterations. *Cytoskeleton*. **71**:230–240.

Lombardi, M.L. and Lammerding, J. (2011) Keeping the LINC: the importance of nucleocytoskeletal coupling in intracellular force transmission and cellular function. *Biochemical Society Transactions*. **39**:1729–1734.

Luxton, G.W.G., Gomes, E.R., Folker, E.S., Vintinner, E., and Gundersen, G.G. (2010) Linear arrays of nuclear envelope proteins harness retrograde actin flow for nuclear movement. *Science*. **329**:956–959.

Luxton, G.W.G. and Starr, D.A. (2014) KASHing up with the nucleus: Novel functional roles of KASH proteins at the cytoplasmic surface of the nucleus. *Current Opinion in Cell Biology*. **28**:69–75.

Madej-Pilarczyk, A. (2018) Clinical aspects of Emery-Dreifuss muscular dystrophy. *Nucleus*. **9**:314–320.

Maeda, K., Nakata, T., Noda, Y., Sato-Yoshitake, R., and Hirokawa, N. (1992) Interaction of dynamin with microtubules: its structure and GTPase activity investigated by using highly purified dynamin. *Molecular Biology of the Cell*. **3**:1181–1194.

Malone, C.J., Fixsen, W.D., Horvitz, H.R., and Han, M. (1999) UNC-84 localizes to the nuclear envelope and is required for nuclear migration and anchoring during C. elegans development. *Development*. **126**:3171–3181.

Mattioli, E., Columbaro, M., Capanni, C., Maraldi, N.M., Cenni, V., Scotlandi, K., Marino, M.T., Merlini, L., Squarzoni, S., and Lattanzi, G. (2011) Prelamin A-mediated recruitment of SUN1 to the nuclear envelope directs nuclear positioning in human muscle. *Cell Death and Differentiation*. **18**:1305–1315.

Mazumdar, A. and Mazumdar, M. (2002) How one becomes many: Blastoderm cellularization in Drosophila melanogaster. *BioEssays*. **24**:1012–1022.

McEntagart, M., Parsons, G., Buj-Bello, A., Biancalana, V., Fenton, I., Little, M.,

Krawczak, M., Thomas, N., Herman, G., Clarke, A., and Wallgren-Pettersson, C. (2002) Genotype-phenotype correlations in X-linked myotubular myopathy. *Neuromuscular Disorders*. **12**:939–946.

McMahon, H.T. and Gallop, J.L. (2005) Membrane curvature and mechanisms of dynamic cell membrane remodelling. *Nature*. **438**:590–596.

McNiven, M.A. (2005) Dynamin in disease. *Nature Genetics*. **37**:215–216.

Meinke, P., Mattioli, E., Haque, F., Antoku, S., Columbaro, M., Straatman, K.R., Worman, H.J., Gundersen, G.G., Lattanzi, G., Wehnert, M., and Shackleton, S. (2014) Muscular Dystrophy-Associated SUN1 and SUN2 Variants Disrupt Nuclear-Cytoskeletal Connections and Myonuclear Organization. *PLoS Genetics*. **10**.

Meinke, P., Nguyen, T.D., and Wehnert, M.S. (2011) The LINC complex and human disease. *Biochemical Society Transactions*. **39**:1693–7.

Melcon, G., Koslov, S., Cutler, D.A., Sullivan, T., Hernandez, L., Zhao, P., Mitchell, S., Nader, G., Bakay, M., Rottman, J.N., Hoffman, E.P., and Stewart, C.L. (2006) Loss of emerin at the nuclear envelope disrupts the Rb1/E2F and MyoD pathways during muscle regeneration. *Human Molecular Genetics*. **15**:637–651.

Mercuri, E. and Muntoni, F. (2013) Muscular dystrophy: new challenges and review of the current clinical trials. *Current Opinion in Pediatrics*. **25**.

Metzger, T., Gache, V., Xu, M., Cadot, B., Folker, E.S., Richardson, B.E., Gomes, E.R., and Baylies, M.K. (2012) MAP and kinesin-dependent nuclear positioning is required for skeletal muscle function. *Nature*. **484**:120–124.

Mislow, J.M.K., Holaska, J.M., Kim, M.S., Lee, K.K., Segura-Totten, M., Wilson, K.L., and McNally, E.M. (2002) Nesprin-1α self-associates and binds directly to emerin and lamin A in vitro. *FEBS Letters*. **525**:135–140.

Mittelbronn, M., Hanisch, F., Gleichmann, M., Stötter, M., Korinthenberg, R., Wehnert, M.S., Bonne, G., Rudnik-Schöneborn, S., and Bornemann, A. (2006) Myofiber degeneration in autosomal dominant Emery-Dreifuss muscular dystrophy (AD-EDMD). *Brain Pathology*. **16**:266–272.

Mooren, O.L., Kotova, T.I., Moore, A.J., and Schafer, D.A. (2009) Dynamin2 GTPase and cortactin remodel actin filaments. *Journal of Biological Chemistry*. **284**:23995–24005.

Mosley-Bishop, K.L., Li, Q., Patterson, K., and Fischer, J.A. (1999) Molecular analysis of the klarsicht gene and its role in nuclear migration within differentiating cells of the Drosophila eye. *Current Biology*. **9**:1211–1220.

Nakagawa, O., Arnold, M., Nakagawa, M., Hamada, H., Shelton, J.M., Kusano, H., Harris, T.M., Childs, G., Campbell, K.P., Richardson, J.A., Nishino, I., and Olson, E.N. (2005) Centronuclear myopathy in mice lacking a novel muscle-specific protein kinase transcriptionally regulated by MEF2. *Genes and Development*. **19**:2066–2077.

Navarro, A.P., Collins, M.A., and Folker, E.S. (2016) The nucleus is a conserved mechanosensation and mechanoresponse organelle. *Cytoskeleton*. **73**:59–67.

Nicot, A.-S., Toussaint, A., Tosch, V., Kretz, C., Wallgren-Pettersson, C., Iwarsson, E., Kingston, H., Garnier, J.-M., Biancalana, V., Oldfors, A., Mandel, J.-L., and Laporte, J. (2007) Mutations in amphiphysin 2 (BIN1) disrupt interaction with dynamin 2 and cause autosomal recessive centronuclear myopathy. *Nature Genetics*. **39**:1134–1139.

Oddoux, S., Zaal, K.J., Tate, V., Kenea, A., Nandkeolyar, S.A., Reid, E., Liu, W., and Ralston, E. (2013) Microtubules that form the stationary lattice of muscle fibers are dynamic and nucleated at golgi elements. *Journal of Cell Biology*. **203**:205–213.

Owen, D.J., Wigge, P., Vallis, Y., Moore, J.D.A., Evans, P.R., and McMahon, H.T. (1998) Crystal structure of the amphiphysin-2 SH3 domain and its role in the prevention of dynamin ring formation. *The EMBO Journal*. **17**:5273–5285.

Patterson, K., Molofsky, A.B., Robinson, C., Acosta, S., Cater, C., and Fischer, J.A. (2004) The Functions of Klarsicht and Nuclear Lamin in Developmentally Regulated Nuclear Migrations of Photoreceptor Cells in the Drosophila Eye. *Molecular Biology of the Cell*. **15**:1623–1634.

Peter, B.J., Kent, H.M., Mills, I.G., Vallis, Y., Butler, P.J.G., Evans, P.R., and McMahon, H.T. (2004) BAR domains as sensors of membrane curvature: the amphiphysin BAR structure. *Science*. **303**:495–499.

Piccirillo, R., Demontis, F., Perrimon, N., and Goldberg, A.L. (2014) Mechanisms of muscle growth and atrophy in mammals and Drosophila. *Developmental Dynamics*. **243**:201–215.

Praefcke, G.J.K. and McMahon, H.T. (2004) The dynamin superfamily: Universal membrane tubulation and fission molecules. *Nature Reviews Molecular Cell Biology*. **5**:133–147.

Prokic, I., Cowling, B.S., and Laporte, J. (2014) Amphiphysin 2 (BIN1) in physiology and diseases. *Journal of Molecular Medicine*. **92**:453–463.

Rajgor, D. and Shanahan, C.M. (2013) Nesprins: from the nuclear envelope and beyond. *Expert Reviews in Molecular Medicine*. **15**:e5.

Ramachandran, R., Surka, M., Chappie, J.S., Fowler, D.M., Foss, T.R., Song, B.D., and Schmid, S.L. (2007) The dynamin middle domain is critical for tetramerization and higher-order self-assembly. *EMBO Journal*. **26**:559–566.

Reinsch, S. and Karsenti, E. (1997) Movement of nuclei along microtubules in Xenopus egg extracts. *Current Biology*. **7**:211–214.

Ribeiro, I., Yuan, L., Tanentzapf, G., Dowling, J.J., and Kiger, A. (2011) Phosphoinositide regulation of integrin trafficking required for muscle attachment and maintenance. *PLoS Genetics*. **7**.

Richardson, B.E., Beckett, K., Nowak, S.J., and Baylies, M.K. (2007) SCAR/WAVE and Arp2/3 are crucial for cytoskeletal remodeling at the site of myoblast fusion. *Development*. **134**:4357–67.

Rogers, G.C., Rusan, N.M., Peifer, M., and Rogers, S.L. (2008) A Multicomponent Assembly Pathway Contributes to the Formation of Acentrosomal Microtubule Arrays in Interphase Drosophila Cells. *Molecular Biology of the Cell*. **19**:3163–3178.

Roman, W. and Gomes, E.R. (2018) Nuclear positioning in skeletal muscle. *Seminars in Cell and Developmental Biology*. **82**:51–56.

Roman, W., Martins, J.P., Carvalho, F.A., Voituriez, R., Abella, J.V.G., Santos, N.C., Cadot, B., Way, M., and Gomes, E.R. (2017) Myofibril contraction and crosslinking drive nuclear movement to the periphery of skeletal muscle. *Nature Cell Biology*. **19**:1189–1201.

Sakaki, M., Koike, H., Takahashi, N., Sasagawa, N., Tomioka, S., Arahata, K., and Ishiura, S. (2001) Interaction between Emerin and Nuclear Lamins. *Journal of Biological Chemistry*. **129**:321–327.

Salpingidou, G., Smertenko, A., Hausmanowa-Petrucewicz, I., Hussey, P.J., and Hutchison, C.J. (2007) A novel role for the nuclear membrane protein emerin in association of the centrosome to the outer nuclear membrane. *Journal of Cell Biology*. **178**:897–904.

Schindelin, J., Arganda-Carreras, I., Frise, E., Kaynig, V., Longair, M., Pietzsch, T., Preibisch, S., Rueden, C., Saalfeld, S., Schmid, B., Tinevez, J.Y., White, D.J., Hartenstein, V., Eliceiri, K., Tomancak, P., and Cardona, A. (2012) Fiji: An open-source platform for biological-image analysis. *Nature Methods*. **9**:676–682.

Schmalbruch, H. and Lewis, D.M. (2000) Dynamics of nuclei of muscle fibers and connective tissue cells in normal and denervated rat muscles. *Muscle and Nerve*. **23**:617–626.

Schulman, V.K., Dobi, K.C., and Baylies, M.K. (2015) Morphogenesis of the somatic musculature in Drosophila melanogaster. *Wiley Interdisciplinary Reviews: Developmental Biology*. **4**:313–334.

Schulman, V.K., Folker, E.S., Rosen, J.N., and Baylies, M.K. (2014) Syd/JIP3 and JNK signaling are required for Myonuclear Positioning and Muscle Function. *PLoS Genetics*. **10**.

Sewry, C.A., Brown, S.C., Mercuri, E., Bonne, G., Feng, L., Camici, G., Morris, G.E., and Muntoni, F. (2001) Skeletal muscle pathology in autosomal dominant Emery-Dreifuss muscular dystrophy with lamin A/C mutations. *Neuropathology and Applied Neurobiology*. **27**:281–290.

Shaw, S.L., Maddox, P., Skibbens, R. V., Yeh, E., Salmon, E.D., and Bloom, K. (1998) Nuclear and spindle dynamics in budding yeast. *Molecular Biology of the Cell*. **9**:1627–1631.

Shpetner, H.S. and Vallee, R.B. (1989) Identification of dynamin, a novel mechanochemical enzyme that mediates interactions between microtubules. *Cell*. **59**:421–432.

Shpetner, H.S. and Vallee, R.B. (1992) Dynamin is a GTPase stimulated to high levels of activity by microtubules. *Nature*. **355**:733–735.

Small, J.V., Herzog, M., and Anderson, K. (1995) Actin filament organization in the fish keratocyte lamellipodium. *Journal of Cell Biology*. **129**:1275–1286.

Sosa, B.A., Kutay, U., and Schwartz, T.U. (2013) Structural insights into LINC complexes. *Current Opinion in Structural Biology*. **23**:285–291.

Soulet, F., Schmid, S.L., and Damke, H. (2006) Domain requirements for an endocytosis-independent, isoform-specific function of dynamin-2. *Experimental Cell Research*. **312**:3539–3545.

Spear, P.C. and Erickson, C.A. (2012) Apical movement during interkinetic nuclear migration is a two-step process. *Developmental Biology*. **370**:33–41.

Spiro, A.J., Shy, G.M., and Gonatas, N.K. (1966) Myotubular myopathy: Persistence of fetal muscle in an adolescent boy. *Archives of Neurology*. **14**:1–14.

Starr, D.A. and Fischer, J.A. (2005) KASH 'n Karry: The KASH domain family of cargo-specific cytoskeletal adaptor proteins. *BioEssays*. **27**:1136–1146.

Starr, D.A. and Fridolfsson, H.N. (2010) Interactions between nuclei and the cytoskeleton are mediated by SUN-KASH nuclear-envelope bridges. *Annual Review*

of Cell and Developmental Biology. **26**:421–44.

Starr, D.A. and Han, M. (2002) Role of ANC-1 in tethering nuclei to the actin. *Science*. **298**:406–409.

Starr, D.A., Hermann, G.J., Malone, C.J., Fixsen, W., Priess, J.R., Horvitz, H.R., and Han, M. (2001) Unc-83 Encodes a Novel Component of the Nuclear Envelope and Is Essential for Proper Nuclear Migration. *Development*. **128**:5039–5050.

Suetsugu, S. and Gautreau, A. (2012) Synergistic BAR-NPF interactions in actin-driven membrane remodeling. *Trends in Cell Biology*. **22**:141–150.

Sullivan, K.M., Scott, K., Zuker, C.S., and Rubin, G.M. (2000) The ryanodine receptor is essential for larval development in Drosophila melanogaster. *Proceedings of the National Academy of Sciences*. **97**:5942–5947.

Tapley, E.C. and Starr, D.A. (2013) Connecting the nucleus to the cytoskeleton by SUN-KASH bridges across the nuclear envelope. *Current Opinion in Cell Biology*. **25**:57–62.

Tassin, A.M., Maro, B., and Bornens, M. (1985) Fate of microtubule-organizing centers during myogenesis in vitro. *Journal of Cell Biology*. **100**:35–46.

Taylor, G.S., Maehama, T., and Dixon, J.E. (2000) Myotubularin, a protein tyrosine phosphatase mutated in myotubular myopathy, dephosphorylates the lipid second messenger, phosphatidylinositol 3-phosphate. *Proceedings of the National Academy of Sciences*. **97**:8910–8915.

Taylor, M. V. (2006) Comparison of Muscle Development in Drosophila and Vertebrates. *Muscle Development in Drosophila*. 169–203.

Theadom, A., Rodrigues, M., Roxburgh, R., Balalla, S., Higgins, C., Bhattacharjee, R., Jones, K., Krishnamurthi, R., and Feigin, V. (2014) Prevalence of muscular dystrophies: A systematic literature review. *Neuroepidemiology*. **43**:259–268.

Thompson, H.M., Cao, H., Chen, J., Euteneuer, U., and McNiven, M.A. (2004) Dynamin 2 binds γ-tubulin and participates in centrosome cohesion. *Nature Cell Biology*. **6**:335–342.

Tosch, V., Rohde, H.M., Tronchère, H., Zanoteli, E., Monroy, N., Kretz, C., Dondaine, N., Payrastre, B., Mandel, J.L., and Laporte, J. (2006) A novel PtdIns3P and PtdIns(3,5)P2 phosphatase with an inactivating variant in centronuclear myopathy. *Human Molecular Genetics*. **15**:3098–3106.

Toussaint, A., Cowling, B.S., Hnia, K., Mohr, M., Oldfors, A., Schwab, Y., Yis, U., Maisonobe, T., Stojkovic, T., Wallgren-Pettersson, C., Laugel, V., Echaniz-

Laguna, A., Mandel, J.L., Nishino, I., and Laporte, J. (2011) Defects in amphiphysin 2 (BIN1) and triads in several forms of centronuclear myopathies. *Acta Neuropathologica*. **121**:253–266.

Tran, P.T., Marsh, L., Doye, V., Inoué, S., and Chang, F. (2001) A mechanism for nuclear positioning in fission yeast based on microtubule pushing. *Journal of Cell Biology*. **153**:397–411.

Trivedi, N. and Solecki, D.J. (2011) Neuronal migration illuminated: A look under the hood of the living neuron. *Cell Adhesion and Migration*. **5**:42–47.

Tsujita, K., Itoh, T., Ijuin, T., Yamamoto, A., Shisheva, A., Laporte, J., and Takenawa, T. (2004) Myotubularin Regulates the Function of the Late Endosome Through the GRAM Domain-Phosphatidylinositol 3,5-Bisphosphate Interaction. *Journal of Biological Chemistry*. **279**:13817–13824.

Vallee, R.B., Seale, G.E., and Tsai, J.W. (2009) Emerging roles for myosin II and cytoplasmic dynein in migrating neurons and growth cones. *Trends in Cell Biology*. **19**:347–355.

Velichkova, M., Juan, J., Kadandale, P., Jean, S., Ribeiro, I., Raman, V., Stefan, C., and Kiger, A.A. (2010) Drosophila Mtm and class II PI3K coregulate a PI(3)P pool with cortical and endolysosomal functions. *Journal of Cell Biology*. **190**:407–425.

Welte, M.A., Gross, S.P., Postner, M., Block, S.M., and Wieschaus, E.F. (1998) Developmental regulation of vesicle transport in Drosophila embryos: Forces and kinetics. *Cell*. **92**:547–557.

Wilson, M.H. and Holzbaur, E.L.F. (2012) Opposing microtubule motors drive robust nuclear dynamics in developing muscle cells. *Journal of Cell Science*. **125**:4158–4169.

Wilson, M.H. and Holzbaur, E.L.F. (2015) Nesprins anchor kinesin-1 motors to the nucleus to drive nuclear distribution in muscle cells. *Development*. **142**:218–228.

Worman, H.J. and Bonne, G. (2007) "Laminopathies": A wide spectrum of human diseases. *Experimental Cell Research*. **313**:2121–2133.

Xiang, X. and Fischer, R. (2004) Nuclear migration and positioning in filamentous fungi. *Fungal Genetics and Biology*. **41**:411–419.

Yang, L., Munck, M., Swaminathan, K., Kapinos, L.E., Noegel, A.A., and Neumann, S. (2013) Mutations in LMNA Modulate the Lamin A - Nesprin-2 Interaction and Cause LINC Complex Alterations. *PLoS ONE*. **8**.

Yeh, E., Skibbens, R. V., Cheng, J.W., Salmon, E.D., and Bloom, K. (1995) Spindle

dynamics and cell cycle regulation of dynein in the budding yeast, Saccharomyces cerevisiae. *Journal of Cell Biology*. **130**:687–700.

Yin, H., Price, F., and Rudnicki, M.A. (2013) Satellite cells and the muscle stem cell niche. *Physiological Reviews*. **93**:23–67.

Yu, H., Chen, J.K., Feng, S., Dalgarno, D.C., Brauer, A.W., and Schrelber, S.L. (1994) Structural basis for the binding of proline-rich peptides to SH3 domains. *Cell*. **76**:933–945.

Yu, J., Lei, K., Zhou, M., Craft, C.M., Xu, G., Xu, T., Zhuang, Y., Xu, R., and Han, M. (2011) KASH protein Syne-2/Nesprin-2 and SUN proteins SUN1/2 mediate nuclear migration during mammalian retinal development. *Human Molecular Genetics*. **20**:1061–1073.

Zelhof, a C., Bao, H., Hardy, R.W., Razzaq, a, Zhang, B., and Doe, C.Q. (2001) Drosophila Amphiphysin is implicated in protein localization and membrane morphogenesis but not in synaptic vesicle endocytosis. *Development*. **128**:5005–5015.

Zhang, J., Felder, A., Liu, Y., Guo, L.T., Lange, S., Dalton, N.D., Gu, Y., Peterson, K.L., Mizisin, A.P., Shelton, G.D., Lieber, R.L., and Chen, J. (2009a) Nesprin 1 is critical for nuclear positioning and anchorage. *Human Molecular Genetics*. **19**:329–341.

Zhang, Q., Bethmann, C., Worth, N.F., Davies, J.D., Wasner, C., Feuer, A., Ragnauth, C.D., Yi, Q., Mellad, J.A., Warren, D.T., Wheeler, M.A., Ellis, J.A., Skepper, J.N., Vorgerd, M., Schlotter-Weigel, B., Weissberg, P.L., Roberts, R.G., Wehnert, M.S., and Shanahan, C.M. (2007) Nesprin-1 and -2 are involved in the pathogenesis of Emery-Dreifuss muscular dystrophy and are critical for nuclear envelope integrity. *Human Molecular Genetics*. **16**:2816–2833.

Zhang, Q., Skepper, J.N., Yang, F., Davies, J.D., Hegyi, L., Roberts, R.G., Weissberg, P.L., Ellis, J. a, and Shanahan, C.M. (2001) Nesprins: a novel family of spectrin-repeat-containing proteins that localize to the nuclear membrane in multiple tissues. *Journal of Cell Science*. **114**:4485–4498.

Zhang, X., Lei, K., Yuan, X., Wu, X., Zhuang, Y., Xu, T., Xu, R., and Han, M. (2009b) SUN1/2 and Syne/Nesprin-1/2 Complexes Connect Centrosome to the Nucleus during Neurogenesis and Neuronal Migration in Mice. *Neuron*. **64**:173–187.